Improved application of remote referencing data in aeromagnetic processing: insights and applications from global geomagnetic modelling

Thesis submitted in accordance with the requirements of the University of Liverpool for the degree of Doctor in Philosophy by

Kelly Barker

April 2016

Improved application of remote referencing data in aeromagnetic processing: insights and applications from global geomagnetic modelling.

Kelly Barker

Abstract

Magnetic surveys are an important method of understanding subsurface geology, however there are several reasons why correction by remote referencing may fail, including local induced effects, activity levels of the field, and simple distance between survey and base station. We look for ways to improve correction by remote referencing using insights from global field models and comparisons of data from a wide range of observatories. We investigate the conditions in which the behaviour of nearby observatories differ from each other, and where the CM4 comprehensive model fails to match the observed behaviour of the local geomagnetic field. The misfits are separated by cause: those due to the activity level of the geomagnetic field, and the location of the observatory. We see that CM4 is a good match to observatories in the conditions it was designed for (mid-latitudes and Kp up to 2), but also that it can produce a good fit to stations out of this range (up to Kp of 3 or 4). The correlation of misfits to CM4 allows us to separate effects due to latitude, and location on the coast. Further investigation allows us to suggest some corrections that may improve the quality and extent of magnetic data gained by surveys in these locations. High latitude stations show changes in behaviour which fall into latitudinally split groups, most likely due to the presence of induced fields from ionospheric currents. Ensuring base station and survey fall into the same grouping would eliminate many of the problems this causes. Geomagnetic storms often lead to survey data being unusable due to their effects. We find that while X component data contains mostly storm signal, the Y and Z components at many stations contain retrievable data. The recovery period of the storm can, for most stations, be used after a regression is applied. We also consider the effects of induced fields due to the tides and the coast effect -well-known effects that can be seen at many stations. We find a correction for the dominant M_2 tidal effect using cosine waves. We also find an approximate correction for the coast effect, using cosine or sine waves of the Sq period as appropriate for the station pair chosen. It is also noted that small differences in location can have a large effect on the induced fields, as seen at GUI and TAM, where storms seem to have a smaller than expected effect.

Acknowledgements

My supervisor, Richard Holme, for providing ideas and impetus to this project, attempting to explain things neither of us understood, and pointing out that nothing worth doing is always easy.

ArkeX, for partial funding of this study, test datasets, and providing an insight into the practicalities of survey correction.

Andy McDonald, for proof-reading things he didn't understand, 80's fantasy films, and supplying endless mugs of coffee.

The various incarnations of the Dags, for endless encouragement and hilarity, weekends of being competent liabilities, and therapeutic sword fighting.

My parents, for allowing me to take over their dining room to write this, and all their support.

All the other PhD students through my time in Liverpool, for bouncing ideas, swapping skills, mutual encouragement/distraction, and the reminder to have fun along the way.

The various people who run the world data centres, and Intermagnet, for providing the data that this study is based on.

Contents

List of Figures

Introduction and Project Aims

Magnetic surveys are an important area of geophysical work, and contribute much to our understanding of underlying geology. This is particularly the case for the exploration industry, where aeromagnetic surveys can ensure coverage of otherwise inaccessible areas. An important part of processing the data captured by surveys is remote referencing – correcting the data from the survey to another set collected nearby, to remove time variant effects such as Sq. In this work, we aim to use findings from global magnetic field models, and comparison of observatory data, to find, understand, and correct for some of the sources of error in this process. The overall aim is to find relatively simple, rule of thumb, corrections for problems that may be encountered with remote referencing, which could be used by industry to improve the quality of their datasets and extend the conditions they can be used under.

Thesis Outline

A discussion of the data and ideas that form the background to this work is provided in chapter 1. This discusses the geomagnetic field, and the indices used to describe its activity levels, the observatories and satellite missions that have collected magnetic data, and the models which use this data. We also discuss magnetic surveying, and the benefits of improved remote referencing.
Chapter 2 focuses on work with the CM4 model, covering what conditions can be successfully modelled, and what conditions start to result in misfits to the model, as well as establishing where observatories are behaving differently to each other. These differences are then looked at individually, with the intention of establishing the cause, and attempting to correct for them.
Chapter 3 looks at the high latitude region, and the particular problems found within it. We investigate latitude based regional differences between observatories, and discuss possible methods of correlating between the regions.
Chapter 4 looks at magnetically active periods of time, discussing geomagnetic storms, investigating patterns in storm behaviour as recorded in various locations, and examining whether data collected during storms may corrected.
We then look at the effects of electrical conductivity and induced features in the geomagnetic field (chapter 5). We consider and attempt to correct for, the effects of tides, and the coast. We also discuss induction effects around the equatorial electrojet, and in high latitudes.
Finally, chapter 6 reviews the main conclusions of this work, and discusses the potential for future work in this area.

Chapter 1. Background

1.1 The Geomagnetic Field

1.1.1 The Geomagnetic Field

The geomagnetic field is the magnetic field surrounding the Earth, generated by dynamo actions in the Earth, and modified by crustal magnetism and the solar wind. At the Earth's surface, it is dominantly dipolar, similar to a bar magnet titled approximately 10 degrees with respect to the rotation axis, with higher degree fields making lesser contributions.

The vector field, **B**, may be described by orthogonal components (B_x for north, B_y east and B_z down), or by its total intensity, T, plus the inclination and declination angles:

$$T = \sqrt{(B_x^2 + B_y^2 + B_z^2)}$$
$$I = \arctan (B_z / \sqrt{(B_x^2 + B_y^2)})$$
$$D = \arcsin B_y/\sqrt{(B_x^2 + B_y^2)}$$

These relationships are shown in figure 1.1. Declination is the angle from north (positive in the eastward direction), and inclination the angle from the horizontal (positive down). The B components are conventionally written as X, Y and Z, and will be used this way thought this document. The total field intensity is also written as F (Blakely 1996).

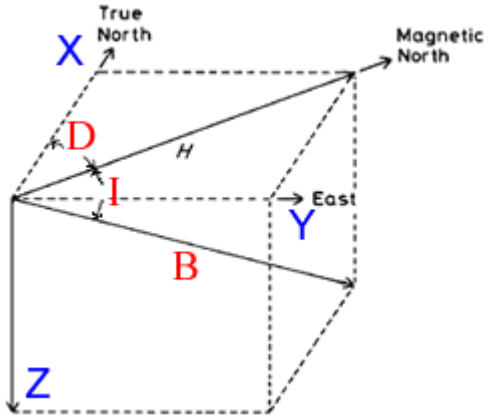

Figure 1.1. Magnetic field components related to geographic directions (Lanza and Meloni 2006)

The geomagnetic field lines converge at the north pole (the north pole is a magnetic south; this is why the north pole of smaller magnets are attracted to it). The magnetic dip poles are offset from the geographic poles by several degrees, and not precisely antipodal (figure 1.2). Over time these poles wander, due to the variation of the core field due to dynamo action. The field has a strength of around 70,000 nT at the poles, and 25,000 nT at the equator (Campbell 1997).

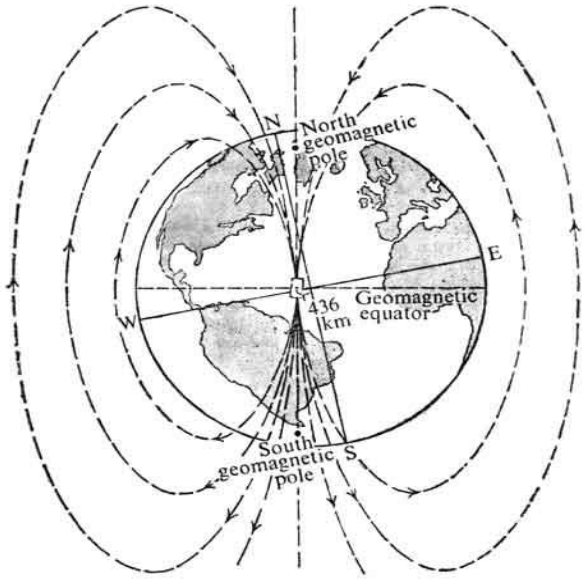

Figure 1.2 Schematic diagram of the geomagnetic field (Haymes 1971)

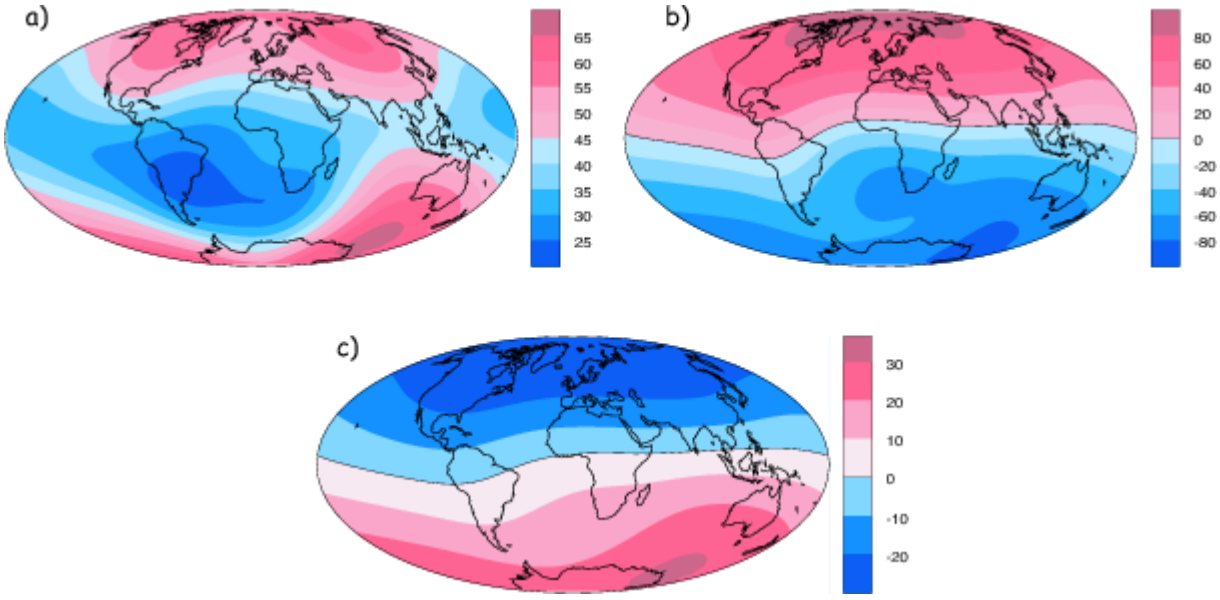

Figure 1.3 Maps of geomagnetic field of the IGRF for 2005. a) Intensity (μT), b) inclination, c) potential (nT) (Maus et al 2005)

The precise strength varies with latitude (figure 1.3), but also due to higher degree features distorting the purely dipolar features. The strength and orientation of the field also varies over long periods of time, this change is known as secular variation, and may be seen in long records of field direction and intensity, such as magnetic observatories. The strength and position of the poles varies with time, as the field is capable of flipping orientation, an event known as a geomagnetic reversal. Events which involve changing field orientations, but which fall short of full reversals, are termed excursions. These happen over long time scales, and as such are outside the scope of this work. Shorter decadal changes in the field are termed geomagnetic jerks. Study of long records of data has identified many potential jerks in field behaviour. Since all of these events have relatively long time-scales as compared to industry-type field measurements, they are not overly relevant to those conducting and interpreting magnetic surveys- certainly reversal/excursions are well outside of the relevant time frames (magnetic surveys will tend to run to a few weeks or months, depending on the nature and objectives of the survey) (Reeves 2005). In the case of jerks, while they are not likely to be important to individual surveys, comparison of old survey data, and the satellite and observatory records used in creating global field models, will likely include jerk effects. Data from some satellite missions has been used to identify current directions of polar wander, and intensity changes in the global field. This could become relevant if surveys undertaken in a 'jerk' are compared to other surveys, or old data for an area compared to newer data, but in theory base station correction should remove all such effects from processed survey data since it is a much longer period signal (Knecht and Shuman 1985). Further details about magnetic surveying practice and corrections are given in section 1.3.

The geomagnetic field extends outwards to the point it meets and is exceeded by the solar wind and the interplanetary magnetic field (figure 1.4). The area where the Earth's magnetic field is dominant is called the magnetosphere; charged particles within this region move as dictated by the magnetic field of the Earth and the currents generated within this region. Outside of this region, charged particles are controlled by the solar wind – the stream of plasma flowing out from the Sun. This also carries the solar magnetic field, the orientation of which is frozen in when the plasma leaves the Sun. The magnetosphere is asymmetric with respect to the sun because of this solar wind – on the sunward side the magnetosphere is pushed closer to the Earth, forming a bow shock, while on the opposite side it is stretched out into the magnetotail. The interactions between the solar wind and the geomagnetic field depend on the magnetic polarity, charge, speed, and density of the solar wind – higher densities in the solar wind compress the magnetosphere more, plasma with southward direction or energetic plasma, with different relative speed, may couple with or break and reconnect

the field lines, allowing solar particles into the magnetopause. This influx of charged particles may cause aurorae in polar regions, raise the strength of the currents that normally flow within the magnetosphere, and cause geomagnetic storms.

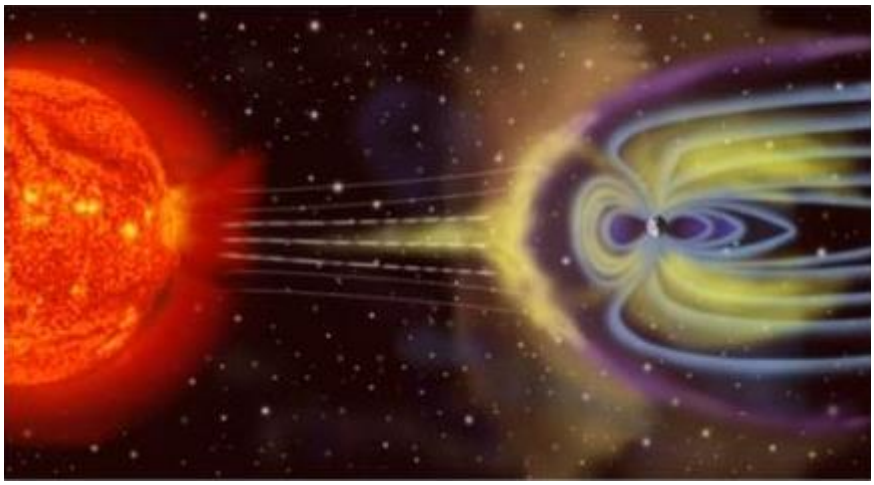

Figure 1.4 Solar wind interacting with the magnetosphere (BGS)

Within the magnetosphere, the region of space where the geomagnetic field dominates the Solar magnetic field, several currents flow, such as the ring current, a stream of charged particles flowing equatorially around the Earth, clockwise as viewed from the north (west to east). The magnetosphere extends many thousands of kilometres from the Earth.
Other currents flow within the ionosphere, a region of charged particles in the upper atmosphere, between about 85 and 600km above the surface. This encompasses the thermosphere, and parts of the mesosphere and exosphere. During the day, the whole ionosphere is ionised, while at night the lower D and E region's ionisation mostly disappears, leaving only the F region as a layer of significant ionisation (figure 1.5). This is because the ionisation in the ionosphere is predominantly created by particles from the Sun; while cosmic rays can also ionise, in general only particles on the sunward side are being ionised, and the ionisation is soon lost when the energy input is removed. Lightning may cause disturbances in the upper atmosphere which causes additional ionisation to occur in the D region. Plasma flow in the E region results in the equatorial electrojet. Currents also flow in the F region. During geomagnetic storms, the F2 layer becomes unstable; it may fragment or disappear completely. Solar heating also drives ionospheric winds, and a thermotidal motion is present. These combine to generate a dynamo current in the ionosphere. At the magnetic dip equator, the Hall current polarises opposite to flow, enhancing conductivity, and concentrating the flow of east-west currents. This is the equatorial electrojet. The ionospheric dynamo is affected by the local field strength, which varies with latitude. Similar effects at the poles create the auroral

electrojets. The Hall effect is the production of a voltage difference across an electrical conductor, transverse to an electric current in the conductor and a magnetic field perpendicular to the current. This means the electrojets are driven by charge build up related to the geomagnetic field, and the field aligned currents in the ionosphere/magnetosphere (McPherron et al 2013, Lanza and Meloni 2006, Pirjola 1998).

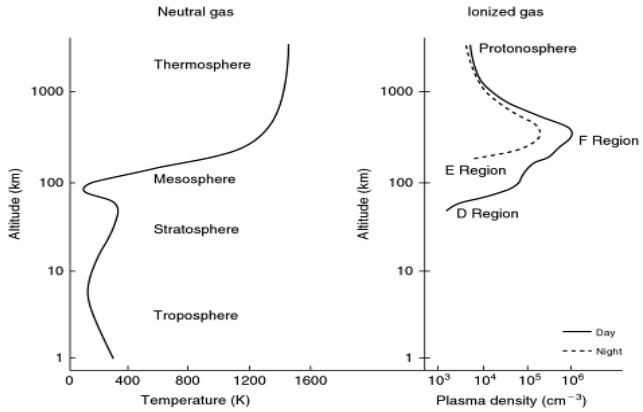

Figure 1.5 The layers of the atmosphere (Kelley, 2009)

The geomagnetic field behaviour over long periods is due to the action of the dynamo region, while on a daily basis it is mainly dominated by the effect of the solar magnetic field. As the Earth rotates, the field becomes stronger as the sun passes overhead, and weaker at local midnight. This is a combination of two effects -the shaping of the field by the solar wind draws the field lines further apart on the night side, giving the 'weakening' effect, vice versa for the compression on the day side; but additionally ionospheric ionisation and heating, which drive the currents which generate the Sq variation, is driven by solar radiation, and so only present on the day-side of the planet (Campbell 1997). The relative activity level of the solar field (and thus the strength of the solar wind), also known as 'space weather', changes the amplitude of this effect, and also the likelihood of shorter period features in the geomagnetic field, as areas of higher solar flux are encountered. The most extreme of these flux patches are associated with solar flares or coronal mass ejections, and create storms in the geomagnetic field, short duration events of very high disturbance, with associated recovery periods where the field returns to its undisturbed state. A geomagnetic storm is defined by the rapid drop of Dst (disturbance storm time index – a measure of the strength of the ring current, see chapter 4 for more details), from its normal value around +/- 20nT to below -50nT. The amount it drops by determines the severity of the storm. During storms, magnetic surveys are often difficult or impossible to interpret, as the normal behaviour of the field is almost completely overprinted with the storm signature. Storms cause large disturbances to the magnetic field, and also to the ionic composition of the upper atmosphere. The influx of solar particles and the disturbance of normal

flow of charged particles around the Earth adds to existing currents, and also creates induced currents, in the ionosphere and magnetosphere, and in the case of large storms, large currents in the ground and ocean may occur. The more disturbance, the farther the field behaviour deviates from Sq (solar-quiet, or 'normal' variation), and so the more noise is introduced into the survey – and the correction. The level of disturbance is measured by the Kp and Dst indices.

1.1.2 Field Activity Levels and Magnetic Indices

Sq

The activity level of external part of the geomagnetic field is mainly dependent on the activity levels of the Sun, and the resulting space weather this sends towards the Earth. This is also dependent on the geometry of the system, since the active areas of the sun will only affect the geomagnetic field if directed towards the Earth at that point in time. Normal, undisturbed time periods are known as Sq, solar quiet time. During quiet times, the geomagnetic field experiences a 24-hour period variation, peaking around local noon and at its lowest at local midnight, with a range of around 10-40 nT (Campbell 1997). This is due to the influence of radiation from the Sun. The solar emissions both ionise and heat up the atmosphere. This creates the charged layers of the ionosphere, in the F, D and E regions during the day; when the solar effect is not creating new ions (during night time, where no ionising radiation is striking the atmosphere) the ions recombine, and the D and E layers disappear. Since the emissions also heat and expand the atmosphere, winds are generated, which couple with the tidal winds (also driven partly by the sun, but mainly by the gravitational pull of the moon). This combination of winds and charged particles creates closed loop currents in the sunward side ionosphere, driving the ionospheric dynamo. These currents give rise to induced magnetic fields, which is what creates the distinctive 24-hour field variation. Due to flowing only on the sunward side of the Earth, the currents loop and reconnect; separate loops are generated in the northern and southern hemispheres (figure 1.6). The two loops, and their shape, which is confined by the extent of sunlight hitting, and so heating and ionising, the upper atmosphere, defines the shape of the Sq variation, which is effectively a sine wave, with '0' points at dawn and dusk, a peak at noon and a trough at midnight (technically midnight is the zero point, as this is where there is no effect from the sun). This variation is best seen at periods of low disturbance; while it is still present during disturbed time, it is over-printed by disturbance effects. In the case of the very high disturbance of storm periods, it is mostly invisible; this is particularly the case for large storms, as they may break down the F region of the ionosphere, removing a large part of the charged particle source for the ionospheric dynamo current. The overall pattern and

amplitude of Sq also varies with hemisphere, and with the seasons, as the varying distance between the Earth and the Sun changes the amount of radiation hitting the atmosphere (Campbell 1997).

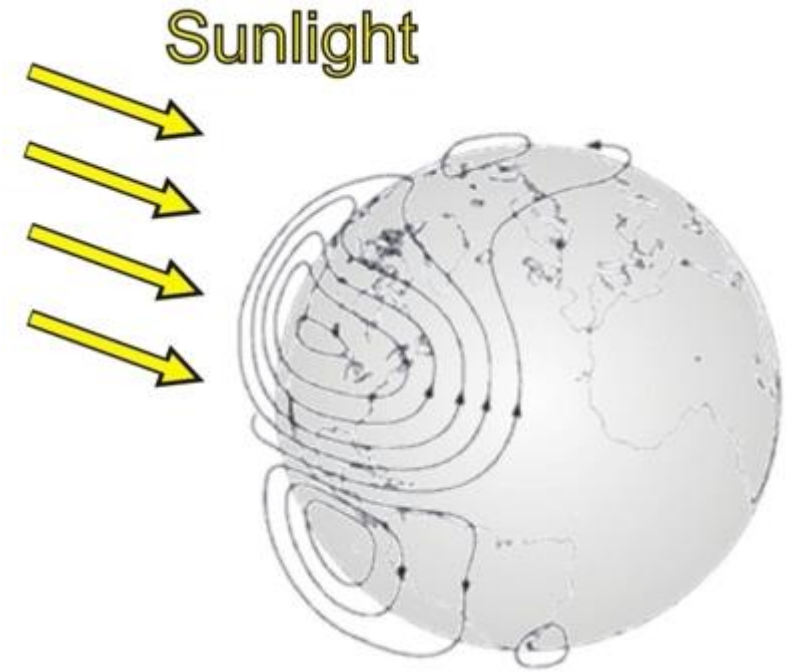

Figure 1.6 Ionospheric Sq currents (BGS; after Torta et al 1997)

The Sq variation of the magnetic field is dominantly in 24, 12, 8 and 6 hour periods (during days which are not affected by magnetic storms, or similar features). After the lunar tidal component is removed, the remaining field is termed Sq (solar quiet). Sq is the relatively stable part of the field variation, which is seen at all times. It is thought of as daily or diurnal variation, though strictly, only the 24hr period part of Sq is the diurnal. Sq is controlled by the sun; it changes with sunspot activity, and varies in amplitude and phase through the year. The Sq field is also asymmetric (in two senses – it is different in each hemisphere at a given time, and also the northern hemisphere tends to be higher intensity compared to the southern hemisphere in the same season). The source of Sq is in the ionosphere. High latitudes may be dominated by magnetospheric fields and not show Sq variation. The Sq field has a sudden local transition at sunrise and sunset, but there is often drift between sunset and sunrise, which may be due to the decay of the night-time F region of the ionosphere. There is also a small contribution from distortion of the dipole field by the solar wind. Viewed from above, the Sq field has an anticlockwise current vortex in the northern hemisphere, and a clockwise vortex in the southern hemisphere. This becomes far more complex in the polar regions. The field is larger in the summer region, since the additional solar radiation can drive stronger currents.

Midnight values of Sq at low and mid latitudes track a night side magnetospheric distortion which stretches anti-sunward and is seasonal/annual/semi-annual, depending on axis component looked at (Campbell 1997). Variation in horizontal components is annual at mid latitudes, semi-annual at low latitudes. Variation in declination is annual, with high/low points at the equinoxes. Variation in the vertical component is significantly modified by latitude (figure 1.7).

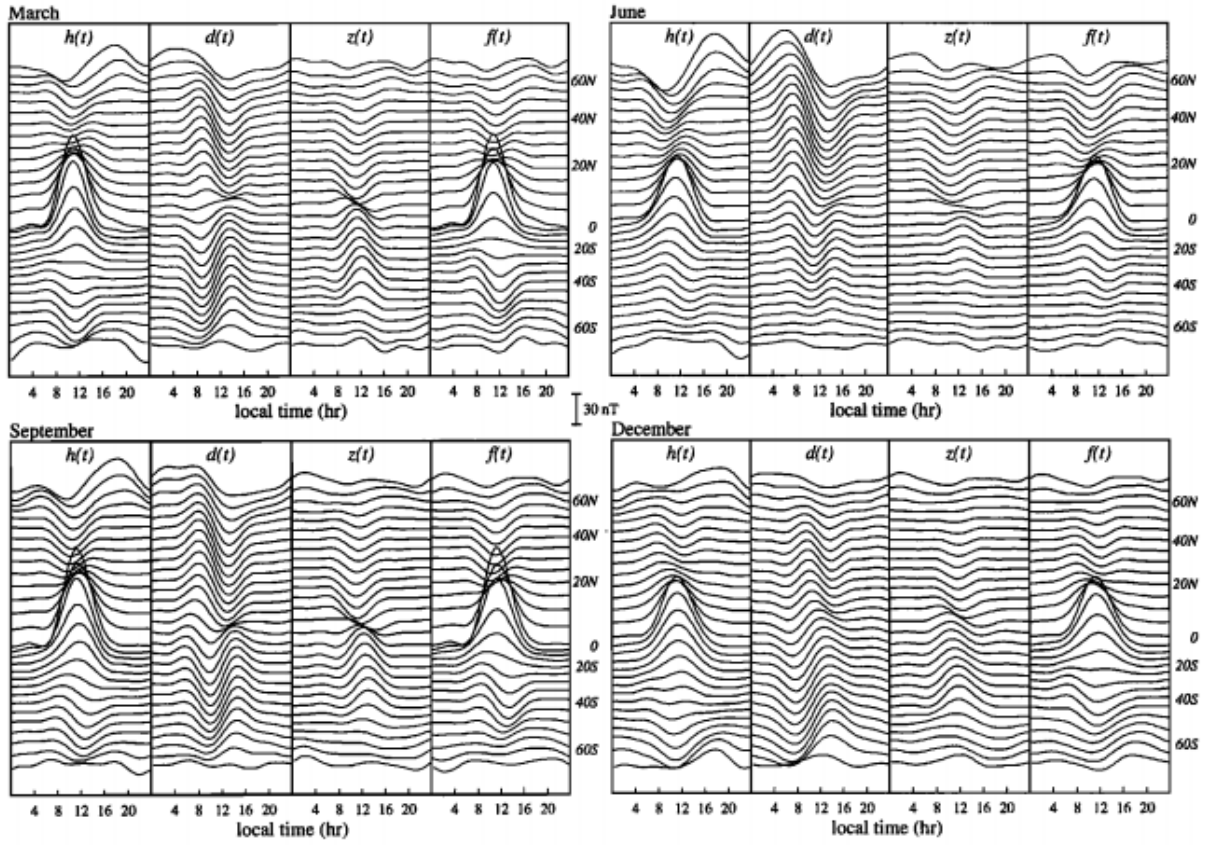

Figure 1.7. Global Sq curves for each season, showing averaged Sq variations for each latitudinal band (Hitchman et al 1998).

Very short period features are not part of Sq, though some shorter features are present as higher harmonics of Sq. Polar currents are separate to Sq and very sensitive to the solar wind. Solar activity changes the amount of heating in the ionosphere, which modifies Sq in active years. The induced component of Sq depends on the conductivity profile, up to depths of 500km (or more). Tidal flow of the ocean, island effects, and flow of salt water currents may also affect Sq.

Kp

K-indices are the measure of disturbance in the two horizontal components of the magnetic field. First, the stations normal Sq variation is removed from the data. Then, the range of disturbance on the most disturbed of the two indices, is calculated for each three-hour period. These give a local K value for the station, which is reported as values from 0-9 in a quasi-logarithmic scale (the range of

the disturbance corresponds to a value of 0-9, which is standardised for the station to balance the frequency of occurrence of a particular level of disturbance). These data are local only, and still contain various cycles of activity related to the station location, time of year/day etc. Conversion tables are used to normalise the data, creating Ks values for each station, which are reported in thirds (0o, 0+, 1-, 1o, 1+ etc.). Thee standardised values are then used to calculate the global Kp index, by averaging the Ks values of the Kp network of stations.

Kp is therefore the weighted average of K-indices from a network of 13 sub-auroral observatory stations over a three-hour period (table 1). It is reported as first as quick look (rapidly collected, unchecked/corrected data used to give an indication of the current activity levels), then provisional data, which has been calibrated and checked, but may be replaced or confirmed as necessary. Definitive values are reported once data from all observatories in the network has been received and verified, these may be displayed as a musical diagram (figure 1.8). (Mayaud 1980, Chapters 4 and 5; GFZ Potsdam http://www.gfz-potsdam.de/en/research/organizational-units/departments/department-2/earths-magnetic-field/services/kp-index/theory/)

The Kp Observatories					
Station Code	Location	Operating Dates	Replacement Station Code	Location	Operating Dates
ABN	Abinger, England	1932-1957	HAD	Hartland, England	1957-present
AGN	Agincourt, Canada	1932-1969	OTT	Ottawa, Canada	1969-present
AML	Amberley, New Zealand	1932-1978	EYR	Eyrewell, New Zealand	1978-present
CHL	Cheltenham, USA	1932-1957	FRD	Fredericksberg, USA	1957-present
ESK	Eskdalemuir, Scotland	1932-present			
LER	Lerwick, Scotland	1932-present			
LOV	Lovo, Sweden	1954-2004	UPS	Uppsala, Sweden	2004-present
MEA	Meanook, Canada	1932-present			
RSV	Rude Skov, Denmark	1932-1984	BFE	Brorfeld, Denmark	1984-present
SIT	Sitka, Alaska	1932-present			
TOO	Toolangi, Australia	1972-1981	CNB	Canberra, Australia	1981-present
WIT	Witeveen, Netherlands	1932-1988	NGK	Niemegk, Germany	1988-present
WNG	Wingst, Germany	1938-present			

Table 1 Kp observatories

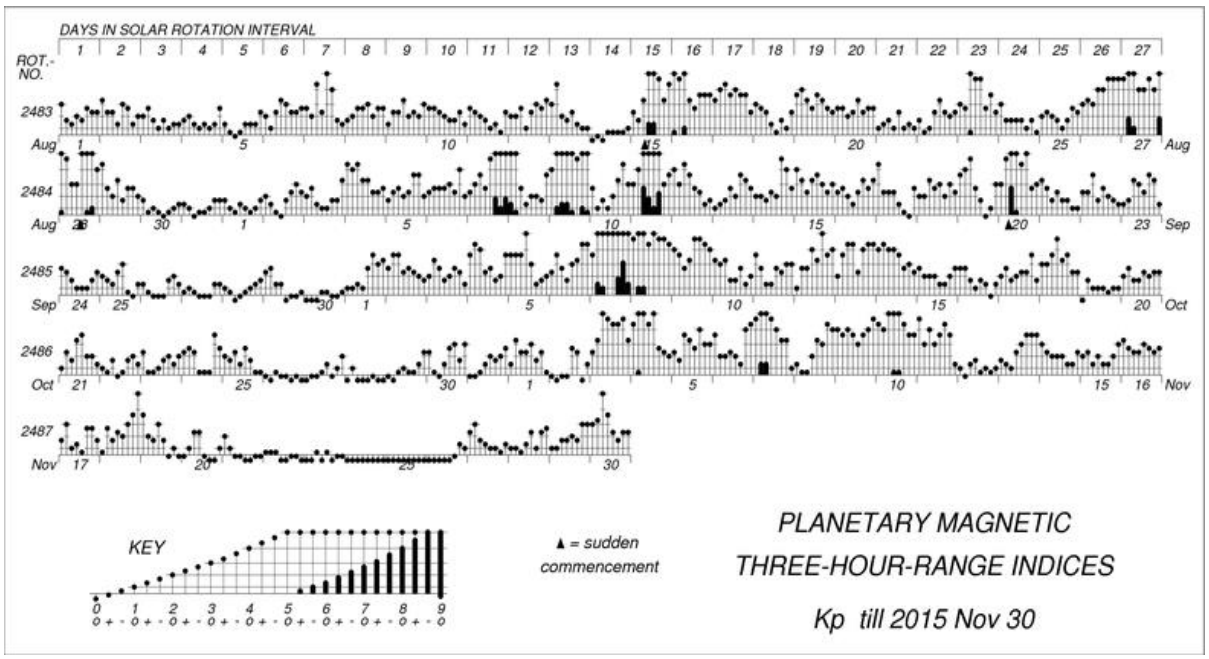

Figure 1.8 Example musical diagram of Kp to 30th November 2015 (GFZ Potsdam)

Other related indices are also defined: for example, ap, Ap, and Cp. For more details, see Mayaud 1980.

Dst

Dst is the disturbance storm time index. It is a measure of activity based on the intensity of the equatorial magnetospheric ring current. Dst can be used to identify the onset of geomagnetic storms; since the disturbance field strength at low latitudes is related to the strength of the ring current, the strengthening of the ring current during the storm is seen as a rapid fall in Dst. Like Kp, Dst is also based on the horizontal components of the geomagnetic field, as recorded at four near-equatorial stations, Hermanus, Kakioka, Sanjuan and Honolulu. These stations are near but not at the equator, to avoid the effect of the equatorial electrojet. Baseline values of the horizontal components are calculated using the 5 local days that have a maximum overlap with the 5 international quietest days. The normal Sq variations for each observatory are also calculated. Any noncyclic change is removed from Sq by assuming that it is linear from midnight to midnight on the local quiet days selected. From the series of the monthly Sq for a given year, a double Fourier series is expanded as follows:

$$\sum_{n=1}^{6} \sum_{m=1}^{6} A_n^m \cos(mT + \alpha_m) \cos(nM + \beta_n)$$

where T is the local time and M the month. This corresponds to the computation of 48 unknown coefficients while one has 12 x 24 experimental data. The hourly values of a synthetic Sq variation

are computed from the Fourier series (a month number with one decimal is assigned to each day) and are subtracted from the original hourly values. For the definition of the reference level at each observatory a parabola is fitted with respect to the annual means of H for the 5 international quietest days of the months and not for the full annual means. Finally, at each observatory *j*, if $H_{obs\,j}$ is the hourly average of the horizontal field recorded, one obtains a Dst, such that

$$Dst_j = H_{obs\,j} - Sq_j(t) - H_{o,j}(t)$$

Then the Dst_j values are averaged before applying the correction $1/\cos A_j$ necessary for obtaining the value of the ring current effect at the dipole equator. (Mayaud 1980, Chapter 8; WDC Kyoto, http://wdc.kugi.kyotou.ac.jp/dstdir/dst2/onDstindex.html)

A similar index is the AE index, which is effectively Dst for the Auroral electrojet, and calculated in much the same way using stations at high latitudes – ABK (Abisko, Sweden), DIK (Dixon Island, Russia), CCS (Cape Celyuskin, Russia), TIK (Tixie, Russia), CWE (Cape Wellen, Russia) – replaced with PBK (Pebek, Russia) in 2001, BRW (Barrow, USA), CMO (College, USA), YKC (Yellowknife, Canada), FCC (Fort Churchill, Canada), PBQ (Poste-de-la-Baleine, Canada), NAQ (Narsarsuaq, Greenland), and LRV (Leirvogur, Iceland). It is less well resourced, and so not always available, and often provisional for many years. (Mayaud 1980, Chapter 7; http://wdc.kugi.kyoto-u.ac.jp/aedir/ae2/onAEindex.html)

F10.7

F10.7 is a measure of solar radio flux per unit frequency, with a wavelength of 10.7 centimetres (a frequency of 2800MHz) at Earth, and expressed in solar flux units. It is a measure of radio emissions, mainly due to heating of plasma in active areas of the sun, but also containing input from areas of emission outside active regions, and the constant background radio emissions of the quiet Sun; it may be thought of as the 'level' of solar activity, and is strongly linked to the sunspot cycle. Flux measurements may also contain the effect of transient events not part of the 'normal' activity of the Sun at that time. It is used as a measure of solar activity (adjusted flux, Sa, scaled to a standard distance of 1AU), and as an input to ionospheric models as a proxy for the ultraviolet radiation which can ionise the particles in the ionosphere (observed flux, S, which is the actual observed value, which changes through the year as the distance between the Earth and Sun changes with orbital ellipticity); calculated daily at local noon at the Algonquin Radio Observatory (to 1991) and Pentictin Radio Observatory (from 1991), it is one of the longest running measures of solar activity;

only the record of sunspots is longer (ftp.ngdc.noaa.gov/STP/space-weather/solar-data/solar-features/solar-radio/noontime-flux/penticton/documentation/miscellaneous/penticton.txt)

1.2 Geomagnetic Data and Modelling

1.2.1 Observatory Data

A particularly important source of geomagnetic field data is that collected at magnetic observatories (figure 1.9). These are permanent structures housing magnetic equipment, located away from anthropogenic disturbances, which record intensity and direction of the field at that location. Some observatories have a very long operating history, while others may only be active for a few months or years. Different observatory sets are involved in the defining/measurement of the various activity indices, such as Kp, Dst and AE, mainly based on their geographical location. Observatories satisfying certain quality criteria may become part of INTERMAGNET (International Real-time Magnetic Observatory Network, intermagnet.org). Most observatories will contain at least one vector and one scalar instrument. Observatories are positioned and built as carefully as possible, and designed to be able to produce accurate data for long periods of time, and record continuously during that time. The site selected should be stable, with no large local anomalies or field gradients, the buildings must not be magnetic themselves(!), be able to maintain a power supply, and temperature controlled as far as possible.

One of the functions of observatories is to record secular variation, so most are intended to operate over decades. Each regional observatory can be used as a base station for surveys in that region, and in theory the secular variation recorded there can be used to update magnetic maps, removing the need to re-survey an area. They also record much faster variations in the field, such as those associated with Sq, geomagnetic storms and solar flares, which are of interest both to scientists and potentially to those working with communications and infrastructure which may be damaged or otherwise affected by either the magnetic fields or associated electrical currents. Data from observatories in this work come either from INTERMAGNET or the World Data Centre for Geomagnetism (Edinburgh) (http://www.wdc.bgs.ac.uk/catalog/master.html)

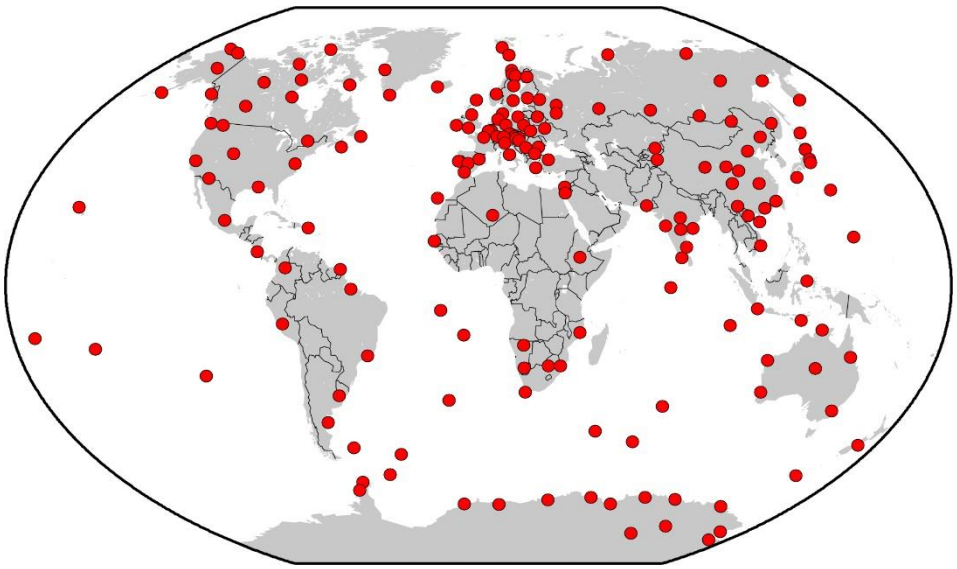

Figure 1.9 Currently operating magnetic observatories (BGS)

1.2.2 Satellite Data

The coverage of good quality magnetic data from observatories is limited by the location of observatories. These are (currently) only located on land, but are also disproportionately more common in the northern hemisphere, particularly in Europe. This means that maps or models based purely on observatory data are much less robust in areas lacking observatories; this is particularly apparent when using historical data. As such, data collected by satellite missions are very important to understanding the global field, as they extend the coverage beyond what is possible with only terrestrial data, and reduces some of the bias. It also allows the collection of data on fields (and currents) which are generated in the ionosphere or upper magnetosphere. While this allows a much more uniform collection of magnetic data, there are still gaps in coverage particularly over the poles, as the satellite missions are temporally and geographically limited by their orbiting patterns, and the length of the mission.

The earliest of the magnetic satellite missions dedicated to modelling the global field collected only scalar data, and were relatively short. They aimed to create a map of the geomagnetic field, which was previously not possible from satellite missions, as they did not carry equipment capable of collecting absolute intensity data (Rajaram 1993). Later missions, such as CHAMP, Ørsted, and now Swarm, have run for much longer periods, collecting both scalar and vector data; this is the same type of data that is recorded at the ground based observatories. The continuing use of satellite missions means our understanding of the geomagnetic field will only improve in coming years. This

is important for many reasons, including our ability to understand the dynamo processes of the core and mantle, and the origin and evolution of the Earth's magnetic field. For purposes of the oil and mineral exploration industry, the increased coverage and understanding of local and short term features of the field could aid in the survey correction process.

Satellite magnetism missions, with their instrument package and aims:

POGO- NASA. 1964- ~1972. Series of satellites designated as orbiting geophysical labs, containing multiple experiments. At least 1 through 5 contained scalar magnetic field experiments.

Magsat – NASA. Autumn 1979 to spring 1980. Scalar and fluxgate magnetometers. Map the Earth's magnetic field.

Ørsted – Danish Meteorological Institute. Feb 1999- . Scalar and fluxgate magnetometers, star imager, charged particle detector, two GPS receivers. Map the Earth's magnetic field, collect data to determine changes (polar motion).

Cluster- II – summer 2000. Four satellites in constellation. Fluxgate magnetometer, ion spectroscopy experiment, several experiments/instruments looking at electric fields, electron/ion plasmas, and radio waves. Studying interactions of magnetosphere and atmosphere with the solar wind.

CHAMP – GFZ/DLR. Jul 2000 to Sep 2010. Scalar and fluxgate magnetometers, accelerometer, laser reflector, GPS receiver, star imager, digital ion drift meter. Gravity (geoid) and magnetic mapping.

SAC-C – CONAE. Nov 2000- . Multi-spectral sensor, high resolution cameras, GOLPE experiment. Launched with Landsat-7, EO-1 and Terra, to create an Earth observation constellation jointly with NASA.

THEMIS- NASA. Feb 2007- . Fluxgate and search-coil magnetometers, electrostatic analyser, electrical field instrument, solid state telescope. Study substorms and reconnection, magnetosphere/solar/lunar field interaction.

Swarm – ESA. November 2013- . Three satellites in constellation. Scalar and fluxgate magnetometers, electric field instrument, accelerometer, laser range reflector. Builds on Ørsted and CHAMP data. High precision magnetic mapping, aiming to understand core dynamics, core-mantle interaction, mantle conductivity, lithospheric magnetisation, and magnetospheric/ionospheric currents.

(Olsen and Kotsiaros 2011; http://www.nasa.gov/missions, http://www.space.dtu.dk/english/Research/Projects/Oersted, http://op.gfz-potsdam.de/champ/, http://www.esa.int/)

1.2.3 Magnetic Field Modelling

Many models of the geomagnetic field (and indeed, planetary magnetic fields in general) have been produced, for a variety of reasons. Each model created allows some improvement in our understanding of the behaviour of the geomagnetic field, and thanks to improved data coverage from satellite missions, these models have become progressively more detailed and extended to cover more of the Earth.

Predictive models attempt to model the future of the field based on its past and present.

Dynamo models attempt to explain many questions, commonly when and how the geodynamo started, why it behaves as it does, how it behaved in the past, and how it may be expected to behave in the future. They may also be used to model other dynamos, such as potential dynamos on other planets. These are outside of the scope of this work, and will not be considered further here.

Other models make predictions of how the field behaves at a particular place and time, based on data recorded at other locations. These may be local or global, and/or concentrated on fitting particular regions. Examples of these include the World Magnetic Model, International Geomagnetic Reference Field (www.geomag.bgs.ac.uk/research/modelling/IGRF.html). CM4 also fits into this category, along with a series of similar models; however, it is different to the IGRF and WMM in the sense that it can be used to create models for different times, and used for different purposes; while the IGRF describes the large-scale field strength and direction globally at one time, and is updated every few years, the CM4 code can be used to create this information for a range of time periods, and look at shorter period variations.

1.3 Comprehensive Modelling (CM3 and CM4)

1.3.1 Use of the Comprehensive Models

In this study, the CM4 model is used extensively as a comparison for observatory data. CM4 is the 4th version of a comprehensive field model developed by Sabaka et al, published in 2004. It is not intended as a true predictive in time model, but generates a standardised model of the magnetic field at a given location, based on prior data. (The predictive capabilities are limited to 'prediction' of expected values in areas without data coverage based on the available data at other locations). The data the model uses to produce its expected behaviour are from both magnetic observatories (fixed stations) and several satellite missions: Magsat, POGO, Ørsted and CHAMP. The code may be

found at http://core2.gsfc.nasa.gov/CM/. CM4 is in this sense an extension and improvement on CM3 (the 3rd version of the model, Sabaka et al, 2002) in that the satellite data includes more vector data as well as scalar data, and the periods covered by both satellites and observatories is greater. CM3 is based on POGO and Magsat data, and observatory data up to 1985. CM4 incorporates both this data, and also the two additional satellite missions (Ørsted and CHAMP), observatory data up to 2000, Dst data, F10.7, and behavioural knowledge from satellite sampling of F-region current-induced fields. It is capable of modelling some of the toroidal magnetic fields in the ionosphere, the effect of the ring current in the magnetosphere, and the effect of increased solar flux, which is treated as scaling the ionospheric field without changing its shape. Currents in the F-region couple with the E-region, which is where the equatorial electrojet is generated. The auroral electrojets are not modelled. The code is designed to fit Sq periods; data from more disturbed periods are not, in general, incorporated into the model parameters.

The CM4 code comes with pre-written driver examples, of which mainly 'example 2' has been used in this study. This outputs model values of induced and external components for the magnetosphere and ionosphere, in X, Y, and Z components (north, east, and vertical respectively), for a user specified location and timeframe, producing six sets of model values for a given time. CM4 as written covers the period to 2002, but adding additional data for Dst and a modification of the code to extend the time series has allowed it to be extended, at least for external and induced fields. Since this study focuses on the magnetic field as used in typical industry surveys, the parts of the model which are more difficult to extend/not designed to extend further, such as the core and lithospheric generated fields, are not so important. The core field can be obtained from IGRF or similar, and the lithospheric field can be assumed to remain constant (or indeed, is the target of the survey). The effect of the core field in the models used here is therefore treated as effectively a linear regression or addition correction. The short period variations of the geomagnetic field are more useful to understand in the situation of a survey, since they are what would be affected by any correction applied, rather than the overall strength of the total field. Since the objective is to improve survey corrections, it is also less vital that the code generate crustal mode fields, since the variance in this feature is the target of the survey.

Since models such as CM4 are constrained by the actual data recorded at observatories and during satellite missions, they can be used to gain greater understanding of how the field is behaving over short time scales. Particularly when this is tied into the behaviour of the field due to solar influences, an averaged model can be of use in extending expected field behaviours to locations where there is poor data coverage, based on the behaviour at locations where observations exist.

This could allow an improvement on remote referencing- if a model value accurately represents the field behaviour over survey-scale time periods, then it could be used as a base station value for surveys where actual stations are far away, unsuitable or unavailable for other reasons. Detailed comparisons of station, satellite, and model data, could also allow an improved understanding of the variation of the field between stations, which would improve the choice of location for a base correction, or an additional set of corrections if alternatives are not available.

More detailed descriptions of CM3 and CM4, taken from Sabaka et al 2002 and Sabaka et al 2004, respectively, are given below. These cover the data selection, and parameterisation of the models, as well as the assumptions used. CM3 is described more thoroughly in section 1.3.2, while section 1.3.3 mainly notes the changes and additions made for CM4. Since work with CM4 within this study focuses on the external (magnetospheric and ionospheric) components, treating the core and lithospheric fields as unchanging in the timespans studied, only a brief description of the core and lithospheric field parameterisation is included. Finally, in section 1.3.4, we discuss the areas where data issues or assumptions used in the parameterisation may affect the performance of the model.

1.3.2 CM3

CM3 (Sabaka et al 2002)

CM3 (or CMP3) developed from the idea of modelling 'comprehensively': using radial positions of various geomagnetic source regions relative to the available data, and simultaneous inversion for parameters from joint analysis of both surface and satellite data. This was intended as an improvement on previous approaches, which treated sources separately.

Data

CM3 incorporates annual and hourly means from magnetic observatories. The hourly means are chosen from the magnetically quietest day of each month, during the operational periods of POGO (September 1965 to August 1971) and Magsat (November 1979 to May 1980), and through to 1982. Only hourly means from every other hour are used.

The Magsat data used in the CM3 model are mainly dawn and dusk data. They were initially screened with the three-hourly Kp index by choosing only data with Kp < 1- and previous Kp ≤ 2o. Vector data poleward of ±50^{o} dipole latitude were excluded to minimize the effects of currents in the auroral regions. Scalar intensity data were retained at all latitudes. Data were then selected within a ±20 nT Dst level for the time intervals of Nov/Dec 1979; Jan/Feb 1980; and Mar/Apr 1980. This was to obtain a uniform data distribution; passes from slightly more disturbed times were added in order to improve geographic coverage. In order to parameterise ionospheric coupling and the EEJ, X and Y vector components from high geomagnetic latitude were added at sampling points already providing scalar measurements.

The POGO data from which the sets used in the CM3 model were extracted, were also used to derive the POGO(2/72) field model, with additional OGO-6 data from 1969 to 1971 for quiet to moderately quiet times. These have an uneven distribution in local time, and were decimated to achieve more uniform distribution. The POGO decimated data set did not admit entire satellite tracks. Data from passes from quiet periods was added, in which the spatial and temporal distributions were considered to sample most of the Sq and EEJ features of the ionospheric current systems.

Parameterization of field sources

Core and lithospheric fields

The current systems responsible for both the core and lithospheric magnetic fields lie entirely below the regions sampled by permanent observatories and satellites. Therefore, these fields may be expressed as gradients of internal potential functions:

$$V = \Re \left\{ a \sum_{n=1}^{N_{max}} \sum_{m=0}^{n} \left(\frac{a}{r} \right)^{n+1} \gamma_n^m Y_n^m(\theta, \phi) \right\}$$

with:

$Y^m_n = P^m_n(\theta) \exp im\varphi$

where a is the mean radius of the Earth (6371.2 km), (r, θ, φ) are geographic spherical polar coordinates, and Y^m_n and P^m_n are the Schmidt normalized surface spherical harmonic and associated Legendre function of degree n and order m, respectively. The γ^m_n are unique complex expansion (Gauss) coefficients. They are related to the usual real Gauss coefficients g^m_n and h^m_n according to $\gamma^m_n = g^m_n - ih^m_n$. The degree truncation level for CM3 is set at $N_{max} = 65$.

The main field is dominated by contributions from the core. Dynamo action means the main field varies on the order of centuries. This secular variation is parameterised using cubic B-splines (b^k_q):

$$\frac{d\gamma^m_n(t)}{dt} = \sum_{q=1}^{h+k} \gamma^m_{nq} b^k_q(t)$$

leading to:

$$\gamma^m_n(t) = \gamma^m_n(e) + \sum_{q=1}^{h+k} \gamma^m_{nq} \int_e^t b^k_q(\tau) d\tau$$

Where k=4, and e (the epoch or expansion point for the series) = 1980; the γ^m_n are the unique complex coefficients of the series. The time span of the model was 1960-1985, allowing for an extension at either end of the satellite missions. The spline knot set was defined at 2.5 yr intervals for all γ^m_n (t), this results in h = 9 and h + k = 13 cubic B-splines per γ^m_n (t). The final expression for the core and lithospheric potential is:

$$V = \Re \left\{ a \sum_{n=1}^{13} \sum_{m=0}^{n} \sum_{q=0}^{13} \left(\frac{a}{r}\right)^{n+1} \gamma^m_{nq} Y^m_{nq} + a \sum_{n=14}^{65} \sum_{m=0}^{n} \left(\frac{a}{r}\right)^{n+1} \gamma^m_n Y^m_n \right\}$$

Ionospheric field

The morphology of geomagnetic variations produced by the ionospheric dynamo is relatively fixed in magnetic local time. However, variation occurs by season, solar cycle, interactions with Earth's main field, etc. It is assumed that primary currents flow horizontally in the E-region at 110 km altitude. The basis functions representing the ionospheric and associated induced potentials are made of a set of potential functions reflecting a single spatial harmonic modulated by single seasonal and diurnal periods. For the region between the Earth's surface, r = a, and the location of the ionospheric equivalent current sheet, r = a + h, these have the form:

$$V_{nsp}^{m} = \Re \left\{ a \left[\iota_{nsp}^{m} \left(\frac{a}{r} \right)^{n+1} + \epsilon_{nsp}^{m} \left(\frac{r}{a} \right)^{n} \right] P_{n}^{m}(\theta_d) \exp i(m\phi_d + \omega_s st + \omega_p pt_m) \right\}$$

where θ_d and φ_d are dipole colatitude and longitude. The fundamental seasonal angular frequency is $\omega_s = 2\pi$ rads/yr with associated wavenumber s and time of year t counted from January 1, 00 UT. The fundamental diurnal angular frequency is $\omega_p = 2\pi/24$ rads/hr with associated wavenumber p and magnetic universal time (MUT) t_m. The ϵ^m_{nsp} and ι^m_{nsp} are unique complex expansion coefficients of the external ionospheric (ϵ) and the internal induced (ι) potentials, respectively. The magnetic local time, t_{mlt}, of an observer is defined as:

$t_{mlt} = (180^o + \varphi_{d;o} - \varphi_{d;s})/15$

where if the dipole longitude of the observer, $\varphi_{d;o}$, and the sub-solar point, $\varphi_{d;s}$, are in degrees, t_{mlt} is in hours. Dipole longitude is measured in the dipole equatorial plane in a positive sense from a line extending from Earth's centre into the half-plane defined by the dipole and geographic axes and containing the south geographic pole. The tilted dipole with north magnetic dipole position ($\theta = 11.2^o$; $\varphi = 289.3^o$), is used to assign dipole longitudes to this data. The magnetic universal time is defined as the MLT of the dipole prime meridian. Hence, it is given by:

$t_m = (180^o - \varphi_{d;s})/15$

where $\varphi_{d;o}$ is now zero.

$\underline{\iota}$ is in general not independent of $\underline{\epsilon}$. The nature of this dependence is related to the conductivity structure of the lithosphere, which leads to the relationship:

$\underline{\iota} = Q\underline{\epsilon}$

where Q is a complex matrix representation of the transfer function between the ionospheric signal and the induced signal. CM3 adopts a one-dimensional radially varying conductivity distribution; a four-layer model derived from Sq and Dst data at selected European observatories. Q then depends only upon n and the frequency f.

Many ionospheric phenomena are organized with respect to the geomagnetic field. Therefore, ionospheric conductivity is highly anisotropic, and "Quasi-Dipole" (QD) coordinates (θ_q; φ_q) are used, in the form of two-dimensional QD symmetry, on a constant-coordinate sphere. The reference model used to define the QD coordinate system for CM3 is IGRF 1980. A set of "elemental" potential functions, may be defined, such that:

$$\begin{aligned} V_{sp} &= \Re\left\{\underline{\tilde{\epsilon}}^H \underline{T}_e + \underline{\tilde{\iota}}^H \underline{T}_i\right\} \\ &= \Re\left\{\underline{\tilde{\epsilon}}^H D^H U_e \underline{S}_e + \underline{\tilde{\iota}}^H D^H U_i \underline{S}_i\right\} \\ &= \Re\left\{\underline{\tilde{\epsilon}}^H D_e^H \underline{S}_e + \underline{\tilde{\iota}}^H D_i^H \underline{S}_i\right\} \end{aligned}$$

Where $\underline{\tilde{\epsilon}}$ and $\underline{\tilde{\iota}}$ are the vectors of $(\underline{\tilde{\epsilon}}\ ^{l}_{ksp})^*$ and $(\underline{\tilde{\iota}}\ ^{l}_{ksp})^*$, $\underline{T}_e$ and $\underline{T}_i$ are the vectors of $T^{l}_{ksp;e}$ and $T^{l}_{ksp;I}$, D is the matrix of d^{lm}_{kn} regression coefficients, and U_e and U_i are real matrix representations of the upward-continuation operators for external and internal fields. Se and Si are vectors with elements:

$$\begin{aligned} S^m_{nsp,e} &= a\left(\frac{r}{a}\right)^n P_n^m(\theta_d)\exp i(m\phi_d + \omega_s s t + \omega_p p t_m) \\ S^m_{nsp,i} &= a\left(\frac{a}{r}\right)^{n+1} P_n^m(\theta_d)\exp i(m\phi_d + \omega_s s t + \omega_p p t_m) \end{aligned}$$

Imposing QD symmetry at r = a + h imposes a linear constraint on the original expansion coefficients:

$\underline{\epsilon} = D_e \underline{\tilde{\epsilon}}$

$\underline{\iota} = D_i \underline{\tilde{\iota}}$

Many satellite measurements are made in the region a + h < r, so the ionospheric and associated induced potentials must be defined here. The ionosphere is now internal to the measurement region:

$\underline{\epsilon}' = D_e \underline{\tilde{\epsilon}}'$

$\underline{\iota} = D_i \underline{\tilde{\iota}}$

The ionospheric potentials above and below the sheet source are not independent because the radial components of the resulting fields are continuous across the sheet. A linear relationship is implied:

$$\underline{\epsilon}' = C\underline{\epsilon}$$

Solving for $\underline{\epsilon}$, $\underline{\epsilon}$' and $\underline{\iota}$ in terms of $\underline{\tilde{\epsilon}}$:

$$\begin{aligned} \underline{\iota} &= QD_e\underline{\tilde{\epsilon}} \qquad \underline{\epsilon}' &= CD_e\underline{\tilde{\epsilon}} \\ &= F\underline{\tilde{\epsilon}} &= G\underline{\tilde{\epsilon}} \end{aligned}$$

Solar flux is used for describing the short term variability of solar activity. The ionospheric expansion coefficients have a linear functional dependence on the F10.7 index:

$\tilde{\epsilon}^{l}_{ksp} = \tilde{\varepsilon}^{l}_{ksp} \cdot (1 + N \cdot F10.7)$

N is not solved for; an *a priori* value is used, which is assumed to be equal for all coefficients. This means that increasing solar flux inflates the whole ionospheric current system without changing its shape. Correlation between annual means of $|\epsilon^1_2|$, the amplitude of the diurnal main term, and solar flux F10.7 yields $N = 14.85 \cdot 10^{-3}$ $[10^{-22}$ W/m^2/Hz$]^{-1}$ with correlation coefficient of r = 0:991. If $\alpha = (1+N \cdot F10.7)$, then the previous equation may be written in matrix notation as:

$\underline{\tilde{\epsilon}} = \alpha\underline{\tilde{\varepsilon}}$

This gives the final potential forms for the ionospheric and associated induced potentials:

$$\begin{aligned} V_{sp} &= \Re\left\{\underline{\tilde{\varepsilon}}^H \left(D_e^H \underline{S}_e + F^H \underline{S}_i\right)\right\} \\ V'_{sp} &= \Re\left\{\underline{\tilde{\varepsilon}}^H \left(G^H + F^H\right) \underline{S}_i\right\} \end{aligned}$$

where the scalar α has been subsumed by the matrices.

Finally, basis functions are selected, defining the expansion limits for s, p, k, l, n, and m. Given the temporal distribution of the magnetic measurements to be analysed, the 24 hr, 12 hr, 8 hr, and 6 hr periods can probably be resolved.

Expressions for the ionospheric and associated induced potentials for the regions $a \leq r \leq a + h$ and $a + h < r$ in explicit summation notation:

$$V = \Re \left\{ \sum_{s=-2}^{2} \sum_{p=0}^{4} \sum_{l=p-1}^{p+1} \sum_{k=\max(1,|l|)}^{|l|+40} \tilde{\varepsilon}^{l}_{ksp} \cdot \sum_{n=1}^{60} \sum_{m=-\min(n,12)}^{\min(n,12)} \left[(d^{lm}_{kn,e})^{*} S^{m}_{nsp,e} + (f^{lm}_{knsp})^{*} S^{m}_{nsp,i} \right] \right\}$$

$$V' = \Re \left\{ \sum_{s=-2}^{2} \sum_{p=0}^{4} \sum_{l=p-1}^{p+1} \sum_{k=\max(1,|l|)}^{|l|+40} \tilde{\varepsilon}^{l}_{ksp} \cdot \sum_{n=1}^{60} \sum_{m=-\min(n,12)}^{\min(n,12)} \left[(g^{lm}_{kn})^{*} + (f^{lm}_{knsp})^{*} \right] S^{m}_{nsp,i} \right\}$$

where $d^{lm}_{kn;e}$, g^{lm}_{kn}, and f^{lm}_{knsp} are elements of D_e, G, and F-type matrices, respectively.

Magnetospheric field

The magnetospheric field can also be represented by the gradient of a potential function. The form and development of this function closely parallel the ionosphere and associated induced fields for the region $r \leq a + h$.

A major source of the magnetospheric field is the ring-current. The resultant field contribution near-Earth is dominated by a simple external dipole. The temporal variation of this field, however, is not simple; exhibiting power across broad frequency ranges. The available measurements cannot resolve a high-precision parameterization of such variations. The desired variation is built into the temporal portion of the basis functions. Given that Dst is a relative measure of disturbance, for the source expansion coefficients, ϵ^{m}_{nsp}:

$\epsilon^{m}_{1sp} = \mu^{m}_{1sp} + \mu^{m}_{1sp,\,Dst} \cdot Dst(t)$

where the Dst index is in units of nT and is tabulated at hourly intervals as a function of universal time. This relationship is adopted only for the dipole terms (n = 1), and the temporal variability of Dst(t) is modulated by both seasonal and diurnal oscillations. Induced fields may be treated as in the ionospheric field. The major difference is the inclusion of basis functions which are dependent upon the modulated Dst(t) index.

At the source region for magnetospheric current systems the Earth's magnetic field is more dipole-like compared to ionospheric current systems thus for this part of the model:

$D_e = I$

$F = Q$

An expression for magnetospheric and associated induced potentials for observatory and satellite data with Dst dependent terms broken out:

$$V = \Re \left\{ \sum_{s=-2}^{2} \sum_{p=0}^{5} \sum_{l=p-1}^{p+1} \sum_{k=\max(1,|l|)}^{|l|+K(p-l)} \mu_{ksp}^{l} \left[S_{ksp,e}^{l} + (q_{kksp}^{ll})^{*} S_{ksp,i}^{l} \right] + \sum_{s=-2}^{2} \sum_{p=0}^{5} \sum_{l=p-1}^{p+1} \sum_{k=\max(1,|l|)}^{1} \mu_{ksp,D_{st}}^{l} \cdot D_{st} \left[S_{ksp,e}^{l} + (q_{kksp,D_{st}}^{ll})^{*} S_{ksp,i}^{l} \right] \right\}$$

Ionospheric coupling currents

When establishing the basis functions used to represent ionospheric fields, it was assumed that source currents flowed entirely below the satellite sampling shells, and a relationship was assumed between the fields from these currents based on an equivalent sheet current. If displacement currents are neglected, then the source currents are solenoidal, and these assumptions may be used for current loops which do not pierce the sampling shell (true for the E-region). However, these ionospheric currents are coupled to the magnetospheric and ionospheric E-region currents. This means that the Magsat sampling region between a + 350 km and a + 550 km is penetrated by F-region currents. For the Magsat sampling shell, this approximation is adopted:

$\delta \underline{B} = \nabla \times \underline{r}\varphi$

with associated current:

$\mu_0 J = \nabla \times \nabla \times \underline{r}\varphi$

The working form of the stream function for the toroidal field due to F-region coupling currents in Magsat sampling region:

$$\Phi = \Re \left\{ \sum_{s=0}^{2} \sum_{k=1}^{40} \sum_{l=0}^{\min(k,4)} \tilde{\phi}_{ks}^{l} \sum_{n=1}^{60} \sum_{m=-\min(n,12)}^{\min(n,12)} (d_{kn,j}^{lm})^{*} S_{ns,j}^{m} \right\}$$

Estimation of model parameters

Since CM3 is solving an inverse problem without a unique solution, and the scalar data are non-linear functions of the model parameters, an iterative least-squares estimator (Gauss method) was used for determining the model. The Gauss estimator allows introduction of additional metrics or norms. These are of two natures: first, regularising the solution; and second, allowing soft physical bounds to be placed upon the model parameter space.

The first norm $Q_{|\underline{J}_{eq}|}$, measures the mean-square magnitude of $\underline{J}_{eq}$ on a spherical region, Ωs, fixed in dipole magnetic local time longitude, defined as $t_{mlt} = \varphi_d + \Omega_p t_m$, over time; this adjusts for the diminished nightside ionospheric E-region conductivity, at mid and low latitudes:

$Q_{|\underline{J}_{eq}|} = \underline{\tilde{e}}^{T} \Lambda_{|\underline{J}_{eq}|} \underline{\tilde{e}}$

where $\Lambda_{|\underline{J}_{eq}|}$ is a real, positive-definite, symmetric matrix representation of the norm. Integration is facilitated by three assumptions: first, the F10.7 index does not vary with time- $\underline{J}_{eq}$ is periodic such that T = 1 yr; secondly, universal time t is treated as magnetic universal time t_m; and thirdly, $\omega_p = 365\omega_s$. The second assumption is best at low and mid latitudes, and the third during non-leap years. The $Q_{|\underline{J}_{eq}|}$ norm works to establish a nightside baseline minimising $\underline{J}_{eq}$. This baseline is a global function, able to adjust to geographic shifts, which varies with season, but not diurnally. Because

there is difficulty in separating this behaviour from secular variation at satellite altitude, the strength of the norm is adjusted via $\lambda_{|\underline{J}_{eq}|}$ such that all p = 0 terms are determined by the norm. This also means the influence of the norm cannot be greatly reduced in polar regions where $\underline{J}_{eq}$ is thought to flow at all magnetic local times. The influence of $Q_{|\underline{J}_{eq}|}$ is limited to magnetic local times of 21 hr - 5 hr. An additional norm is used to minimize roughness on the dayside. This norm, $Q_{|\nabla^2_s \underline{J}_{eq;p>0}|}$, is a quadratic function of $\underline{\tilde{e}}_{p>0}$ which measures the weighted mean square magnitude of the surface Laplacian of $\underline{J}_{eq;p>0}$ on a sphere, Ω, over time:

$$Q_{|\nabla_s^2 \underline{J}_{eq,p>0}|} = \underline{\tilde{e}}_{p>0}^T \Lambda_{|\nabla_s^2 \underline{J}_{eq,p>0}|} \underline{\tilde{e}}_{p>0}$$

where $\Lambda_{|\nabla^2_s \underline{J}_{eq;p>0}|}$, is a real, positive-definite, symmetric matrix representation of the norm.

The surface Laplacian operator multiplies $S^m{}_{nsp;e}\,|_{r=a+h}$ by a factor of -n(n+1), and so $Q_{|\nabla^2_s \underline{J}_{eq;p>0}|}$damps the higher degree harmonics much more severely than $Q_{|\underline{J}_{eq}|}$.

The magnetospheric field expansion includes many more coefficients than can be reliably estimated from the data. Earlier phases of modeling suggested that excessive cross-talk or correlations between the ionospheric and non-Dst dependent magnetospheric expansions would exist due to poor field separation. A reduction of this coupling is achieved by $Q_{|\Delta \underline{B}_{ltd}|}$, which measures the mean-square magnitude of deviations from a dipole in magnetic local time, independent of Dst on a Magsat altitude sphere ($r = a + h_m$ with h_m = 450 km), Ω, over time:

$$Q_{|\Delta \underline{B}_{ltd}|} = \underline{u}^T \Lambda_{|\Delta \underline{B}_{ltd}|} \underline{u}$$

where $\Lambda_{|\Delta \underline{Q}|}$ is a real, positive-definite, diagonal matrix representation of the norm.

The inclination of the Magsat orbit meant no data were acquired within a cap of half-angle of about 7^o centred on the geographic poles. This, and the fact J_r is expressed in dipole coordinates, makes damping polar regions a necessity. EEJ coupling currents are present at dusk along the dip equator, but including an influence function which is small only at low dipole latitudes is complicated, and

so omitted. $Q_{|J_r|}$ measures the mean-square magnitude of J_r on a Magsat altitude sphere ($r = a + h_m$ with $h_m = 450$ km), Ω, over time:

$$\mathcal{Q}_{|J_r|} = \underline{\tilde{w}}^T \Lambda_{|J_r|} \underline{\tilde{w}}$$

$$\underline{\tilde{w}} = \begin{pmatrix} \Re\left\{\underline{\tilde{\phi}}\right\} \\ \Im\left\{\underline{\tilde{\phi}}\right\} \end{pmatrix}$$

The $\Lambda_{|J_r|}$ matrix is real, positive-definite, and symmetric. Because J_r has a period of one year, T = 1 yr. There are separate $Q_{|J_r|}$ for dawn and dusk.

1.3.3 CM4

CM4 (Sabaka et al 2004)

As CM4 is an extension of CM3, many of the data are common to both. CM3 incorporated observatory hourly means (OHMs) for the quietest day of the month, as determined by Kp, at two sampling rates: (i) the OHM values closest to 01:00 local time for 1960–1985, denoted as OHM 1AM, and (ii) OHMs every 2 hr on quiet days during the POGO and Magsat mission envelopes, denoted as OHM MUL. For CM4, the OHM values closest to 01:00 local time on the quietest day per month were extended through 2000.

The POGO and Magsat scalar data sets are identical to those used in CM3. The Magsat vector data have been reselected for denser coverage. They have 20 arcsec accuracy per attitude flags during quiet conditions in which Kp ≤ 1o for the time of observation and Kp ≤ 2o for the previous 3-hr interval. The data were decimated from the original 16 Hz to 1 min^{-1}. Ørsted and CHAMP data were selected for quiet conditions where Kp ≤ 1+ for the time of observation and Kp ≤ 2o for the previous 3-hr interval. In addition, the Dst index was required to be within ±20nT. The Ørsted data span 03/1999 to 07/2002, while the CHAMP data span 08/2000 to 07/2002. During this period both satellite orbits precessed through all local times. The Ørsted dawn and dusk data are few, but complemented by Magsat data; there is a general lack of northern autumn data. Vector and scalar data were used at all latitudes at a sampling rate of 1 min^{-1} and all satellite data were weighted

proportional to sin θ (where θ is geographic colatitude) to simulate an equal-area distribution. To limit outliers, satellite data were initially culled according to their residuals with respect to CM3.

Modified Parametrization

The parametrization of field sources in CM4 closely follows CM3. The core and lithospheric fields are expressed as the negative gradient of a potential function represented by a degree and order 65 internal spherical harmonic expansion in geographic coordinates, with SV represented by cubic B-splines through degree and order 13. The knot spacing was kept at 2.5 yr and extended through mid-2002. Because Observatory Hourly Means are direct measurements of the field, and their close proximity to lithospheric and induced sources, a set of static vector biases is solved for each station. These effectively remove a weighted mean from the OHM residuals at each station. Separate biases are determined for each type of OHM data (two types of OHM data are used, OHM_1AM, the values closest to 01:00 hours 1960-1985, and OHM_MUL, values every two hours on quiet days during the POGO and Magsat missions).

The currents responsible for the ionospheric field are considered to flow in a thin spherical shell at h = 110 km altitude. This field is thus expressed as the negative gradient of a potential function at surface and satellites altitudes and is constrained to have radial continuity across the current sheet. The ionospheric parametrization employs harmonic functions with QD coordinate symmetry, which is aligned with the ambient magnetic field. These functions are mainly sun-synchronous in time, but slightly slower and faster modes are also present with a minimum period of 6 hr, and are modulated with annual and semi-annual seasonal variability. Spatially, they have high QD latitudinal resolution in order to model the equatorial electrojet. Induced contributions are accounted for using a four layer, 1-D, radially varying conductivity model derived from Sq and Dst data at selected European observatories, as for CM3. The influence of solar activity is represented by an amplification factor, assumed equal for all harmonics, which is a function of F10.7 values. Near the Earth, the field is cast as the negative gradient of a potential function represented by an external SH expansion in dipole coordinates, which has regular daily and seasonal periodicities. Ring current variability is modelled as a linear function of the Dst index for external dipole terms only. Provisional Dst has been used during and after 2001. The induced contributions of the magnetosphere are treated in a similar manner as the ionosphere and thus coupled with an internal SH expansion via the same conductivity model.

F-region currents

Magsat and Ørsted sample the magnetic field in thin shells centred roughly at 400 and 750 km altitude, respectively. Consequently, these measurements contain contributions from toroidal magnetic fields as a result of poloidal F-region currents **J**, which couple the ionospheric E region and magnetosphere. This field is not curl-free and cannot be expressed as the gradient of a potential. In CM3, which analysed Magsat vector data only, these coupling currents were assumed to be purely radial and were only sampled at two local times. For CM4 **J** is considered QD meridional. Because Ørsted sampled all local times, a continuous diurnal representation is attempted for toroidal **B** in the Ørsted shell. The toroidal **B** and associated poloidal **J** may be expressed in spherical coordinates (r, θ, φ) as

$$\mathbf{B} = \begin{pmatrix} 0 \\ \frac{1}{\sin\theta}\frac{\partial}{\partial\phi}\Phi \\ -\frac{\partial}{\partial\theta}\Phi \end{pmatrix},$$

$$\mathbf{J} = \begin{pmatrix} -\Delta_s(r\Phi) \\ \frac{1}{r}\frac{\partial}{\partial\theta}(r\Phi)' \\ \frac{1}{r\sin\theta}\frac{\partial}{\partial\phi}(r\Phi)' \end{pmatrix}\frac{1}{\mu_0},$$

where Δ_s is the angular part of the Laplacian, the prime indicates differentiation in r and φ is the toroidal scalar function

$$\Phi(t, \mathbf{r}) = \Re\left\{\sum_{n,m,s,p} \phi^m_{nsp}(r) T^m_{nsp}(t, \theta_q, \phi_q)\right\}.$$

The $\Re\{\cdot\}$ operator used here takes the real part of the complex expression and

$$\begin{aligned} T^m_{nsp}(t, \theta_q, \phi_q) = {} & Y^m_n(\theta_q, \phi_q) \\ & \times \exp is\phi_s(t) \\ & \times \exp ip\phi_p(t_{mut}(t)) \end{aligned}$$

are the QD symmetric basis functions. $Y^m{}_n(\theta_q, \varphi_q)$ is the Schmidt quasi-normalized surface SH function of degree n and order m evaluated at QD coordinates $(\theta_q(\theta, \varphi), \varphi_q(\theta, \varphi))$, but these may be expanded in terms of $Y^k{}_l(\theta, \varphi)$ via spherical transforms. Thus, $T^m{}_{nsp}$ is QD symmetric on a particular reference sphere and is simply a linear combination of the $Y^k{}_l$ over k and l, modulated by periodic time functions in QD longitude φ_q. The arguments of these time functions include s and p, which are the seasonal and diurnal integer wave numbers, respectively, the seasonal time angle φ_s,

which has a period of 1 yr and is a function of universal time (UT) t, and the diurnal time angle φ_p, which has a period of 24 hr and is a function of magnetic universal time (MUT) t_{mut}. The MUT of an observer is closely related to the observer's magnetic local time (MLT) t_{mlt} defined as $t_{mlt}(t) = (180^o + \varphi_{d,o} - \varphi_{d,s}(t))/15$ where, if the dipole longitude of the observer, $\varphi_{d,o}$, and the sub-solar point, $\varphi_{d,s}(t)$, are in degrees, then $t_{mlt}(t)$ is in hours. Thus, MUT is simply the MLT at the dipole prime meridian ($\varphi_{d,o} = 0^o$), which runs roughly through central South America. In CM3, the radial dependence of φ was chosen to be 1/r, which leads to $J_\theta = J_\varphi = 0$. To obtain QD meridional **J**, one selects from two classes of admissible φ: (i) those with a radial dependence of 1/r and (ii) those that are QD zonal, i.e. m = 0. Only this second class will contribute to the horizontal portion of the currents $\mathbf{J}_h = (J_\theta, J_\varphi)^T$, where the ^{T} denotes transposition. The component of $\mathbf{J}_h$ denoted $J_{\theta q}$ lies in QD meridional planes. The φ parametrizations used for Magsat dawn and dusk are

$$\Phi(t,\mathbf{r}) = \Re\left\{\sum_{s=0}^{2}\sum_{n=1}^{40}\sum_{m=0}^{\min(n,4)}\phi^m_{ns00}T^m_{ns0}(t,\theta,\phi) + \sum_{s=0}^{2}\sum_{n=1}^{40}\rho\phi^0_{ns01}T^0_{ns0}(t,\theta,\phi)\right\}\left(\frac{R}{r}\right)$$

where b = 6801.2 km for dawn and b = 6786.2 km for dusk and R = 6371.2 km for both. As with CM3, the seasonal phase angle is fixed as a result of the limited seasonal coverage of Magsat. This results in retaining only terms in cos $s\varphi_s(t)$, giving a total of 1164 coefficients in each expansion.

For Ørsted, the φ parametrization used is

$$\Phi(t,\mathbf{r}) = \Re\left\{\sum_{s=-2}^{2}\sum_{p=0}^{4}\sum_{m=p-1}^{p+1}\sum_{n=\max(1,|n|)}^{|n|+40}\phi^m_{nsp0}T^m_{nsp}(t,\theta,\phi) + \sum_{s=-2}^{2}\sum_{p=0}^{4}\sum_{n=1}^{40}\rho\phi^0_{nsp1}T^0_{nsp}(t,\theta,\phi)\right\}\left(\frac{R}{r}\right)$$

where now b = 7121.2 km and R = 6371.2 km. The second term, describing $\mathbf{J}_h$, only contains terms with m = 0, whereas the first terms allows for more variability with m. The total number of coefficients in the expansion is 6120. These ranges on s, p, n and m were chosen to match those of the ionospheric E-region, which it couples, because Ørsted vector data give full local time coverage.

Estimation Procedure

The iteratively reweighted least-squares (IRLS) approach with Huber weights is employed. Large residuals are treated as Laplacian to avoid unduly influencing the parameter estimate. The starting model was CM3 or zero for new parameters.

Regularization and *a priori* information

In addition to magnetic field observations, information has been introduced either to restrict the set of admissible parameter estimates as a result of insufficient data (regularization) or, for external fields, to impart some physical knowledge to the problem that is otherwise not supplied. With the exception of F-region currents, is the same as in CM3. Main field SV is smoothed by two norms: the mean-square magnitude of $\ddot{B}_r$ over the core– mantle boundary (CMB) over the span of the model, $Q_{|\ddot{B}_r|}$, and the mean-square magnitude of the surface Laplacian of $\dot{B}_r$, $Q_{|\nabla^2_h \dot{B}_r|}$. Night-side ionospheric E-region currents are minimized by $Q_{|\mathbf{J}_{eq}|}$ which measures the mean-square magnitude of the E-region equivalent currents, $\mathbf{J}_{eq}$, flowing at 110 km altitude over the night-time sector through the year. In addition, these are further smoothed by $Q_{|\nabla^2_s \mathbf{J}_{eq,p>0}|}$ which measures the mean-square magnitude of the surface Laplacian of the diurnally varying portion of $\mathbf{J}_{eq}$ at mid-latitudes at all local times. In the magnetosphere, the mean-squared magnitude of deviations from a dipole field in MLT is damped at Magsat altitude (450 km), independent of Dst. For CM3, the mean-square magnitude of the radial F-region currents were minimized at Magsat altitude at dawn and dusk. For CM4, the mean-square magnitude of the surface Laplacian of J_r ($Q_{|\nabla^2_h J_r|}$) and $\mathbf{J}_h$ ($Q_{|\nabla^2_h \mathbf{J}_h|}$) were damped separately. The damping was on spheres at 430 and 415 km for Magsat dawn and dusk, respectively, and at 750 km for Ørsted. In addition, because Ørsted samples continuous diurnal variations, the weighted mean-square magnitude of J_r was damped over the same night-time sector used in $Q_{|\mathbf{J}_{eq}|}$ in order to stabilize meridional coupling currents associated with the EEJ and allow coupling currents to still flow via $\mathbf{J}_h$ ($Q_{|J_r|}$). The function $\sin^8\theta_d$, where θ_d is the dipole colatitude, was used to weight the norm more heavily at low and mid-dipole latitudes.

1.3.4 Assumptions and potential failings in the models

Data used in the parametrisation of the CM3 and CM4 models is chosen within a range of Kp to preferentially use days of low activity, unless lack of geographic coverage requires the use of more disturbed times. For CM4, the data is resampled and weighted to simulate equal area coverage.

Magsat vector data is not used for polar regions, to avoid auroral current systems, and due to the lack of coverage (both a physical gap in coverage, and only sampling certain times). This necessitates damping of the polar data. The auroral electrojet is not modelled.

Where CM3 assumed ionospheric currents were radial only (which fails at mid latitudes), CM4 models them as QD meridional, and attempts to represent them continuously, as Ørsted samples all local times. Ionospheric currents are assumed to flow below the satellite sampling region, at 110km altitude, and the relationship between the internal and external fields is based on an equivalent sheet current. Coupling currents associated with the EEJ are either ignored, or in the case of Ørsted, the data is damped to stabilise the model in this region.

Solar activity is based on F10.7 data, and is assumed to amplify all harmonics equally, treated as inflating the ionosphere with no change in shape. Maximum amplitudes of temporal variation in the external fields are fixed to the solstices and equinoxes. Dst is used to model temporal variations in the magnetosphere, which are assumed to have periods of a few days. The models are smoothed to ensure ionospheric conductivity is lowest at night time, and periodic over 1 year. This does not work so well over the poles, due to the presence of currents flowing at all local times. Ring current variability is included in CM4 as a linear function of Dst, for the external dipole terms only.

Errors are assumed to be uncorrelated for scalar and observatory data; vector satellite data contains correlated errors, which are well defined for Ørsted, but less so for Magsat.

The same starting model is used for all parts of the model, before using least squares methods. An *a priori* 4-layer, 1D conductivity model is used, based on data from European observatories, in which conductivity varies only with radius. Fields generated by tidal motion are not modelled.

These assumptions and noted difficulties suggest that CM4 will not work as well for high activity periods (since its parametrisation is based mainly on low activity data), may fail over high latitudes (since there is a lack of coverage of all time periods and a certain amount of damping due to both this and the auroral current systems), and may have issues with atmospheric current systems (due to damping of data containing them, not modelling some coupling currents, smoothing of temporal

variations, and fixed locations for the currents in the model). The initial conductivity model may also lead to errors or poor performance, since it only varies radially, and is based on European data. In this work then, we test the model and its limitations to determine if these failings are indeed present, and how extensive they are.

1.4 Magnetic Surveying

1.4.1 Surveying Methods

Magnetic surveys are conducted using magnetometers which may be carried either by people or vehicles. In the case of smaller scale surveys, continuous or closely spaced discreet readings of magnetic field intensity and/or direction can be recorded by a human operator carrying a small magnetometer. In the case of larger surveys, magnetometers are mounted on ships or planes, which give them several advantages in acquiring data in areas that might otherwise be inaccessible. Unlike seismic or similar methods, magnetic surveys do not require contact with the ground surface, or a network of fixed receiver/observation stations, and particularly in the case of airborne surveys, can be conducted over areas which are prohibitively large to survey on foot, or are inaccessible to other vehicles. Airborne surveys can be completed very quickly, and ship-borne surveys can be conducted at the same time as (for example) seismic surveys, or combined gravity/magnetic survey schemes. In the case of dual survey types, this means that not only is there a larger amount of data collected with only a slight increase in 'work' or expenditure, but this also gains the benefit of surveying the same thing with two geophysical methods, allowing an additional constraint on interpretation, and reducing the non-uniqueness of inverse problems.

Magnetic surveys should generally be planned to extend beyond the area of interest to at least the maximum depth of the target anomaly, and measurements should be spaced closer together than the expected minimum depth of the anomaly (based on the assumption that the field due to an anomaly falls to around 10% of its total strength at a distance similar to the depth of the centre of the anomaly). The precise pattern and location of measurements will of course depend on the nature of the terrain and the target. As much noise as possible is excluded by designing the survey with this in mind – obvious magnetic objects such as power cables or barbed wire fences are avoided; sensors can be raised to avoid ferrous soil content. The major consideration however, is the removal of temporal magnetic variations – mainly, Sq variations. Sq tends to fall in the range of 10-40nT over

the course of a day, which can be a similar value to the survey target, which for exploration industry may be anomalies of tens to hundreds of nT (metal near the surface may result in much higher anomalies). This is done by monitoring and recording the ambient field, and later removing that variation from survey data. This is a base station correction, or remote referencing. The aim is to remove all variations which are common to both locations. If this correction works in an ideal manner, all which is left in the survey data is the changes in the magnetic field due to the local geology. This may be done by re-recording the values at a given location at consistent time periods, by returning to a particular point, by crossing survey lines so tie points are created, or (particularly for large surveys where returning to locations would be difficult or time consuming) by using a base station, which will constantly record the temporal variation of the field. The base station may be one of the magnetic observatories, or if an observatory is not conveniently located, a magnetometer set up in a location specifically to record data as a correction for the survey. Base stations should be located away from ferrous material, and high magnetic gradients, able to be re-occupied to check for instrument drift, and within a few tens of kilometres of the survey. During quiet periods, especially at night, the temporal variation in the field is likely to be (much) less than 10 nT/hour, so can be sampled less often. During periods of high activity, this may reach hundreds of nT in the space of a few minutes. The frequency of sampling of the varying field therefore should increase with the activity levels, but times of particularly rapid variation may prevent accurate measurement and correction. (Hinze et al 2013, Gambetta et al 2007, Reeves 2005, Milson 2003).

1.4.2 Problems with Remote Referencing

There are several reasons why the ideal situation may not be the case when remote referencing surveys. If the base and survey locations are too far apart (not within a few tens of kilometres, or closer depending on the local conditions) the field may behave differently – particularly if they are at different magnetic latitudes. One area may be affected by strongly localised effects, either spatially or temporally, such as the coast effect, or the effect of the auroral or equatorial electrojets. They may also be affected by short-period features differently, as there may be a lag, or features may be exaggerated or damped by local effects. If the locations contain very different geology, the base correction may not be at an appropriate level, due to varying conductivity or magnetic mineral content. Changes of this type may potentially require an additional correction to account for an overall increased or decreased magnetic intensity in the region (Hinze et al 2013).
If this correction can be improved, then the quality of data for surveys can be improved. This has

benefits in that

1) Smaller scale features may be able to be interpreted, allowing more potential exploration targets to be seen.

2) 'Ghost' anomalies due to under-correction, over-correction, or noise, can be better corrected for, and so removed, reducing the risk of misidentification.

3) The overall level of noise and unusable data can be reduced.

4) The times where data can be used may be able to be extended, so allowing surveys to be carried out in conditions (such as non-solar quiet days) that might otherwise prevent them.

All these benefits may be summed up as improving data quality, extending useful conditions, and reducing noise. This allows better understanding of the survey area, but is also a financial gain – less data is unusable, less potential missing of targets or beginning exploration of an area with no viable targets. This is of course to the advantage of all concerned, particularly if corrections can be made with the minimum amount of extra effort in terms of time or computing power.

Disturbances in the behaviour of the geomagnetic field, such as geomagnetic storms, are also of particular importance in the collection of survey data, since they may produce features of much larger amplitudes than both normal Sq variations and the anomalies which are the target of the survey. Storm times generally are considered unsuitable for magnetic surveys (although they can be used for magnetotelluric work, since magnetotellurics depends on naturally occurring currents, which are enhanced by increased magnetic activity). The amount of disturbance that can be worked with is potentially critical to the success of a survey – if only low levels of disturbance can be corrected and interpreted, then the times that data can be used in are greatly reduced. Improving the correction to allow times of greater disturbance to be corrected for then allows more data to be used from a given survey. Since large geomagnetic storms also pose threats to satellites, and potentially to large infrastructure, they are monitored, and when conditions that may produce a storm are spotted, they are publicised. This can help avoid wasting effort collecting magnetic survey data during these periods, however since there is only a short warning period, storms are still likely to result in the loss of survey time.

1.4.3 Survey Data

Survey data, and observatory data may be recorded in several different ways. The most common records the intensity of the field in the three orthogonal component directions – north, east and vertical (X, Y and Z, respectively). This may also, particularly in older records, be seen as DHZ, which records the horizontal magnitude, the declination (the eastward angular direction of the

horizontal component from geographic north) and the vertical component (these are orthogonal components in a different reference frame). Both systems are representations of the F value- the total field intensity and direction. The two may be converted;

$$X= H \cos(D), Y= H \sin(D)$$

F may be found by

$$F=\sqrt{(X^2+Y^2+Z^2)} =\sqrt{(H^2+Z^2)}$$

Some surveys record data in three components, much as the observatory stations do. However, many record only F (total field) intensity values, so to compare the two, the three component data must be converted to F values.

1.4.4 Magnetometers

The two basic types of magnetometer are the vector and scalar. Vector magnetometers measure vector components of the field – giving a magnitude and direction, while scalar magnetometers measure only the magnitude or total strength of the field. Generally, proton magnetometers are used, which are absolute, where the data recorded is calibrated to physical properties of the instrument, to give an absolute value; Scalar magnetometers may be relative (also called variometers), where the data is referenced to a fixed base, and requires calibration from another source (Milsom 2003). Magnetometers may also be classified based on intended use, e.g. stationary, mobile etc. The most commonly used magnetometers for geophysical surveying are fluxgate and proton precession magnetometers.

Scalar magnetometers

- Proton precession magnetometer
- Overhauser magnetometer
- Vapour magnetometers

Vector magnetometers

- Fluxgate magnetometer
- SQUID

Fluxgate magnetometers consist of strips of iron-nickel alloys with low coercivity and high

susceptibility, such that they can be magnetised by a very weak field, and the Earth's field can produce a magnetisation that is a large portion of the saturation value. These strips are wound in opposite directions, such that when current flows in energising coils attached to them, they magnetise in opposite directions. A secondary coil is wound around the pair, and detects the change in magnetic flux. If there is no external field, the flux in the two coils are equal and opposite, if an external field is applied, and the axis is aligned with it, one saturates before the other, producing a voltage in the secondary coil. The voltage produced in the secondary coil is proportional to the strength of the external field along the axis. This property makes it a vector instrument. For three component field readings, three sensors are aligned at right angles to each other, and rotated so that two of the sensors record zero field and the third is aligned with one component of the geomagnetic field. The output is not an absolute field value, but rather a voltage which must be calibrated to the field. However, it can record field strength continuously, and has a sensitivity of around 1nT. Fluxgate instruments are capable of measuring most anomalies of geophysical interest, and are robust enough to be mounted on, or towed behind, a plane or ship.

Proton precession magnetometers depend on the properties of the proton – particularly, that it has a magnetic moment proportional to the angular momentum of its spin, which can only fall into given values. The ratio of magnetic moment to angular momentum is the gyromagnetic ratio, a fundamental constant with the value of 2.675 13x10^{8} s^{1} T^{1}. The sensor of a proton precession magnetometer consists of a flask of proton rich fluid (e.g. water, alcohol, lighter fluid), with a magnetising solenoid and a detector coil would around it. When the solenoid is switched on, it produces a magnetic field much stronger than that of the Earth (on the order of 10 mT), which aligns the magnetic moments of the protons within the flask along its axis. The axis is arranged at approximate right angles to the geomagnetic field, so that when the solenoid field is switched off, the protons react to the coupling of the geomagnetic field, processing around the field direction at a known rate. This motion produces a signal in the detector coil, which is then amplified and used to calculate field strength. The strength of the field measured is directly proportional to the frequency of the signal. Accurate measurement of this signal gives an instrument sensitivity of around 1 nT, but it requires a few seconds to achieve, as the instrument calibrates the frequency measured by counting a few cycles. Proton precession magnetometers give an absolute field value, but do not provide a continuous record. They measure the total field (B_t, the vector sum of the Earth field, B_E, and ΔB, the field from a local anomaly), but cannot provide vector components as the fluxgate magnetometer can (Lowrie 2007)

Chapter 2. CM4 Tests

This section deals with work on observatory data and CM4 models. CM4 model outputs are expected to be good fits to observatory data in the conditions it is designed for, but misfits are expected to occur based on some of the assumptions used, and base parameters of the model:

- CM4 is primarily based on magnetically quiet data, so is not expected to model disturbed conditions well.
- The conductivity model used in the parameterisation does not vary radially, so CM4 is not expected to model conductivity based features, such as those related to the coast effect, and the conductivity structure may not be appropriate for all locations.
- Data from polar regions was not used, only available at certain times, or heavily damped when parameterising CM4. It also does not model auroral current systems, so it is expected that high latitude regions may not be modelled as successfully.

First, we establish how well CM4 external components fit data from observatories, and where there are trends in the misfit. This is initially done using European stations, and then extended to other geographic locations. Several months of data are used to establish how disturbance level affects fit. Since misfits are identified, we look at the possibility of making adjustments to the CM4 model components to improve the fit, correcting for the differences due to latitude and location, by increasing the amplitude of each of the four model components. This also allows us to establish the relative size of error in the model due to the unmodelled effect.
We also investigate whether there are differences in the way the model creates signals of certain periods compared to those recorded at observatories, by taking discrete Fourier transforms of both model values and observatory data, and comparing the power spectra to look for over or underestimated signal periods.

2.1 CM4 Model Fit

CM4 produces half hourly averaged models of ionospheric and magnetospheric magnetic variations at a given location. The model can be viewed as four components for each element of the field, or combined to produce a single variation for X, Y, and Z, as is mostly used here to compare to observatory data. The initial output of CM4 used for these tests consists of the primary and induced

ionospheric and magnetospheric variation for a given location and time period (in this case, one calendar month was used, with values calculated for half-hourly means). These are produced for each of the three directional components X, Y and Z, and centre around zero, showing the change with time, but not the overall intensity of the geomagnetic field. This can be produced by modelling the core and/or lithospheric fields, but is not of great use here, since these fields do not vary on such short timescales. The four values for X are combined to produce a single X value (and so on). This creates the overall external field variation used for comparison to observatory data in these tests. Since this value (and those of the two other components) centre on zero, we add or subtract values from the model values to produce a separation between the lines, allowing them to be viewed more clearly. This is also done to the observatory data, removing the large overall strength of the field, and allowing us to see the daily variations (and compare these to the CM4 models). This adjustment has been applied to all following model/observatory data diagrams, normally scaling Y values near zero, with higher X and lower Z.

We begin by testing how well CM4 fits real data from a variety of stations, and also looking for differences/similarities in behaviour between observatories. The first tests were on Valentia (VAL) station, located on the Atlantic coast of County Kerry, Ireland, and Niemegk (NGK), in Brandenburg, Germany. Niemegk was chosen as it is generally a stable, magnetically quiet, and otherwise well-behaved station, with well understood and laterally homogeneous underlying geology, with no nearby sources of induced magnetic effects or noise. Valentia was chosen, as it is also generally well behaved, but is located at the coast, and previous studies have found a normal coast effect there (an induction effect created by the presence of highly conductive seawater next to less conductive land, which affects the Z component of the field, giving larger variations. See Chapter 5 for more details) (Parkinson 1962). Both stations have long data records. Since they are also at similar latitudes, they should be affected by similar external field variations. Comparisons were extended with other stations: Eskdalemuir (ESK), in Scotland, which was used as a comparison for Valentia due to being close by but further inland, Furstenfeldbruck (FUR), which is similar to Niemegk, and Chambon-le-Foret (CLF), in France. Since all of these stations are located at similar latitudes, and all have long operating histories, including being part of INTERMAGNET, which ensures certain standards are met, they should all be of a similar quality, and be recording the variations of similar overall fields. As such, they should behave very similarly. This is indeed what is shown by the CM4 modelled data for these stations – all the models are very similar to each other (in some cases to the point of being indistinguishable – figure 2.1).

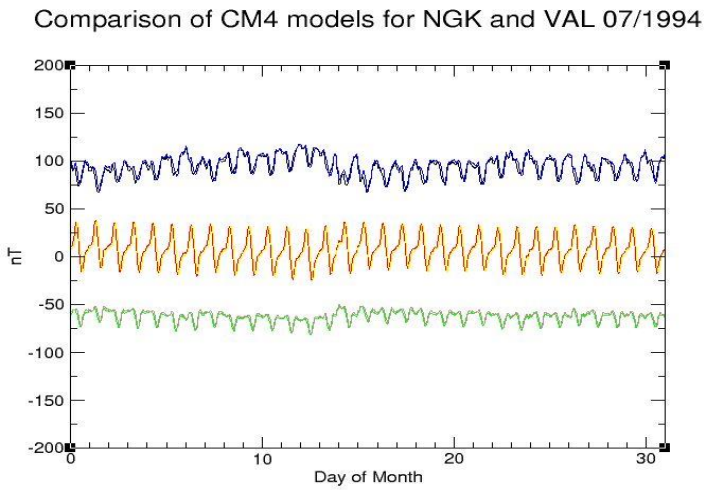

Figure 2.1 CM4 model for VAL and NGK July 1994 (X component blue/black, Y red/yellow, Z green/brown) These are the combined values of the ion_pri, ion_ind, mag_pri and mag_ind CM4 output, combined into single values for X, Y, and Z. X component values have then been offset +75, and Z components -60, to allow them to be seen more clearly.

This suggests that, as expected, differences in the data from these stations is due to effects on the geomagnetic field that CM4 does not account for well, or different behaviours in the response to changes in field behaviour (for example, geomagnetic storms, or disturbed periods of time which are not full storms). In order to look at overall behaviours, the various model series generated by the example 2 code (ion_ind, ion_pri, mag_ind and mag_pri) were combined into single series for each of the three-way components X, Y and Z. This does not prevent analysis of the origin of an anomaly however, as they can still be separated to view contributions from the magnetosphere or ionosphere (induced and external) as required. Most disturbed time effects are seen more prominently in the Z component, or the ratio of Z to H, as are induced effects, and are contained in both magnetospheric and ionospheric fields (e.g., the change in disturbance level around the 27th May 1994 is seen as a larger increase in amplitude variation for Z compared to X at European observatories, figure 2.2).

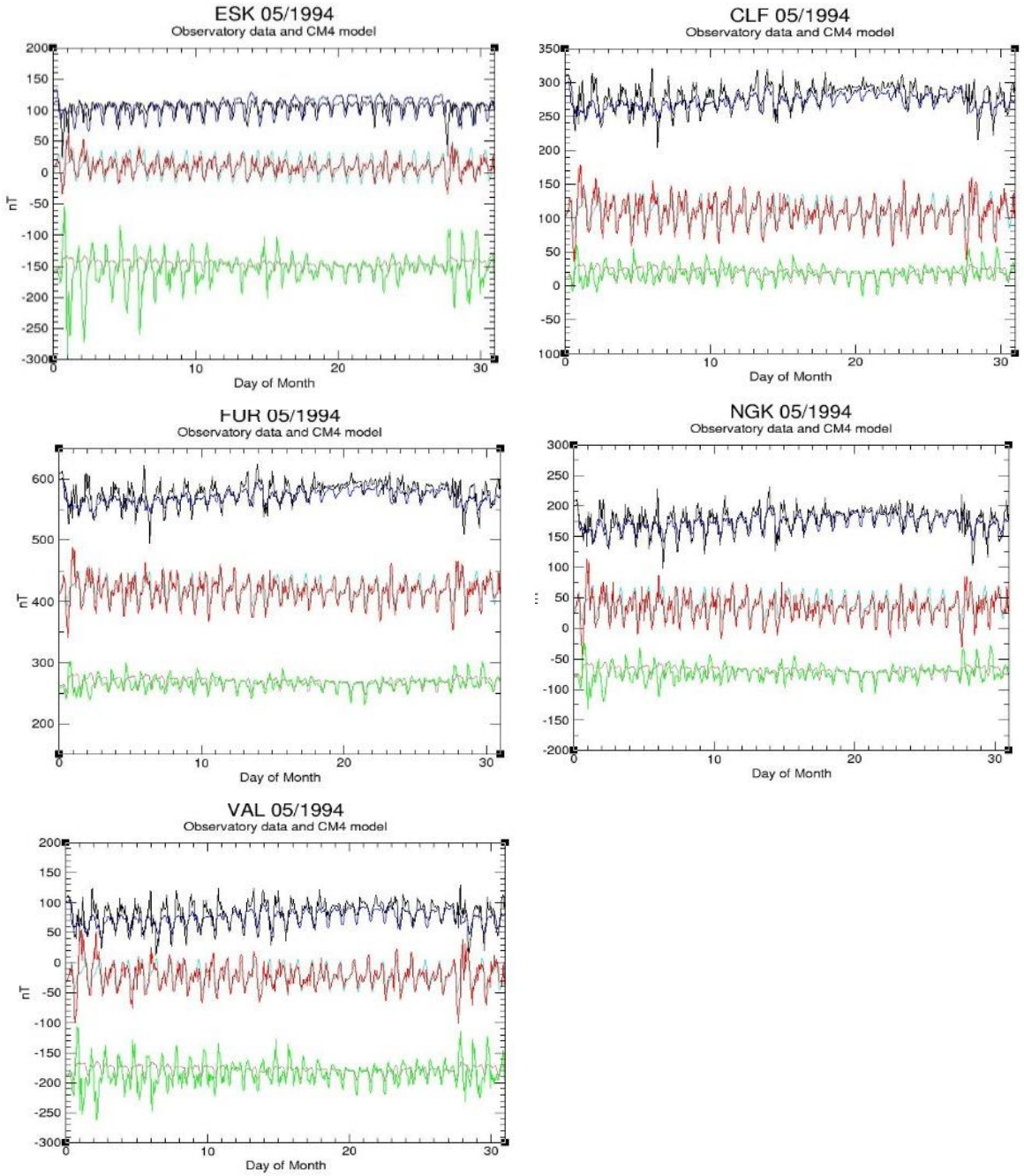

Figure 2.2 Observatory data (X in black, Y red and Z green) compared to CM4 models (X in blue, Y turquoise, and Z brown) for several stations in May 1994

Generally, the pattern of daily variations shown in the models are good fits to the behaviour of the data (figure 2.2). Certainly for the inland European stations, the fit is very good. For VAL and ESK, the fit is less good, but the 24-hour period variations are captured, though the amplitudes and shorter features are less good. For all stations, the fit to the vertical (Z) component is less good than the fit to X and Y. This is most noticeable in VAL. The fit also becomes worse as the activity levels in the outer field increase, as measured by the Dst and Kp indices. CM4 generated data is most similar to the real data on days of low Kp (0 or 1), but is a reasonable approximation up to a Kp of

about three, so long as the change is gradual. This can be seen for whole months in table 2, showing the decreasing RMS misfit for various stations for May, June and July 1994 – months with progressively decreasing disturbance levels. For individual days at VAL, the generally low disturbance period around 20-25th May 1994 has an RMS misfit of 7.62nT, while the higher disturbance days 1st-5th May have a misfit of 13.78nT.

VAL consistently shows a misfit in amplitude in the model data. Generally, the amplitude of the model is not high enough to match the daily variations at VAL; this is particularly noticeable for the Z component, and in a lesser manner for the X component. Only very quiet days, with Kp values of 0 or 1, have the same amplitude as the models would expect.
Since induction features are likely to be seen mainly in the Z component, and to a lesser extent on the horizontal components (Campbell 1997, Kuvshinov 2008), this mismatch in the model data is expected – VAL station is near the coast, and previous work has shown a normal coast effect present here. This would increase the Z amplitudes, in a way that is not modelled by CM4, which does not generate modelled induction features. While there is a conductivity element involved in CM4, it assumes only a radially varying conductivity structure, and does not include the oceans, so corrections for induction effects cannot be carried out using CM4, but must instead be modelled separately.

To test whether the misfit seen at VAL was due to an induced coast effect or something peculiar to the station, other stations located near the coast were also compared to CM4 models. These included Baker Lake and Fort Churchill (BLC and FCC, Canada), and Abisko (ABK, Sweden). These also seemed to show poor fits to CM4, in a similar way to VAL, suggesting the coastal position/induction effects due to this are causing at least some of the misfit. However, the amplitudes of the model, particularly for BLC and FCC are also not fitted well by the model data, suggesting that this is not the only effect occurring (figure 2.3). Comparing the level of fit to the Dst and Kp indexes, suggests that while undisturbed days may be well fit at these coastal stations, the fit decreases rapidly with increasing disturbance, much more so than for the inland stations. Since these stations are located at high latitudes, they were judged likely to contain effects which are not modelled by CM4.

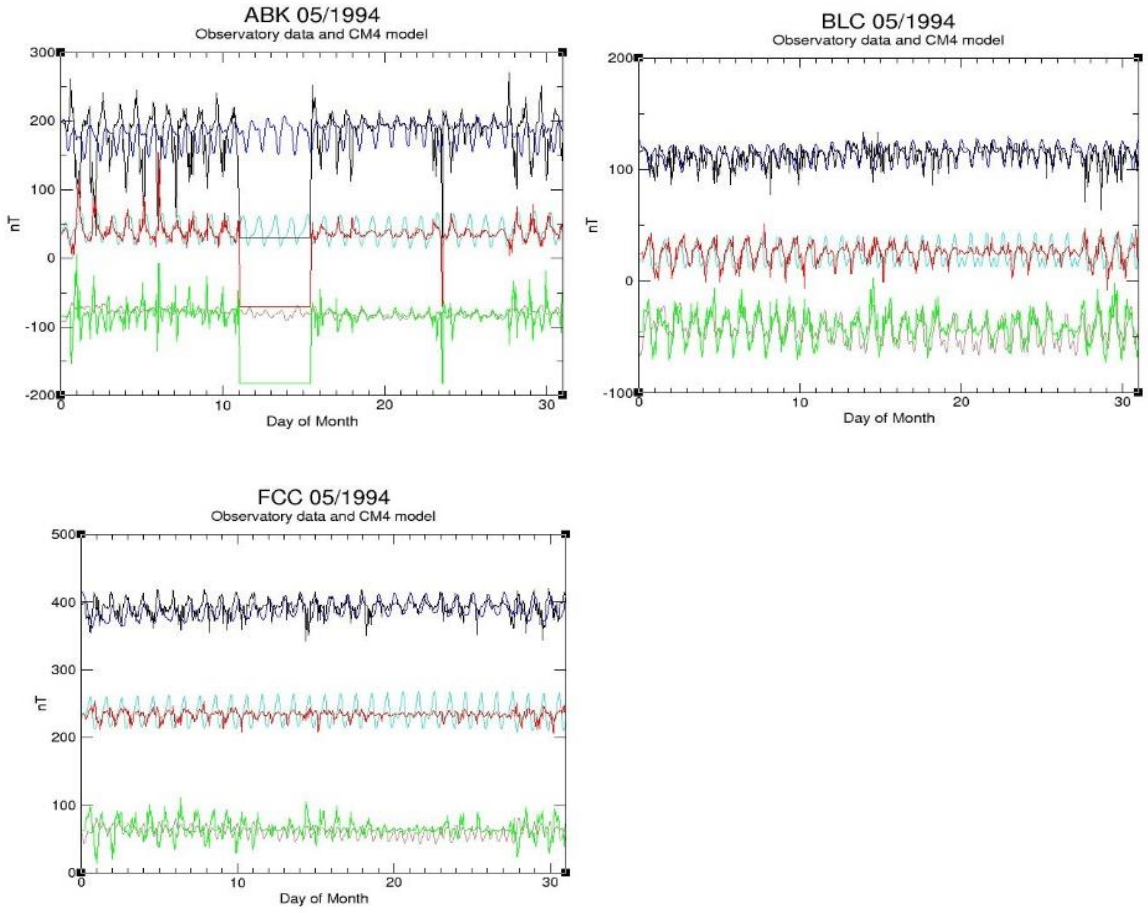

Figure 2.3 Observatory data (X in black, Y red and Z green) compared to CM4 models (X in blue, Y turquoise, and Z brown) for several stations in May 1994. The drop in ABK values between the 12th and 16th is due to missing data.

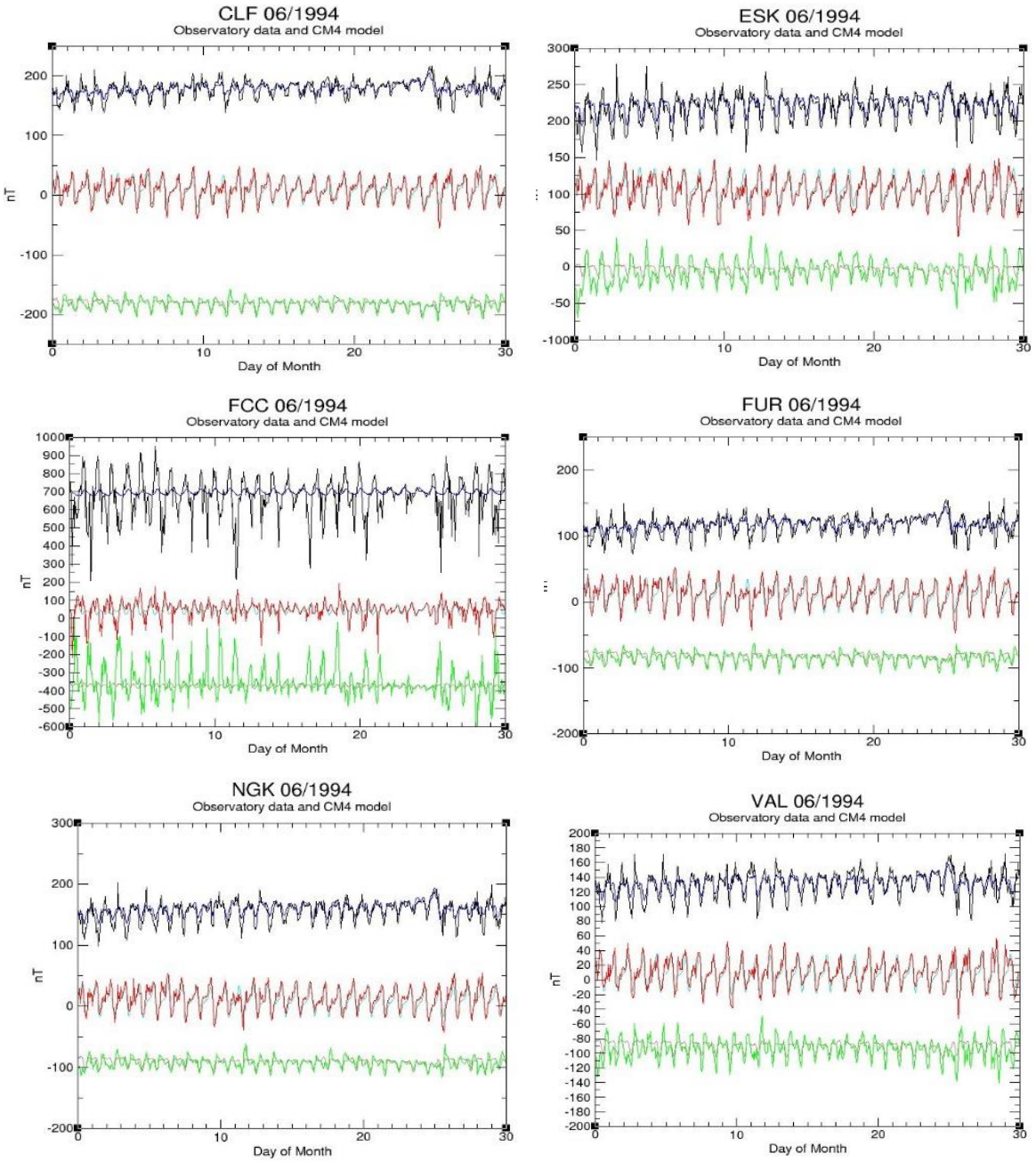

Figure 2.4 Observatory data (X in black, Y red and Z green) compared to CM4 models (X in blue, Y turquoise, and Z brown) for several stations in June 1994

Observatory	05/1994	06/1994	07/1994
VAL	27.88	20.16	17.59
NGK	17.53	11.84	10.18
ESK	32.73	26.74	18.68
FUR	14.44	14.95	12.37
CLF	21.03	17.82	
FCC	131.75	121.06	
BLC	146.63	136.83	
ABK	132.69	101.94	

Table 2 RMS misfit of CM4 model ionospheric and magnetospheric components to observatory data for May, June and July 1994 (misfit values in nT)

When looking at stations in high latitudes, as seen before, the pattern the model creates fits well, but the amplitudes are almost always too low (The RMS misfit between observatory and model data is over 100nT for FCC, BLC and ABK in May and June 1994. As can be seen in figure 2.5, for ABK 06/94, the model predicts X component variations of around 50nT, while the observatory data records up to around 600 nT of variation). This misfit seems to increase with latitude (as can be seen from figure 2.4 and table 2). As such, it suggests that the model is not fitting something related to high latitudes. Since CM4 does not include much data from this region (there are no observatories at the north pole, and it is a difficult location to survey with satellites, coverage here depending greatly on the choice of orbital pattern (while polar orbits allow the sampling of most of the region, the satellite will only sample a given area at particular times of day) and does not include the auroral electrojets, this is to be expected. The geomagnetic field near the poles is much more complicated than elsewhere, which makes it more difficult to fit models to. The north magnetic pole is better sampled, since it is located in northern Canada, where several observatories are located. Most of these stations however, are also located on or near the coast (either of the ocean or large lakes), and many are on islands of varying sizes, making induced effects such as the coast effect of great importance. This is further complicated by the presence of the auroral region. Disturbance in this part of the field is both more likely to occur, more likely to be large, and due to the position of stations on the coast, more likely to generate induction effects which will be recorded in the observatory data. This is discussed further in chapter 5.

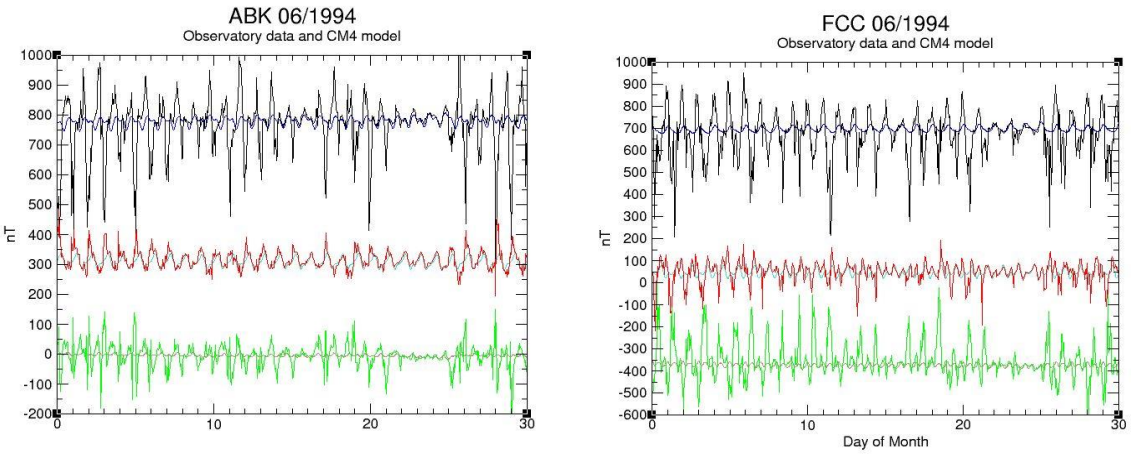

Figure 2.5 Observatory data (X in black, Y red and Z green) compared to CM4 models (X in blue, Y turquoise, and Z brown) for ABK and FCC in June 1994

Since surveys are often considered in this area, and may be more so in the future, it is particularly important to be able to correct data in high latitudes effectively.

The location of all observatories used may be found in Appendices 1 and 2.

2.2 Disturbance Related Behaviour (Kp and the models)

Dst is incorporated into the CM4 model as one of the initial parameters. When model data is generated for a station/time combination, the effect of Dst can be seen in the way the model values vary from the standard Sq pattern (removing Dst from the model gives a smoothed, idealised model of behaviour). Particularly in months when the Dst variation is large, the inclusion of the magnetospheric fields for that month in the model improves the fit to real data (for NGK in May 2009, comparing the model with and without Dst produces RMS misfits of 10.22nT and 10.41nT, respectively). Removing Dst from the models removes some of the variation which is superimposed on the Sq pattern (figure 2.8). It also tends to lower the amplitudes, and remove the shortest of the features the CM4 model is capable of generating, particularly in the form of 'spikes'; the model is generally flatter than the real data, with Dst removed this effect is more pronounced.

On less disturbed days of the month, where Kp is low, the model and the data fit well, and the same pattern can be clearly seen.

The month chosen for the initial tests was May of 1994. May '94 contains a range of quiet and

disturbed behaviour. When the model is run, the patterns of the real data and the model are generally the same, but the amplitudes of the components in the data are often higher than model values. Stations such as NGK, FUR, are fit well, even on disturbed days. VAL is much less of a good fit, especially when comparing the Z component. The difference between the quiet and disturbed days is less noticeable in VAL data, since even quiet days are less well fit by the model (Kuvshinov 2008).

June 1994 was used for a second set of tests, as it is a much less disturbed month overall (as can be seen from figures 2.2 and 2.4). The fit to the data in all cases is much better (see table 2, at all observatories used here, there is a smaller RMS misfit between the observatory data and the model in June 1994 compared to May). The disturbed days are obvious in the station data, as they are more different to the surrounding quiet days than for the May data. In general, VAL has higher amplitudes on X, and Z becomes far from the prediction on disturbed days. For some stations, such as ABK and FCC, the models only really fit on the quiet days, but these fit very well. On the more disturbed days, the amplitudes are much higher than the modelled values, much more so than for VAL.

July 1994 is a more disturbed month than June, but not so much as May. Again, the model fit is very good for stations like FUR, NGK. In general, the data is still a bit spikier than the model, but not very much. Even on the most disturbed days, Y is a reasonably good fit; X is affected more and Z the most (figure 2.6).

For VAL, again Y is a good fit throughout. X is a generally good fit, but with slightly higher amplitude discrepancies than for NGK. On Z, only the quietest days fit really well, and more disturbed days show progressively higher amplitudes in the real data, as compared to the model. This amplitude misfit affects the fit of the model more, as it exaggerates double peak features that are present in the real data but not the model data.

ESK in general is very similar to VAL, but VAL shows higher amplitudes. ESK therefore could be treated as an intermediate between VAL and stations such as NGK. This is as expected, since the distance to the ocean for ESK is intermediate between VAL and NGK. The fit to VAL and ESK becomes worse at lower activity levels compared to the inland stations.

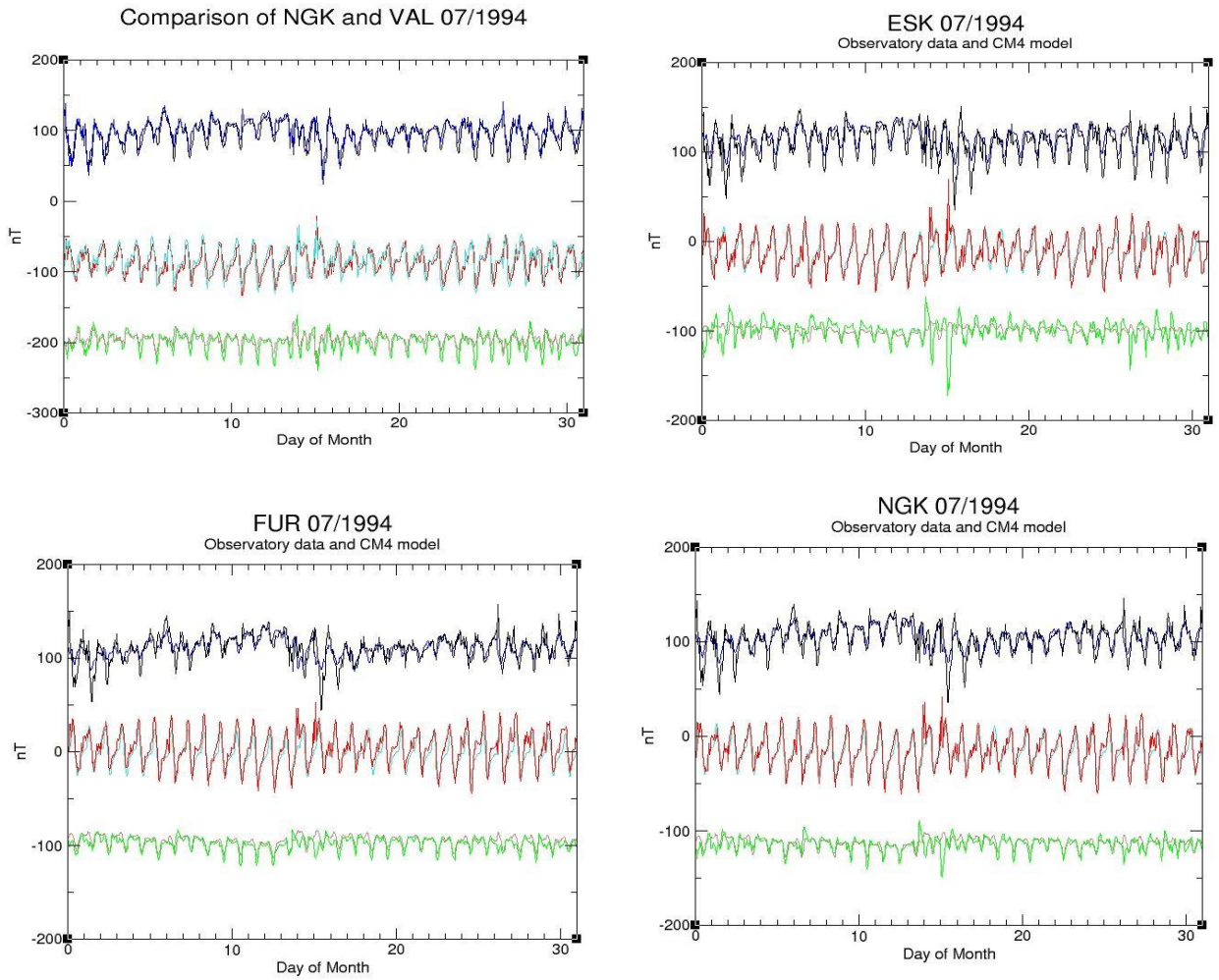

Figure 2.6 Observatory data (X in black, Y red and Z green) compared to CM4 models (X in blue, Y turquoise, and Z brown) for several stations in July 1994

Aside from overall slight issues with amplitudes, for NGK, FUR, and other inland European stations, the CM4 model seems to fit well to station data at times of low disturbance, and up to around Kp 3. However, in some places, a quieter day in among more disturbed days will fit better than a disturbed day in among quiet days (this result is expected, since CM4 is averaged), and some days with a higher Kp index can be fit quite well as long as the change is gradual. Previous work (Shore 2007) also agrees with the finding that CM4 works well in more disturbed times. While Dst data is incorporated into the model, and the difference between the model without Dst and with it is clear (it does improve the fit), it does not seem to be fitting **enough** of the variation to model simply.

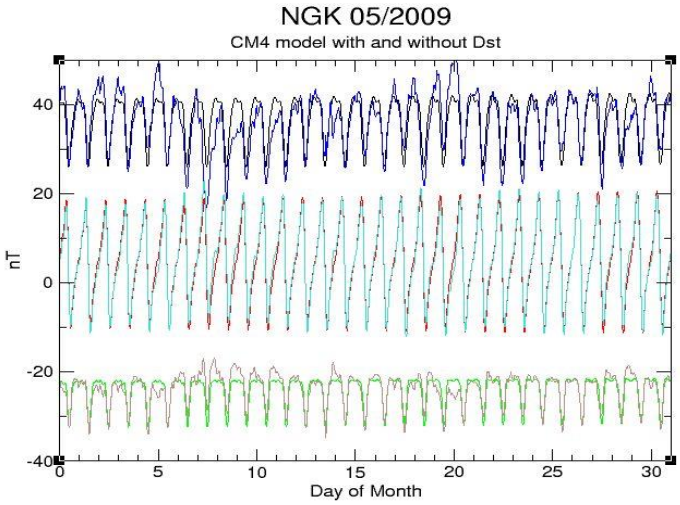

Figure 2.7 CM4 model with Dst (X in black, Y red and Z green) compared to CM4 without Dst (X in blue, Y turquoise, and Z brown) for NGK May 2009

The ability to fit odd days of disturbance is seen most obviously in May of 2009, which is one of the quietest months in that year. While a couple of days have Kp up to 3o, in one case 4o, most of the month has values of 0-1. Despite this, even with the Niemegk data, which is usually well fit by the model, some days do not seem to be behaving as expected. These days have rapid, though fairly low, Dst variations. This shows that Dst is a good estimate for disturbance if there are no other effects involved (figure 2.7 shows the effect of removing Dst from the model), and also agrees with the finding that CM4 can cope with higher disturbance levels than it is strictly designed for (not being intended to work for Kp over 2). That days of higher Kp can be modelled might suggest that Kp is not the best determinant of the point at which CM4 starts to fail.

Recent work by Onovughe has shown that some of the short period features seen in station records correlate well between stations, and also with features seen in the ring current index (Olsen et al 2014). This is a similar index to Dst, but is based on a much larger number of stations, with better global coverage and temporal resolution. Dst and the RC index are similar, but the increased coverage of data for the RC index shows changes that are not captured by Dst. The greater geographical spread of the RC stations also shows features in the field which are global, as opposed to those which may only be found in the near-equatorial region covered by the Dst stations. This suggests that Dst could be improved on as a method of incorporating ring current activity. As such, Onovughes work suggests that it may be more useful to use this index with stations showing short period variations, particularly given it seems to correlate with short features in the X component at a variety of locations, and comparisons of various stations suggest short period features can be seen in across regions (e.g. Europe (Onovughe 2015), or between high latitude stations (see chapter 3).

In order to remove the complication of higher amounts of disturbance in the field, a survey of the activity level of the field was conducted, to establish months which contained generally quiet data, and which were more active. May of 2009 was established as a month of consistently low Kp, small Dst variations, and also had available data for the maximum number of stations. This month was used as a standard quiet month for most of the subsequent tests.

2.3 Adjusting CM4 Model Components

CM4, we have seen, is constrained by, and attempts to fit data, from observatory stations. However, it is not always sufficient to fit the data well when used on its own. We therefore are looking for simple 'rule of thumb' relations which might improve the ability to remote reference surveys, without becoming too complicated or too specifically useful to be applied by a survey company.

An initial test to establish which part/s of the model are not fitting well to the observatory data was made, by arbitrarily increasing the values of the various parts of the model (taking the series generated by the model and multiplying each point value by a factor of 2, or 5 etc.), to adjust their overall contribution to the total; these adjusted models were then compared to observatory data to establish if the fit is improved by the increase. While this sometimes improves the fit of the model – in most cases by increasing the amplitudes – it generally results in over-correction for some components/stations, while under-correcting others. A single change of this type is therefore unlikely to result in an improved correction for all stations. The results of the series of changes tested do show, however, that very little appears to affect the Y component - while it will gain overall amplitude, the shape rarely distorts; larger differences are taken up by the X and Z components (figure 2.8). Increasing the relative strength of the ionospheric or magnetospheric components changes the model shape, in some cases improving the fit, but in other cases any improvement is balanced by a decrease in fit elsewhere, an improvement in X will have a negative response in Z, and so on. For example, when increasing the induced ionospheric component, the amplitudes of Z at VAL were increased, which was a desired result, as the model values are consistently too low; however, this resulted in the pattern of the variations being lost, and very little change to either X or Y. This suggests that the values for the relative contributions of the magnetosphere and ionosphere are well modelled by CM4, certainly for quiet periods, but it is not capturing all of the detail, probably in particular the induced currents relating to specific locations.

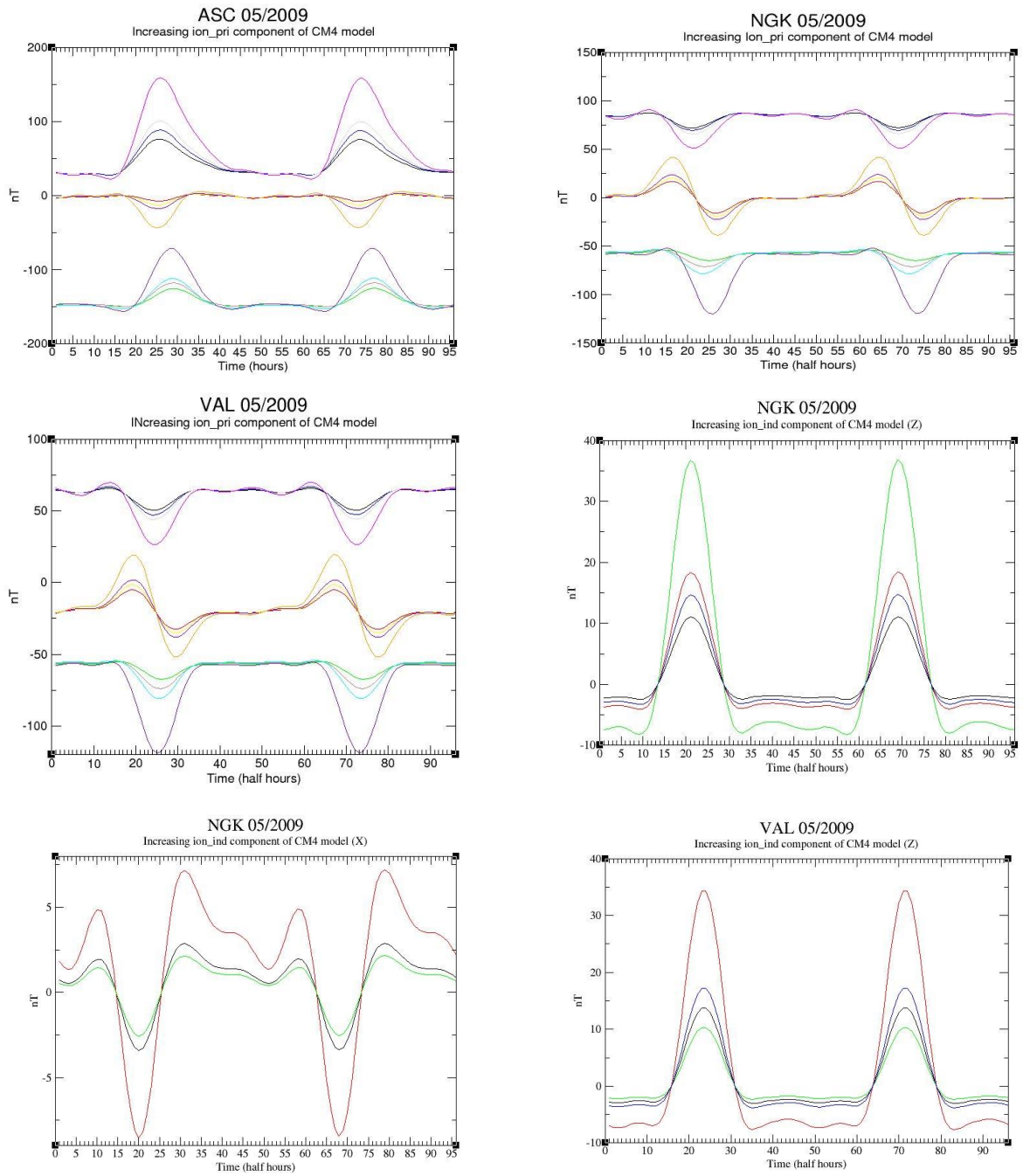

Figure 2.8 Results of increasing CM4 model data components at various stations. Models are increased x1.5, x2, x2.5 and x5

Further tests focused on looking at which parts of the model could be adjusted to incorporate the appropriate amount of variation. Tests of various step increases of each of the four CM4 model components were performed.

Each external component (primary and induced ionospheric, and primary and induced magnetospheric) was increased x1.5, x2, x2.5 and x5. The resulting 'new' data were then combined

with the original model of the other three components, giving a new model. These new models were then compared to the observatory data to establish which model gave the best fit. Results may be seen in figures 2.9 and 2.10, and tables 3 and 4.

NGK 05/2009	Component adjusted	Size of increase	RMS misfit (nT)
Original RMS misfit: 10.22	Ion_pri	1.5	8.49
		2	8.54
		2.5	10.36
		5	27.94
	Ion_ind	1.5	10.67
		2	11.25
		2.5	11.94
		5	16.55
	Mag_pri	1.5	9.37
		2	9.5
		2.5	10.57
		5	22.48
	Mag_ind	1.5	10.28
		2	10.71
		2.5	11.45
		5	18.1

VAL 05/2009	Component adjusted	Size of increase	RMS misfit (nT)
Original RMS misfit: 13.69	Ion_pri	1.5	11.15
		2	9.51
		2.5	9.28
		5	22.48
	Ion_ind	1.5	14.02
		2	14.45
		2.5	14.99
		5	18.79
	Mag_pri	1.5	12.39
		2	11.83
		2.5	12.11
		5	21.97
	Mag_ind	1.5	13.53
		2	13.64
		2.5	14.04
		5	19.13

Table 3 RMS misfits to CM4 models with increased component values for VAL and NGK

The RMS misfit of each of these tests for VAL and NGK can be seen in table 3. These show patterns of behaviour that are generally consistent across the stations - the best fits were found (as expected from previous tests) from increasing the primary ionospheric component (ion_pri). Most stations are best fitted by an ion_pri increase of 1.5 to 2 times the initial model, with no increase to other components (table 4). Increasing any of the other three components either made less difference, or decreased the fit, as did increasing them together (e.g., increasing both ion_pri and mag_pri). In most/all of the CM4 models, the magnetospheric components are much smaller in amplitude than the ionospheric ones – thus larger increases are needed to make a noticeable difference to the overall model, although small increases in mag_pri do decrease the RMS misfit. Ion_ind – the induced ionospheric component- is often out of phase with ion_pri, which results in the shape of the model no longer fitting if it is increased enough to change the amplitude, or in some cases with an increase in ion_ind causing an overall drop in amplitude of the model. Since for most stations where the CM4 fit is off it is due to smaller amplitude, hence this effect of increasing ion_ind is obviously not helpful. In some cases, large increases of ion_ind results in the combined data switching polarity – troughs become peaks etc. This feature has been observed in data from high latitude stations. Increasing to x5 (of any component) in most cases produces a large over-correction, as the model is already fitting the data quite well. However, for some of the Arctic stations, a much larger increase is possibly appropriate, as the data variation is well beyond the model values.

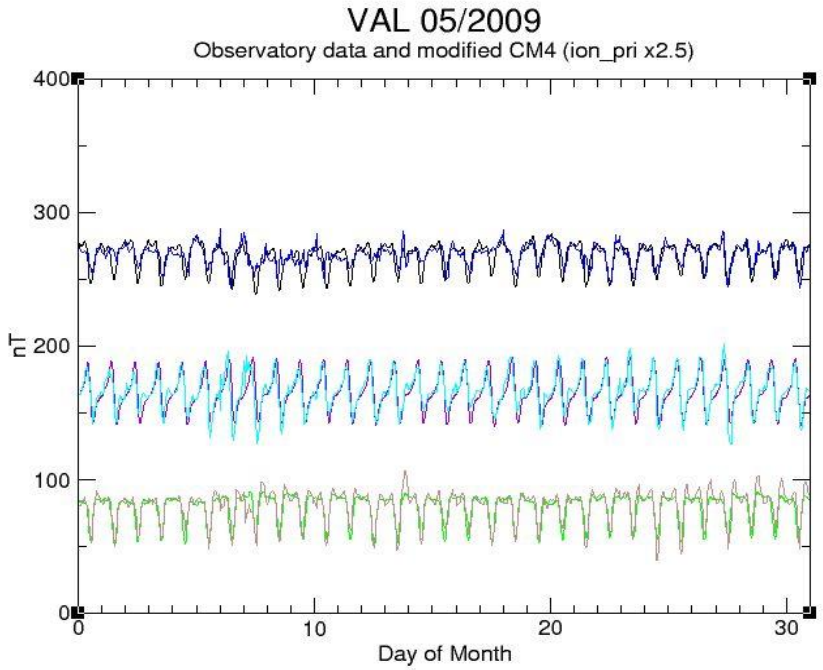

Figure 2.9 Best fitting increased component CM4 model (X in black, Y purple, and Z green) compared to Observatory data (X in blue, Y turquoise, and Z brown) for VAL, May 2009

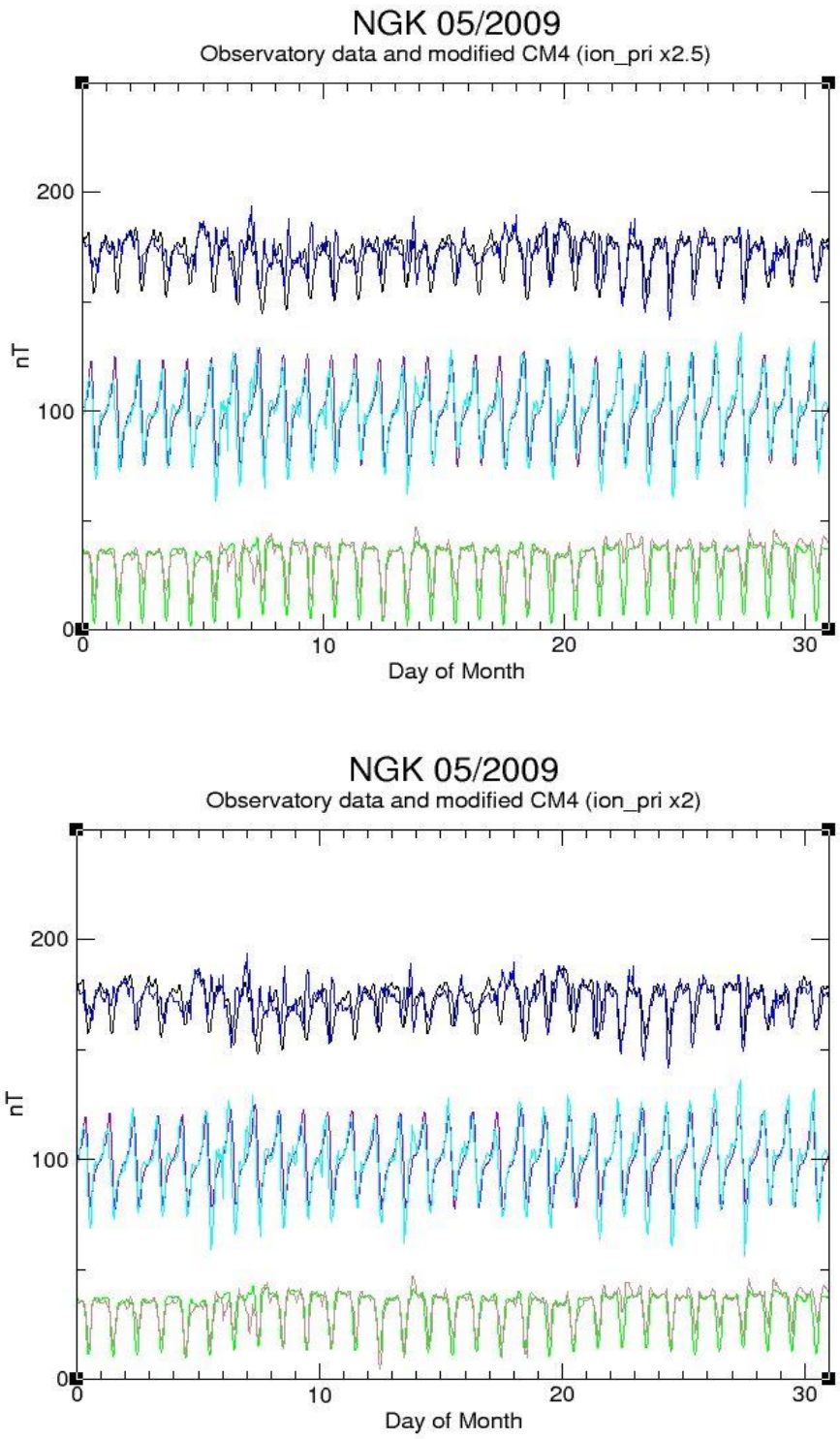

Figure 2.10 Comparison of increased component CM4 models (X in black, Y purple, and Z green) compared to Observatory data (X in blue, Y turquoise, and Z brown) for NGK, May 2009

Observatory	Situation	Original RMS misfit to model (nT)	RMS misfit to best fit model (nT)	Best fit ion_pri increase by RMS value	Best fit ion_pri increase by visual pattern comparison
HRN	Island, Arctic	80.18	77.14	5	2.5
GDH	Coast, Arctic	65.23	61.46	2.5 or higher	5 or higher
VAL	Coast	13.69	9.28	2.5	2.5
MBO	Coast, Equatorial	25.37	24.84	2.5	2.5
BRW	Coast, Arctic	98.18	-	-	2 X, 2.5 Y, Z
NEW	Arctic?	14.53	13.4	2	2 X, 2.5 Y, Z
MEA	Arctic?	24.19	23.97	2	2 or 2.5
LER		14.76	12.04	2	2
MMB	Island	11.23	8.31	2	2
HON	Island	12.57	11.03	2	2
KIR	Arctic	63.89	63.55	2	2
OTT		15.45	14.08	2	2 X, Y, and 1.5 Z
YAK		12.04	8.97	2	2 X, Y, and 1.5 Z
HLP	Coast	10.61	8.77	2	1.5 or 2
SOD		70.71	70.37	2	1.5 or 2
HAD		11.2	8.48	2	1.5 or 2
BEL		99.41	99.08	2	1.5 or 2
ESK		11.96	8.74	2	1.5 or 2
LZH		-	-	-	2 X, Y, 1.5 Z
HER	Coast	7.37	1.81	1.5	2.5
TAM	Equatorial	34.91	23.97	1.5	2
NGK		10.22	8.49	1.5	2
GUI	Island	31.51	31.43	1.5	1.5 or 2
CLF		63	62.88	1.5	1.5 or 2
PST	Island	20.93	20.93	1	2
ASC	Island	13.36	13.36	1	1 or 1.5
DMC	Antarctic	-	-	-	1

Table 4 Best fit ion_pri increases for 05/2009. Highest needed corrections are seen in coastal and/or high latitude stations. The pattern of variation in observatory data at some stations makes it difficult for RMS to be used to calculate the difference between the models – such as CLF, which has a step like drop in the Y component values partway through the month, or BRW, DMC, and LZH, which have large daily spikes which are not replicated by the model.

Since we might expect stations at certain locations to require different (but consistent) adjustments to the model, the best fitting model was determined for a selection of stations giving as wide a coverage as possible, and in a selection of different location types. These were inland (expected to be the control/least affected group), coastal (expected to show an increase in model values needed due to the induction effect), island (which might show an effect due to being surrounded by ocean, but equally might be behave like the inland stations due to the general lack of conductivity contrast), equatorial (which might have unmodelled effects from the equatorial electrojet) and Arctic (which might have unmodelled effects from the auroral electrojet). Of course, there are also stations which fit more than one of these categories in the selection, which could be used to see if the effects stacked, or if one was more important than another. Results are shown in table 4. While there are exceptions (e.g. DMC in the Antarctic being almost perfectly modelled, possibly due to it being located away from the auroral electrojet), the Arctic and coastal stations require the highest correction to the model, and equatorial also require a higher correction. Even with the adjustments to the model (which improve the fit, as can be seen by both visual comparison and calculating misfits) stations in the Arctic region are still worst fit by CM4, with high RMS misfits that suggest CM4 would leave far too high a residual error to use it for survey purposes in this region. Location of a station on an island doesn't seem to make much difference – but the location of the island does - with equatorial islands needing a higher correction, and Arctic ones a higher correction still. This suggests that when it comes to the island stations, there isn't a large difference to inland stations – there isn't a large conductivity effect, but an overall slight increase in conductivity due to the ocean. For both island and inland stations, latitude has an effect on the model fit – those in locations covered by the electrojets are less well fit. This could even be an advantage if conducting a survey over the ocean – there would be no need to correct for a coast effect, and less difference due to the survey being at sea and the base station on land. Locating the station on the coast has a similar effect to locating it at the edge of the Arctic region (e.g., VAL and HRN need a similar scale adjustment to be made) and the highest corrections are needed on stations that are both coastal and Arctic. SOD/KIR/HRN shows an increasing correction as the stations move further north. This is slightly compounded by a concurrent change from inland to coast to island, but as seen from other islands, the change at HRN is more likely to be due to the latitude than the geography (or the coast effect, as Svalbard is a significantly larger island than most of the other island stations). For some coastal and most arctic stations, as well as those stations which have consistent unmodelled effects, CM4 would not be appropriate to use on its own for survey purposes, as the RMS misfits are of a similar scale or higher than many types of survey target anomaly.

There is a general trend in the fit patterns, which implies that there is a consistent difference in stations located at the coast, and in the Arctic region, which are discussed further in chapters 3 and 5. Since certain stations have essentially the same CM4 model, but require different corrections to this model to fit the real data, this could be used to attempt transforms between stations. As noted before however, this is not simply a case of increasing the whole model, but only one part of it. While this is generally the largest part, it does affect the shape of the corrected models. Comparing NGK and VAL (as these have been the primary examples of inland/coastal, and are conveniently located close together), suggests a straight transform is indeed not an appropriate correction for this effect. As the component that makes the most difference to model fit is ion_pri - the major component of Sq - tests were run to see if adding a Sq period set of sine/cos waves would improve the fit. This would effectively increase the ionospheric contribution in a similar manner to ion_pri in the model. This can be found in chapter 5.4.

2.4 Discrete Fourier Transforms of Magnetically Quiet Months

Discrete Fourier transforms are created using the xmgr/qtGrace plotting program. These convert the time series data into the frequency domain, and are displayed by period. This shows the relative power of each frequency period within the observatory data. We calculate the DFT for periods up to 30 hours, since it is expected that Sq periods (harmonics of 24 hours) are likely to be the source of most of the signal, and also because the month long series used are unlikely to be long enough to properly resolve any longer period signal. DFTs can also be used to compare the signals in the model data, to see if certain periods are missing/additional or stronger/weaker than they should be, compared to the real data, and so not being modelled correctly. Depending on the time period, this would also indicate the likely source of the signal, which would affect the correction method.
This also allows a comparison of the relative strengths of each time period between stations – are there periods which are more important at coastal locations? Or at high latitudes?
Firstly, DFTs were performed on the CM4 models (figure 2.11 shows examples of these). All stations show peaks in the power spectra for the harmonics of 24 hours, decreasing in power as the time period becomes shorter. Almost all of the power is concentrated in the 24-hour period. Few other periods are seen as large features, though there are very small spiky features in the low periods of the power spectra. These model DFTs provide a comparison for the observatory data, showing which periods are misfit by the model.

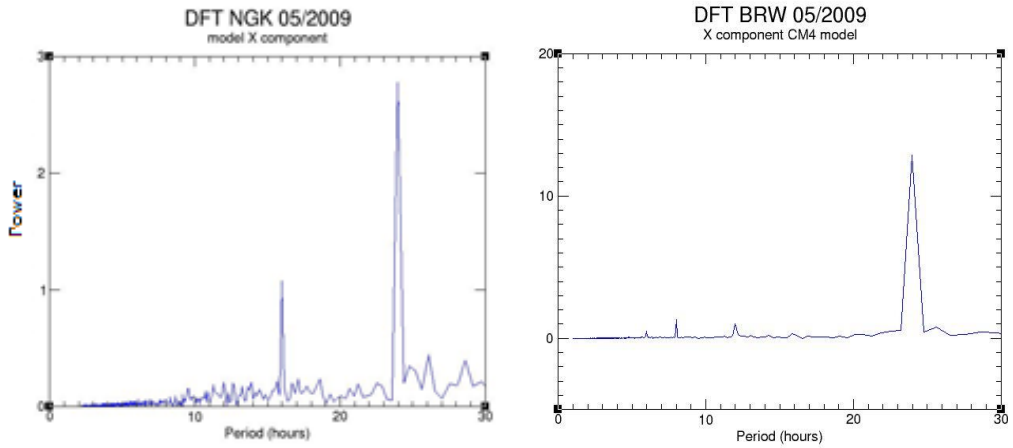

Figure 2.11 Discrete Fourier transforms of CM4 models for May 2009

In most stations, the dominant periods visible in the Fourier transforms are 24-hour and 12-hour, the fundamental and highest harmonic of the solar day. For most stations, 24 hour contains by far most of the signal, though some have a larger 12-hour spike, or very similar heights for 24 and 12. Most stations also show a dropping off in relative power of the harmonics of 24 (which would be expected for daily variation). There are few stations for which any other time period is the dominant part of the power spectra, though in some cases there are other relatively large contributors, or periods 'missing' from the spectrum; for example, BRW 05/2009 Z component contains little power at 24 hours. Variants from the decreasing 24 harmonics pattern include relatively large spikes between 24 and 12 hours (18 and 15 are common), and for some stations 8 is a smaller spike than 6. 8.2 is another common minor spike. This shows most of the variation in the magnetic field on quiet days is driven by the relative position of the sun; these periods are seen at all stations and in both quiet and disturbed conditions. High latitude stations (e.g. HRN, figure 2.12) may show high short period spikes even in quiet months, particularly on the X component. The next noticeable feature (not seen in the model data) is a peak at 12.4 hours, or a modification in the shape of the 12-hour peak (e.g. VAL Z component, figure 2.13). This is the influence of the M_2 tide. This in not present in the model, as CM4 doesn't include tides. See chapter 5.2 for a further discussion of tidal effects.

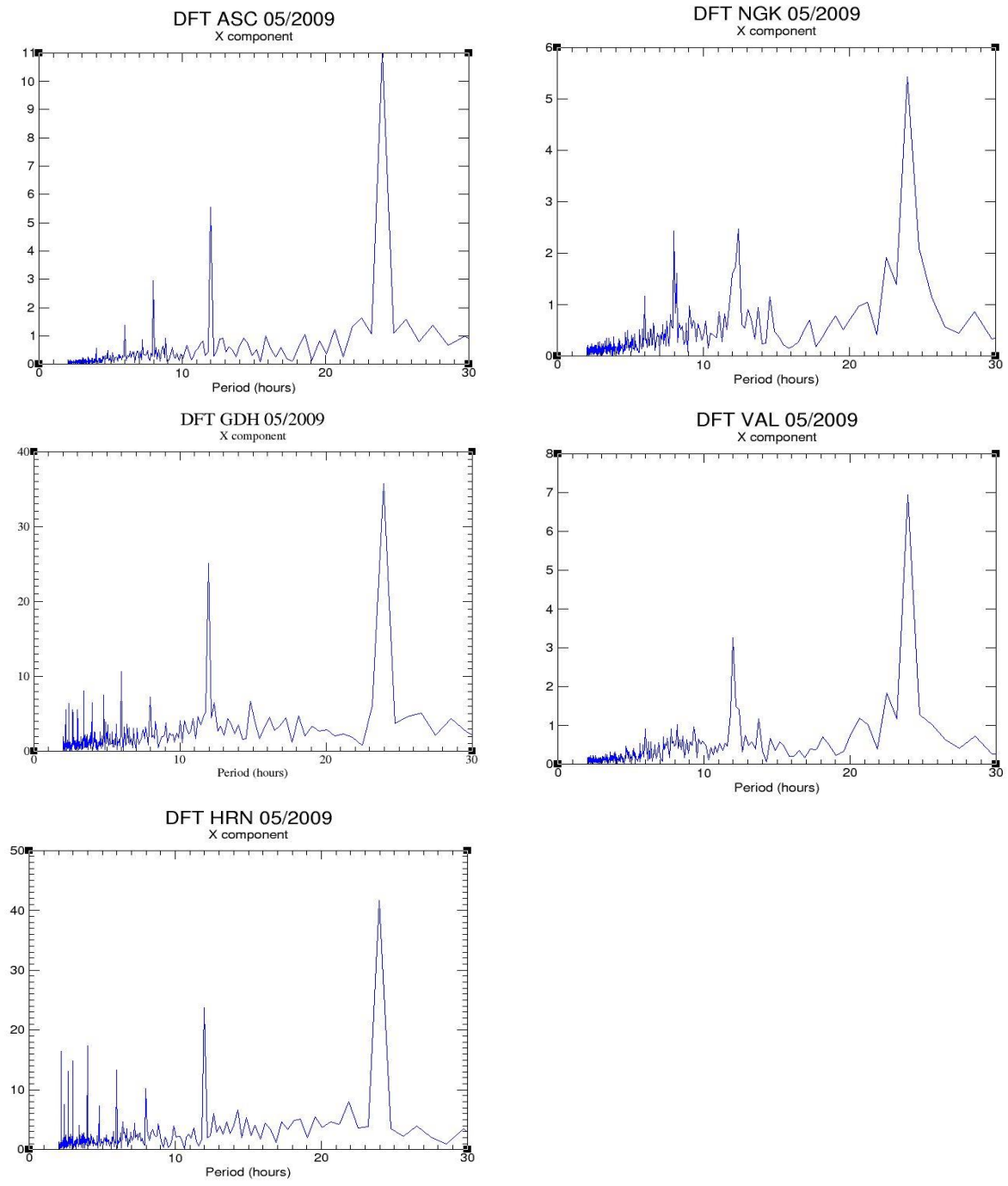

Figure 2.12 Discrete Fourier transforms of X components at several stations, May 2009. Y axis shows the relative power at each period

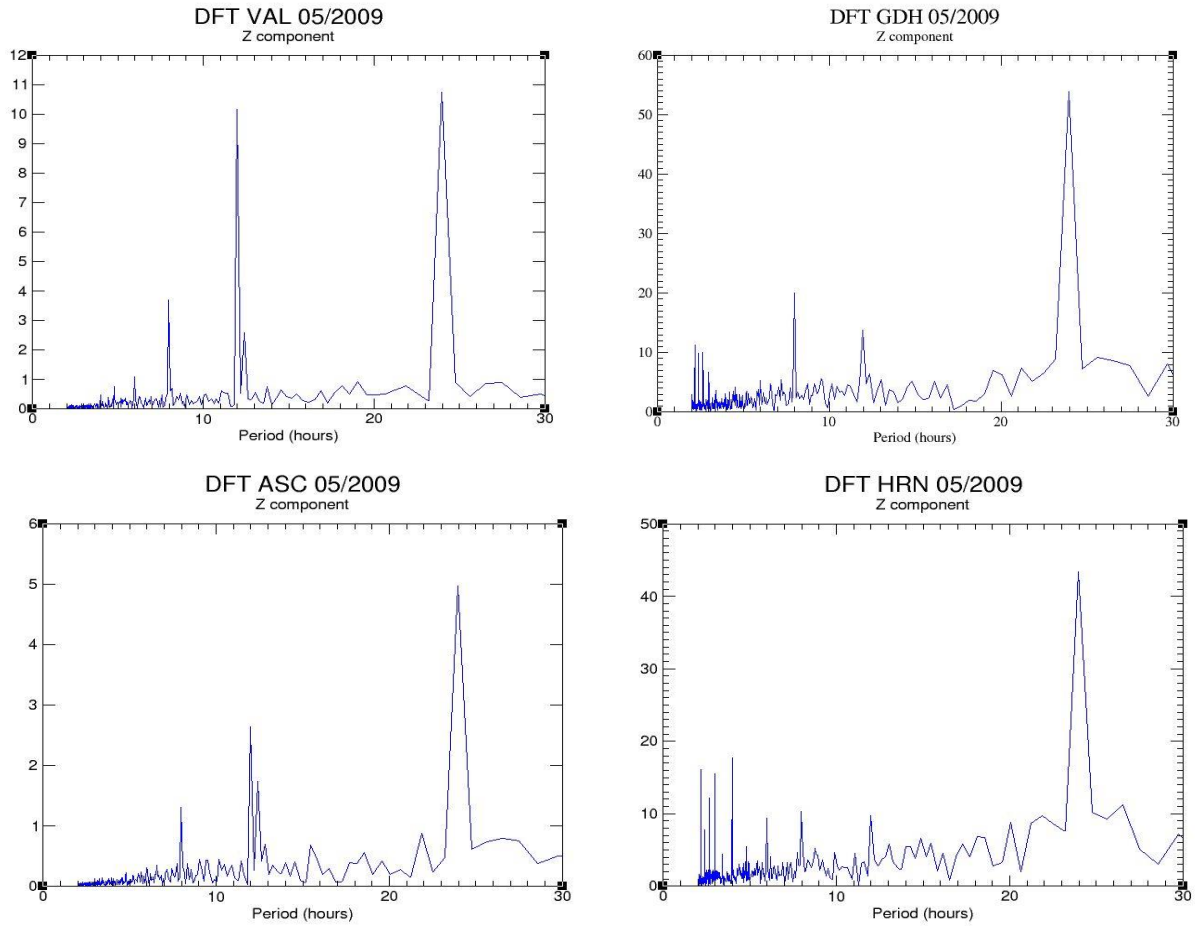

Figure 2.13 Discrete Fourier transforms of Z components at several stations, May 2009. Y axis shows the relative power at each period

DFTs also show that periods longer than 24 hours are relatively less important. While they may appear to be larger spikes than some of the shorter periods, they also tend not to show up at sharp peaks, but as broader features; power is not concentrated in discrete spikes, but more smeared out for periods longer than 24 hours. For observatory data it is likely to be partly due to the length of time series used (the longer the series the better things are likely to be resolved) and also due to smearing out of the effect of similar periods, as seen in the 12/12.4 period at some stations.

Results

In this section, we compared CM models of the external field variations to observatory data. This was begun with European observatories (primarily VAL and NGK). This showed that the model generated for these observatories was very similar, yet the observatory data showed some differences. The most noticeable of these is the misfit to the amplitude of Z axis data at VAL. Generally, the fit of the model to observatories is good for European stations. The fit decreases with

higher magnetic activity (over Kp of 3); this is higher than might be expected from the parametrisation of the model (being mainly based on Kp of 0 or 1).
Since CM4 does not include lateral conductivity variations, it was expected that VAL might be less well modelled due to previous studies noting a coast effect present. Other coastal stations were compared, and showed similar amplitude misfits. Some of the observatories used in this comparison where at high arctic latitudes, and show a similar (indeed, much larger) amplitude misfit in CM4. This was again expected, due to the data used for CM4, and damping/omission of auroral currents. It is also noted that disturbance in the field seems to have more of an effect at coastal and high latitude observatories, and the rapidity of Dst fluctuations may be of more importance to judging exactly where the model will fail than the Kp value. This could likely also be improved by using the ring current index in place of Dst. Very quiet months were used for further tests, to eliminate the extra complication of this variation with disturbance level.
Tests were conducted to see if the model could be adjusted to improve the fit- particularly since the major issue for both coastal and high latitude observatories seems to be an underestimation of the amplitude of variations recorded, but the pattern is correct. This was done by increasing the four external model components (ion_pri, ion_ind, mag_pri and mag_ind) and seeing if the new model showed an improved fit to the data. The fit was determined by both RMS error values and visual comparison. Ion_pri increases produce the best fitting models.
Inland, mid latitude observatories were best fit by CM4. The largest misfits/required adjustments were seen in high latitude observatories, and also coastal observatories. Equatorial observatories show a smaller misfit, and island observatories may have a slightly increased misfit, although this is far outweighed by the effect of latitude.
Since these misfits are both expected, and relatively consistent between observatories in similar locations, this observation might form the basis of a correction between locations at different latitudes or inland/coast pairs, as is discussed in chapters 3 and 5.
DFT power spectra are also compared, to see if CM4 is missing/adding or over/underestimating the relative contributions of particular variation periods. The comparison of model and observatory spectra shows that the model does not contain as much variation, mainly consisting of the 24 and (lesser) 12 hour periods, and missing short period variations seen in most observatory data, as well as the larger contributions seen from other solar period harmonics. The model also does not contain the relatively large 12.4-hour signal seen in observatory data, especially at observatories near the coast. This is the M_2 tidal period, and the source of this signal is discussed further in chapter 5.

Chapter 3. High Latitude Effects

Introduction

Given that the higher amplitudes (e.g., figure 2.5, showing ABK and FCC model variations of tens of nT, but observatory recordings of several hundred nT) seen at high latitude stations relative to the CM4 model appears to be a consistent feature above ~60ºN, this suggests both a systematic issue that the model is not addressing, but also that these stations are behaving consistently – which in turn, suggests that the issue can be corrected for. Ignoring the fit to the model, and instead focusing on how the stations themselves behave, groups of consistent behaviour can be seen, correlating to the geomagnetic latitude.

The first section contains work on a survey conducted north of Iceland, which had proven difficult to correct. Using CM4, and data from both the original base station and other observatories in the region, we investigate why the correction was unsuccessful, and if any data could be recovered. This work established that the base station was reasonably well fit by CM4, but other stations in the region which might have been considered for base station behaved differently to it. This led to a survey of arctic region observatories, to establish which behaved in similar manners, and lead to the separation of groups of station based on magnetic latitude (section 3.2 and 3.3).
These groupings are not noted in CM4 models, which suggests they are created by something which is not modelled. In section 3.5, we look at several pairs of stations that are close to each other, but located in different groups, to establish if any method of correlation or correction can be found, using both observatory data series and DFT power spectra.

3.1 Survey Correction

Using a combination of CM4 models, survey data, and data from stations, the aim of this section of work was to try and understand why the base stations used for two surveys in the Arctic region didn't manage to properly apply a remote base correction, to the extent that large portions of data could not be used. One survey was discounted as being conducted in a time period that was simply too disturbed to correct for accurately, however the other was simply not well corrected by the base stations used. We attempted to understand why this survey was not corrected, and if there were ways to fix the problem causing this to enable this (or data with similar problems) to be used in the future.

The initial survey data used for this work was collected to the north of Iceland, as part of a larger series of ship-based magnetic/seismic surveys in summer 2011. The data was recorded as a total field (F) value at minute intervals, with lines containing between 10 and ~100 hours of data. The base station was SCO variometer station. The data was provided by ArkeX.

The CM4 model, compared to the data collected in the survey, in some parts fits reasonably well, in others it doesn't fit well, and in a few rare cases behaves in exactly the opposite manner. It also has consistently smaller amplitudes than those recorded in either the base station or the survey data, which, as previously noted, is a consistent problem for stations at high latitudes with CM4. DFTs of high latitude data also shows that short periods (e.g. figure 2.13, showing more power in spikes at less than five hours in Arctic stations (GDH, HRN) compared to non-Arctic stations) have a larger influence on the behaviour of stations in this region, even in quiet months, which would not be fitted by CM4. Short period features can be seen in much of the survey data, and also the base station data.

To attempt to roughly correct CM4 for this difference in amplitude, while keeping the pattern of variation (which is generally well fit) we attempted to increase the amplitudes of the model. This was done using a combined (F) data series, since this is the format of the survey data. For CM4 model data, increasing Z increases the amplitudes of the peaks and troughs in the combined model. This roughly corrects for the amplitude difference between the model and base station. As a 'quick fix' then, the data from the survey and base station observatory were compared to CM4 model data with an increased Z value, allowing us to see if (aside from this known issue) the data recorded at the base station is behaving ‘normally’, or at least, as predicted by CM4. For most of the time, this increase in Z improves the match to the data, in others it over or under compensates. The timing of this mismatch is directly related to the activity levels, as the over compensation is on days of low Kp, while on days of higher Kp the correction is good. For the most disturbed days, this was not enough of an increase; however, it was the overall best option, as there were more days of lower Kp than high.

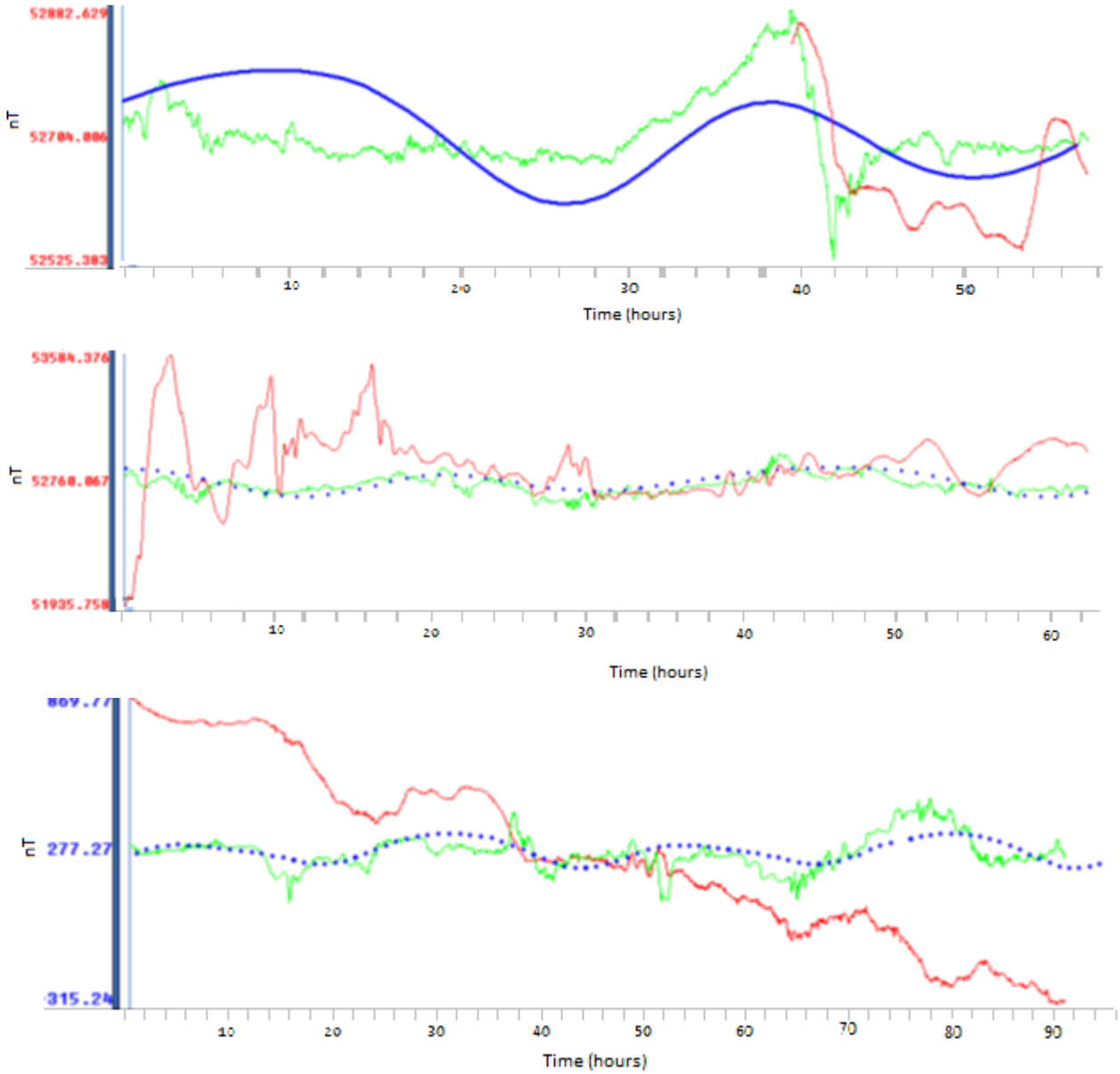

Figure 3.1 Minute F value data for parts of July 2006. Blue – CM4 model (hourly dots). Red - survey data, green - base station SCO. The three datasets are displayed on the same scale, but have had large numbers added or removed to display together for comparison.

Regardless of the increased amplitudes, the CM4 generated model fits relatively well to the pattern of variation recorded by the base station (observatory) data (figure 3.1), and the increased amplitude also fits quite well. This suggests that the inability to correct the survey is not due to any oddity in the base station data, or to magnetic storms distorting the whole time period. In fact, very short duration disturbance effects, on the order of minutes, can be seen occurring at the same time in both the station and survey data, and the overall pattern of the Dst behaviour is also seen in both. Some of these short period features are the same at both locations. Some of them are in opposite senses (a peak on the base station becoming a trough in the survey data, or vice versa), and some of them

show a lag between the station and the survey. The lag is relatively short, being up to an hour maximum. Longer lags may occur, but after a certain lag it becomes difficult to distinguish one event from another, so to avoid misidentification, where spikes could not be clearly correlated, they were ignored. This is particularly because not all of these events are recorded at both the base station and in the survey. This could indicate events occurring and travelling in different directions, or being very localised, but this would require more than just the two locations to constrain properly.

The base station was selected on the basis of being the closest observatory at the same latitude as the survey, but due to the different locations of magnetic and geographic north, this is not actually the case (the observatory, being further west, was at a higher geomagnetic latitude than the survey). Comparing to data from an observatory on Iceland (LRV) suggested that using a base station further south or east (and so close to the geomagnetic latitude of the survey location) might improve the remote correction, however there also appears to be some other effect occurring which prevents this correction from being totally successful for this survey.

3.2 Observatory Data Correlation

Since the comparison of CM4 and the base station used for the survey in section 3.1 shows that the base station is behaving normally, but is not appropriate for correcting the survey, we considered how base stations might be chosen to avoid this type of issue in the future. A first recommendation was to pick based on magnetic rather than simply geographic latitude, but we also wished to see if there was a ‘cut off point’ where the difference in latitude between the locations of survey and base station became overly problematic, but before which could be used. The occasional lag that appeared in the survey/base data also suggested that short period features might drift rather than being instantaneous, which offered a further possibility- that it might be possible to use two stations to correct the data. This would involve using an observatory further south, which based on magnetic latitude should have been used as the initial base station due to the standard option of picking a station at a similar latitude to the survey, and seeing if the features could be tracked across to the original 'northern' station. This might allow a correction to be made based on the distance from the survey and the expected speed of drift.

Stations from the area were surveyed to see which had available data for the same time period, to see if there were regional/latitude differences in behaviour such as were seen with the survey period. This found data available at Fort Churchill (FCC), Baker Lake (BLC), Cambridge Bay

(CBB) and Resolute Bay (RES) (Canada), Leirvogur (LRV, Iceland), Bear Island (BJN) and Tromso (TRO) (Norway), Hornsund (HRN, Svalbard), Abisko (ABK, Sweden), Qeqertarsuaq (GDH), (Qaanaaq (THL), and Narsarsuaq (NAQ) (Greenland), and Barrow (BRW) and College (CMO) (USA – Alaska). Full locations may be found in the Appendices.
Data for Russian stations were unavailable for recent times, so it was not possible to create a dataset which covered the whole Arctic region. This would have been preferable; complete coverage would have allowed features to be tracked across the area. This would also have avoided some of the edge effects in the gridding used to display the data (kriging, discussed further later), and indeed in the suggested correction, as if one station on the edge of the grouping was behaving differently it would be more difficult to distinguish true difference in behaviour from edge effects. Edge effects (as well as within grid effects due to the wide spacing between some stations) are visible in figures 3.13-3.15.

Since Abisko, Tromso, Bear Island and Hornsund form an almost perfect north/south line, these observatory stations were used to test if there was a noticeable difference in how the recorded field behaved moving further north. The CM4 models for these stations are very similar, with some difference for Bear Island. Despite this, the data recorded at the stations show several differences, with the most southern observatory Abisko being quite different to the most northern, Hornsund; the data show a progressive difference in amplitude moving north, but also a definite split in behaviour between the station pairs Abisko/Tromso, and Bear Island/Hornsund. While the stations do have similarities, there are times when they behave quite differently, most noticeably where a peak at one pair is recorded as a trough at the other, the pairs behaving in approximately opposite senses (as seen in figures 3.3, 3.6). Since CM4 does not incorporate data for the auroral electrojets, and is missing data from the poles, the higher latitudes were expected to be less well modelled, so the lack of variance in the model was expected, although the major differences in behaviour seen between the station pairs was not – there is nothing in the models for these four stations that would suggest that the two pairs should behave noticeably differently.

Since a large number of stations had data available for use in this work, and there was the issue of the missing part of the map over Russia, the data was split into two sets for comparison: a North Atlantic/Europe group, and a North America/Greenland group (figures 3.2 and 3.3). However, as these two sets both include stations in Greenland, they can additionally be directly related to each other. For each station both three component data and total field values were taken, and compared qualitatively. These comparisons used data from July 1994, as it is a relatively quiet month with

data available from the largest number of observatories.

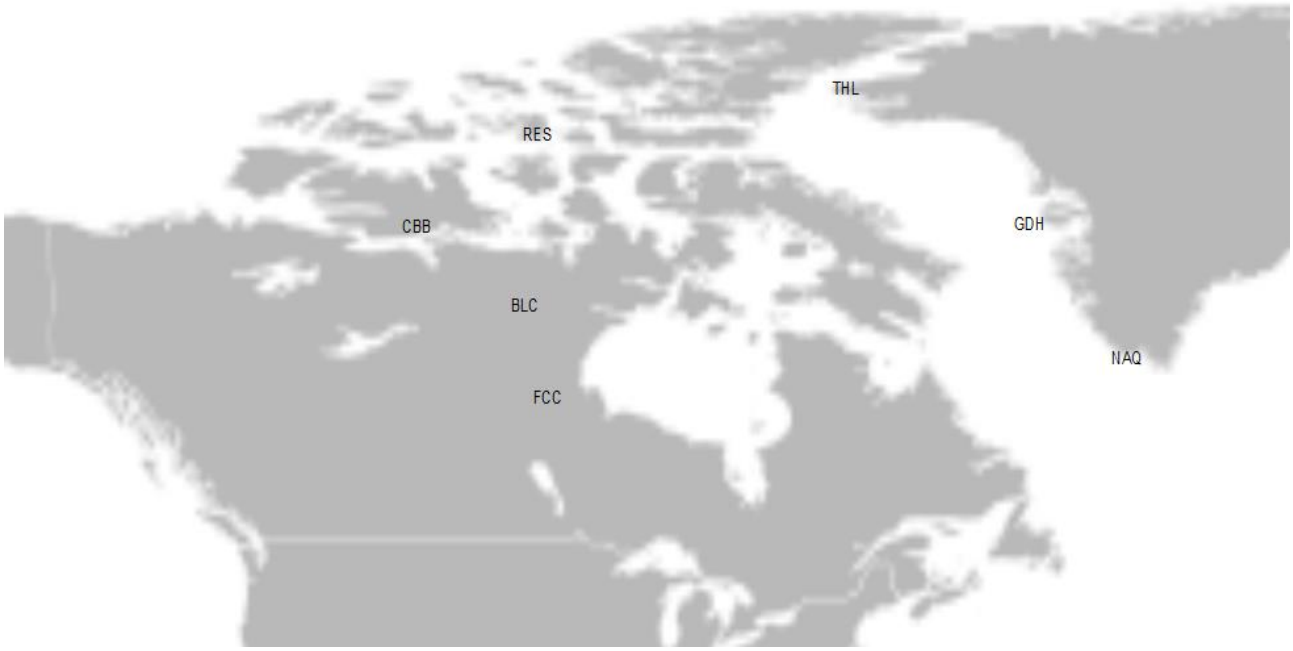

Figure 3.2 Station Locations for the North America/Greenland group

Figure 3.3 Station locations for the North Atlantic/Europe group

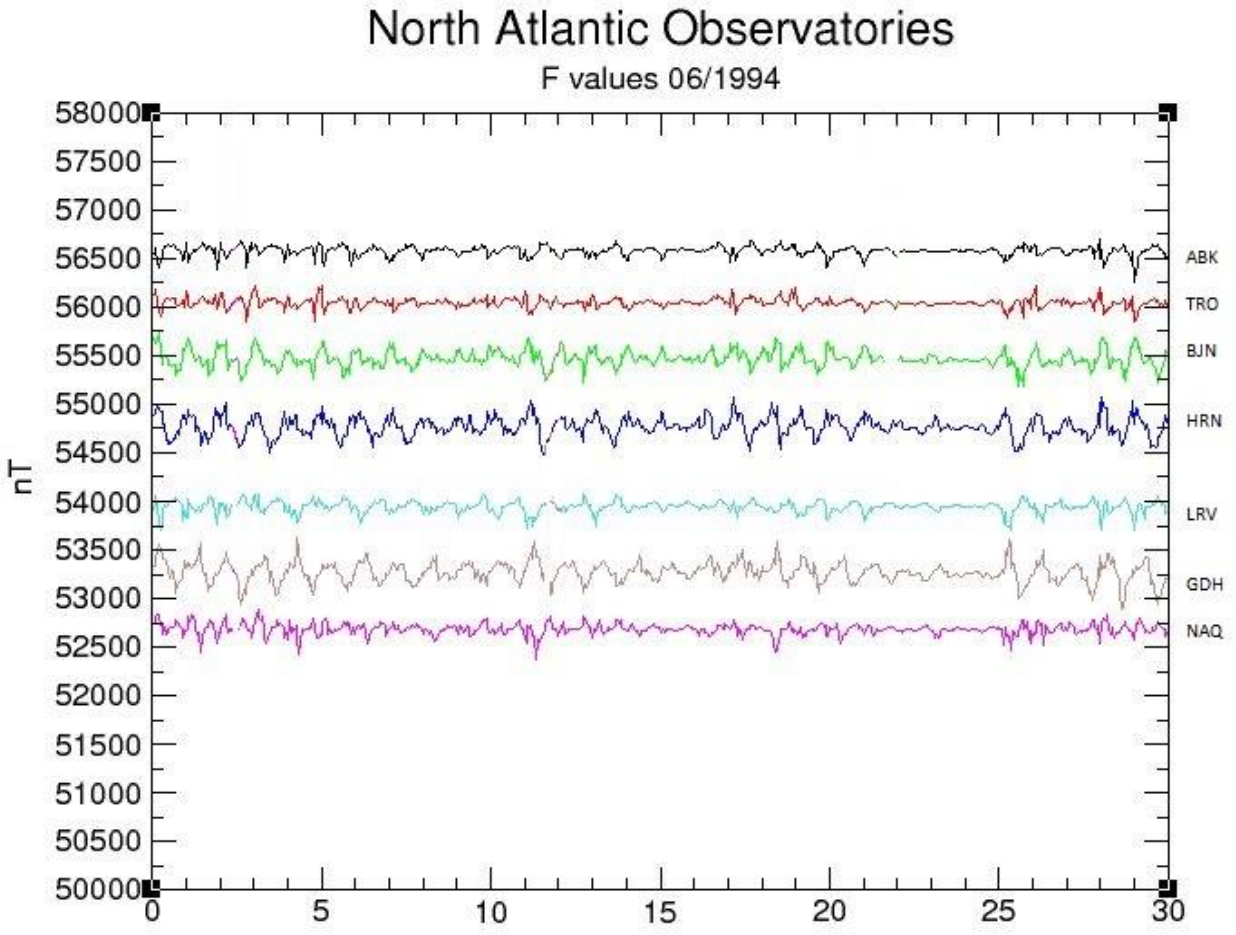

Figure 3.4 North Europe station set F values June 1994. ABK black, TRO red, BJN green, HRN blue, LRV turquoise, GDH brown, NAQ pink

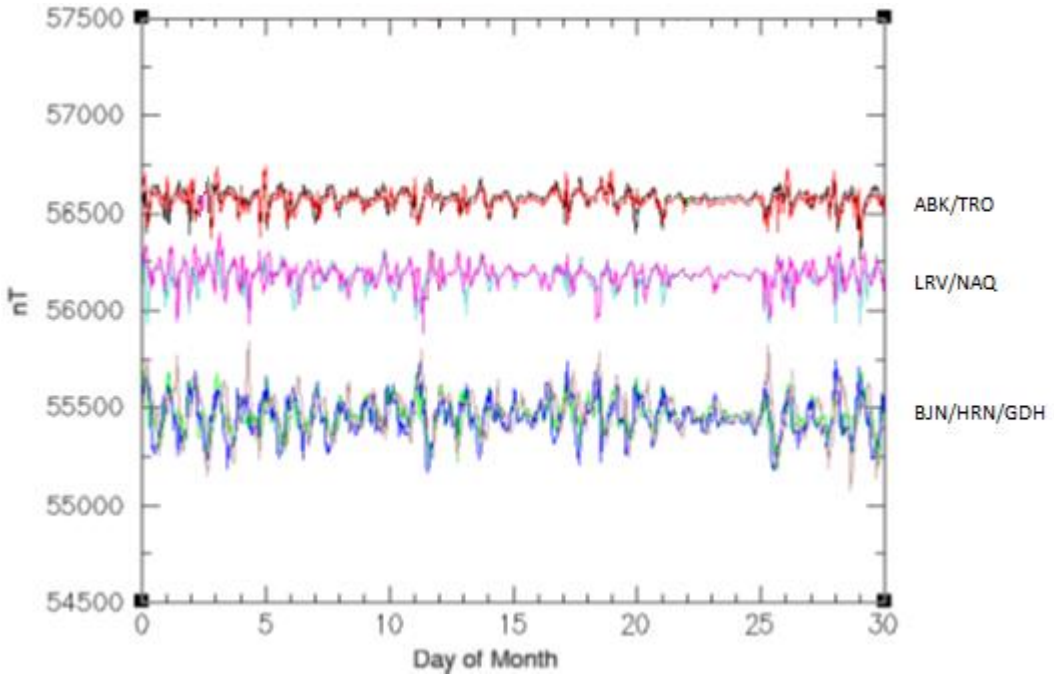

Figure 3.5 F value fits between ABK/TRO (black/red), LRV/NAQ (turquoise/pink), and BJN/HRN/GDH (green/blue/brown)

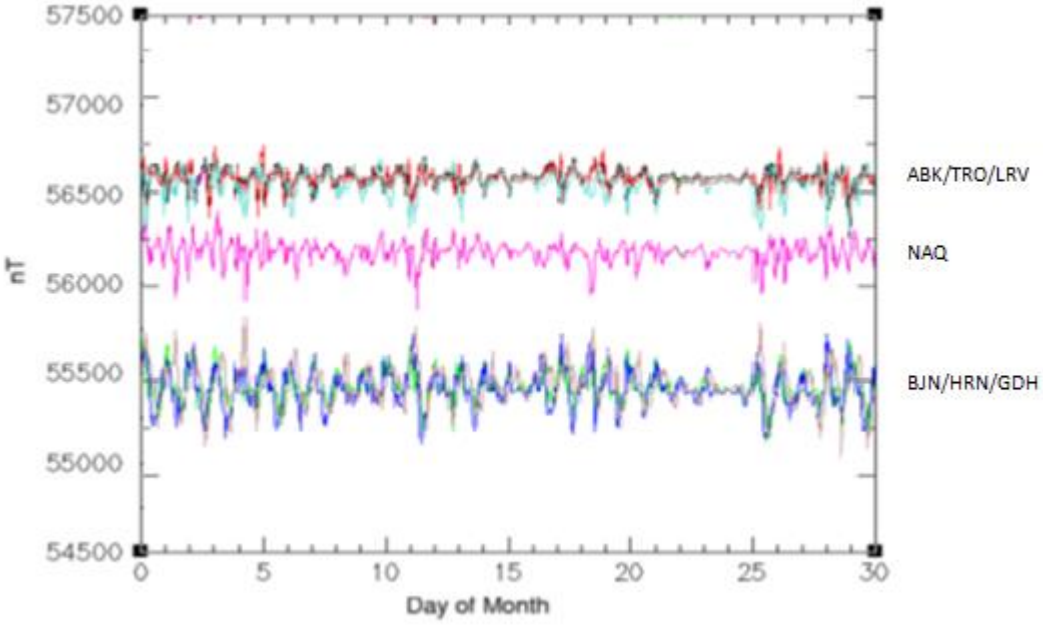

Figure 3.6 As above, but showing fit of LRV (turquoise) to ABK/TRO (black/red)

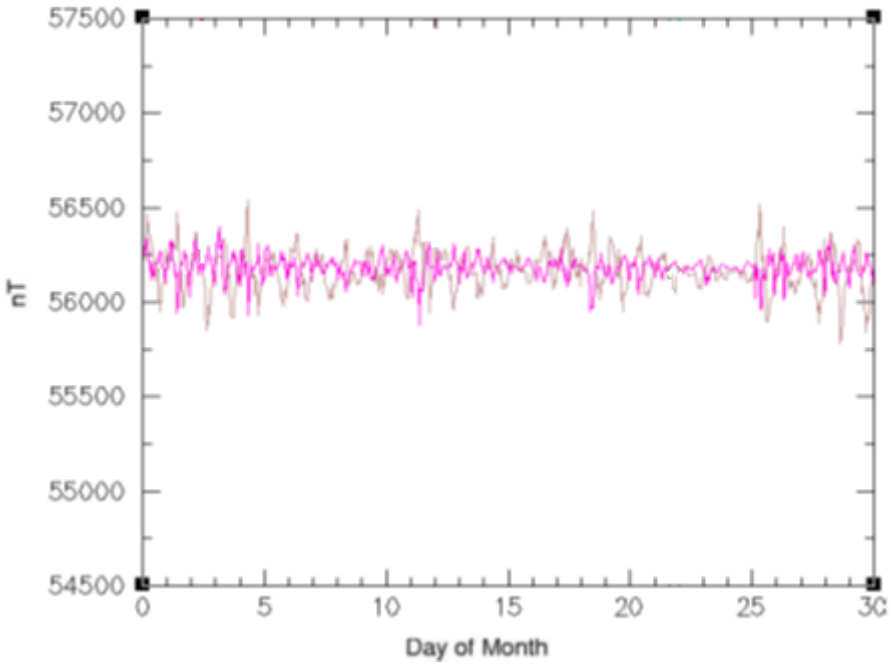

Figure 3.7 Comparison of GDH (brown) and NAQ (pink)

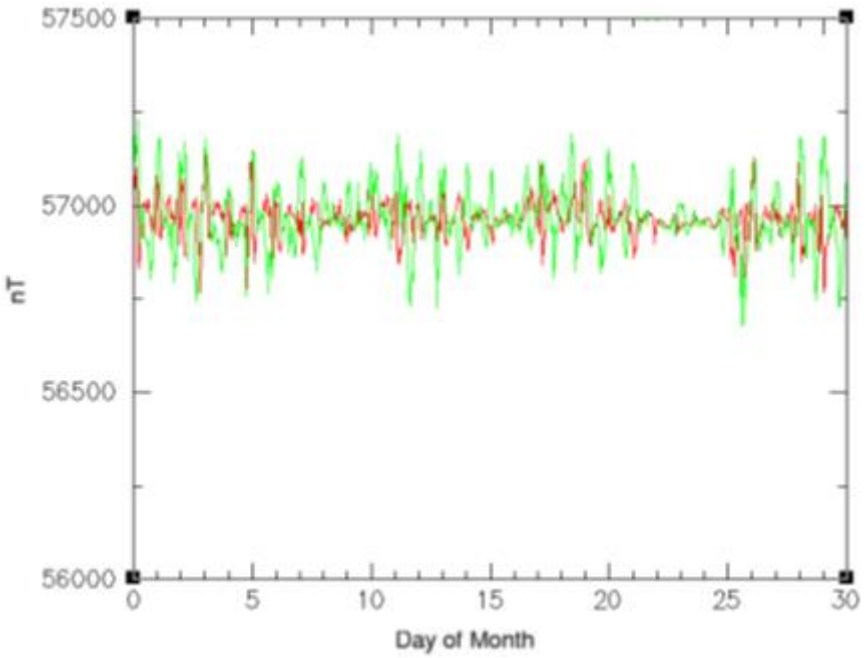

Figure 3.8 Comparison of TRO (red) and BJN (green)

For the European set, there is a north south divide, splitting GDH, HRN and BJN into a northern set, and NAQ, LRV, TRO and ABK into a southern set (figures 3.5 – 3.8). This explains why the survey initially used as an example was badly corrected by the base station chosen – the survey and station fell on opposite sides of this divide in behaviour. The angle the dividing line makes is approximately the angle geomagnetic latitude in this area makes compared to geographic, suggesting this is the reason for the differences – a latitude-related change in behaviour.

Looking at the data from the North American stations (figure 3.9 and 3.11), this pattern can also be seen, with the northern stations THL and RES being very similar to each other in both X and Z components (figure 3.10 and 3.12), southern BLC and FCC being similar, particularly in the Z component (figure 3.12) and CBB and GDH as a sort of transition between the two groups, with some features in common with both groupings. Again, the split appears to be along geomagnetic latitude. Differences between the groups tend to be in more disturbed days (the quiet period around the 20th -25th of the month is similar in all observatories), and mostly expressed as opposite sense features, as with the European stations.

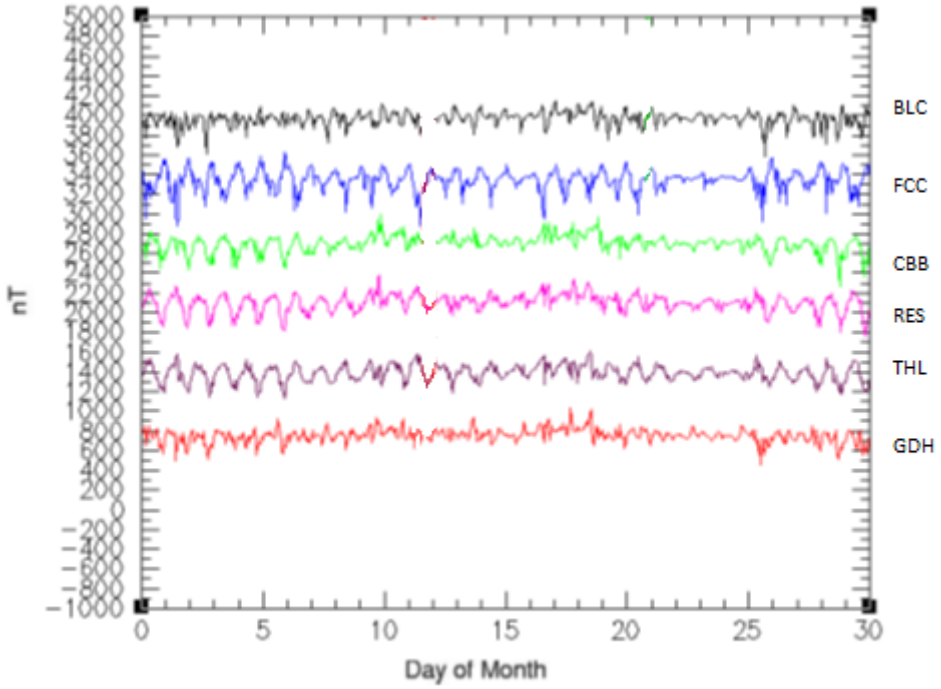

Figure 3.9 Canada/Greenland X components June 1994. BLC black, FCC blue, CBB green, RES pink, THL purple, GDH red

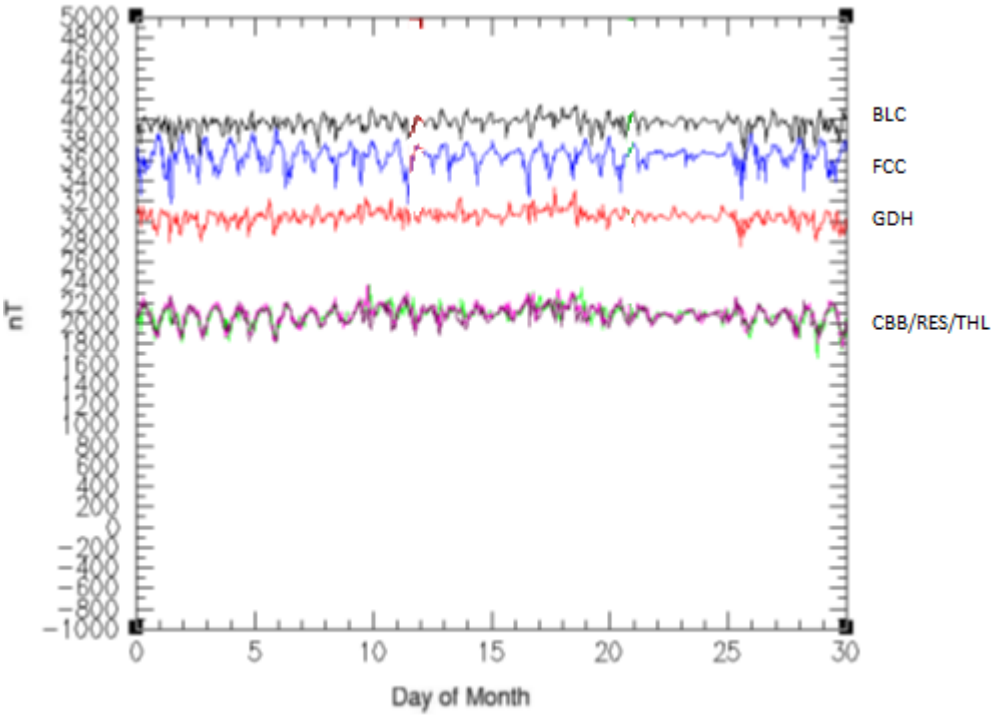

Figure 3.10 Fit matching in X component June 1994 – good match between CBB/RES/THL (green/pink/purple), similarities in FCC/BLC (blue/black) and FCC/GDH (blue/red)

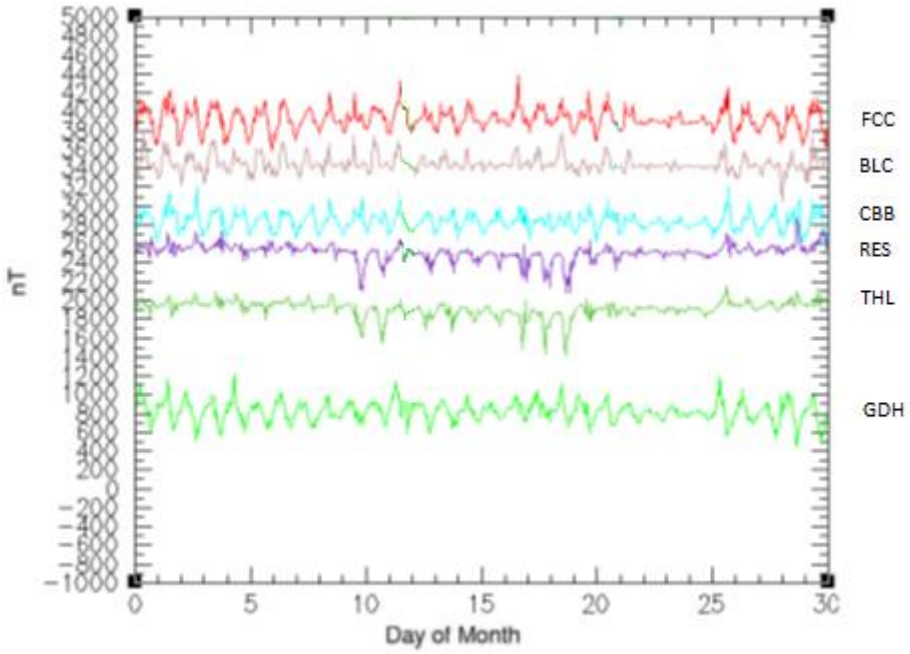

Figure 3.11 Canada/Greenland Z components June 1994. FCC red, BLC brown, CBB turquoise, RES purple, THL dark green, GDH green

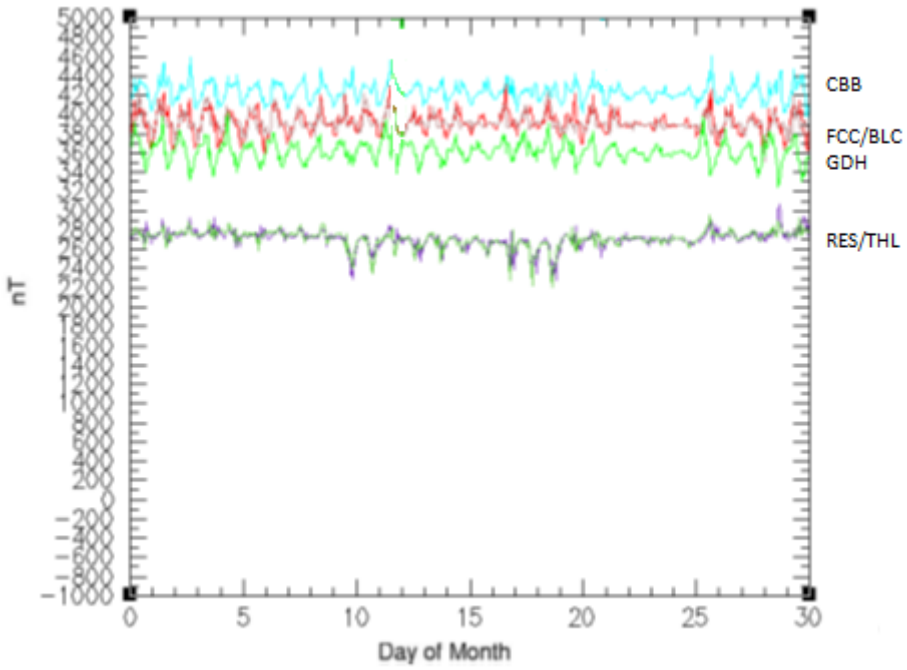

Figure 3.12 Fit matching in Z components June 1994 - good match RES/THL (purple/dark green), and FCC/BLC (red/brown); FCC/BLC also reasonable fits to CBB (turquoise) or GDH(green), which are not fit to each other

3.3 Mapping Latitude Variations

To display the data in a way that might allow the latitude split to be seen more easily, we attempted to map the variations in station behaviour (figure 3.13). An attempt to reduce the data values while keeping variations was made using the IGRF (figure 3.14). However, correcting data by subtracting the IGRF doesn't help in understanding the differences between the stations behaviour, as this involves a constant shift in the data, and all the stations have an overall 'height' of field which doesn't change – i.e. this only shows the overall strength of the field at that latitude, since the changes over the day are very small relative to the overall field strength. This demonstrates the strengthening of the overall field as the stations get closer to the pole.

To display the daily variations more effectively then, the hourly mean values for a month were stacked for each station, monthly average values for each station were calculated, and this value was removed from the data.

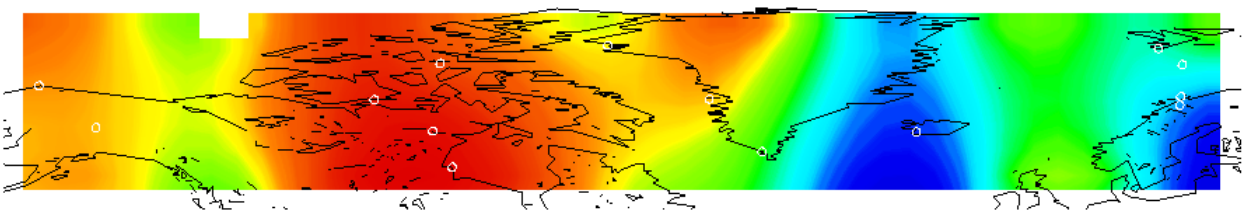

Figure 3.13 Map of F data at each station. Observatories shown as white circles

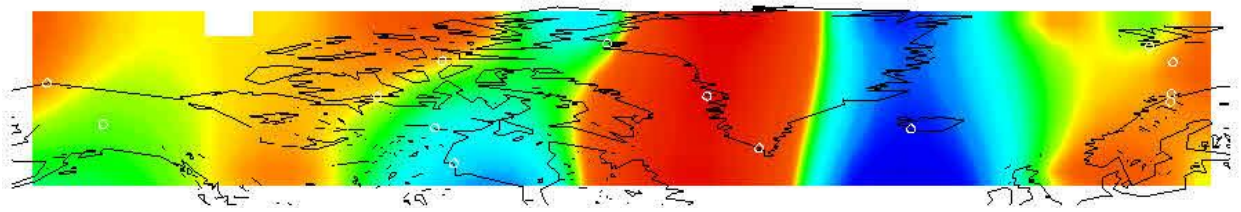

Figure 3.14 Data with IGRF removed. Observatories shown as white circles

The results are shown in figure 3.13, showing the relative change at each station through the day. Figures 3.13, 3.14, 3.15a and 3.15b contain several odd effects around the edge of the diagrams. As mentioned earlier, this is due to edge effects and the gridding method (kriging), mainly affected by the lack of complete data coverage – the missing Russian stations, and the use of only stations above a defined latitude. There are also grid-based changes where the stations are further apart – for example, the highs seen at HRN/BJN and NAQ/THL do not join across the north Atlantic, which is unlikely to be a 'real' effect. Figure 3.15c shows the probable pattern of changes without this effect. This also shows that some stations behave differently at different times of day, for example looking at the Greenland observatories, the central station GDH behaves in the same manner as THL at some points, and NAQ at others. This suggests that depending on conditions, while it is overall more similar to THL, it still has some behaviour in common with the more southern station. This also appears to be true for the HRN/BJN and ABK/TRO region – while as a whole they split into two distinct groups, there are some days or times of day when they behave in a similar manner.

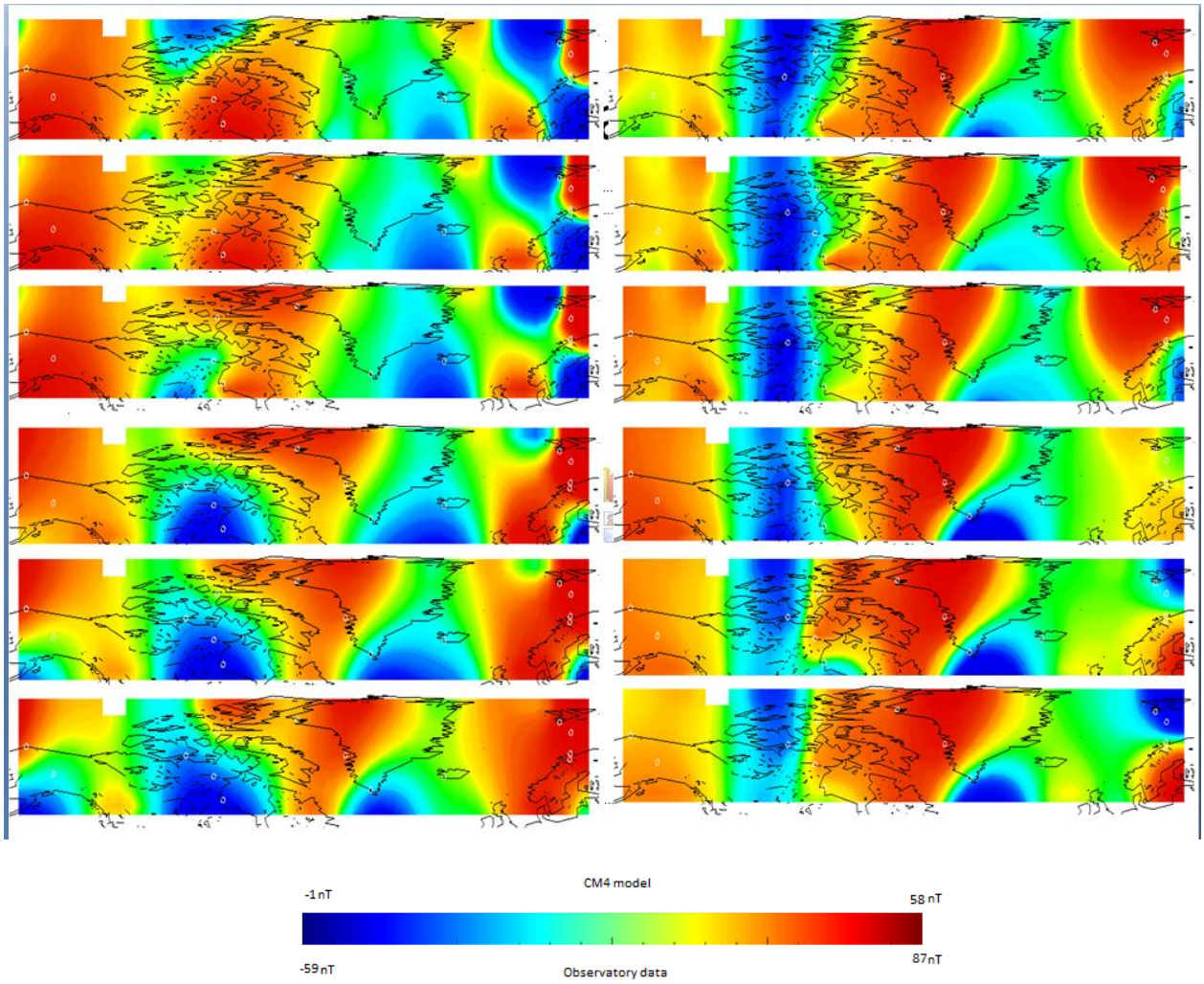

Figure 3.15a Maps showing the CM4 model (left) and observatory data stacked monthly F values with an average removed (right) for each hour time slice, from 00:30 to 06:30, minus 03:30 The model data is scaled from 58nT (red) to -1nT (blue). The adjusted data is scaled from 87nT (red) to -59nT(blue). The difference in scale is approximately the same as the amplitude misfit in CM4. The Sq pattern of variation in CM4 is similar to some observatory data, but does not show enough amplitude change in this region -the difference in scaling roughly accounts for this, enabling comparison of the behavioural trends

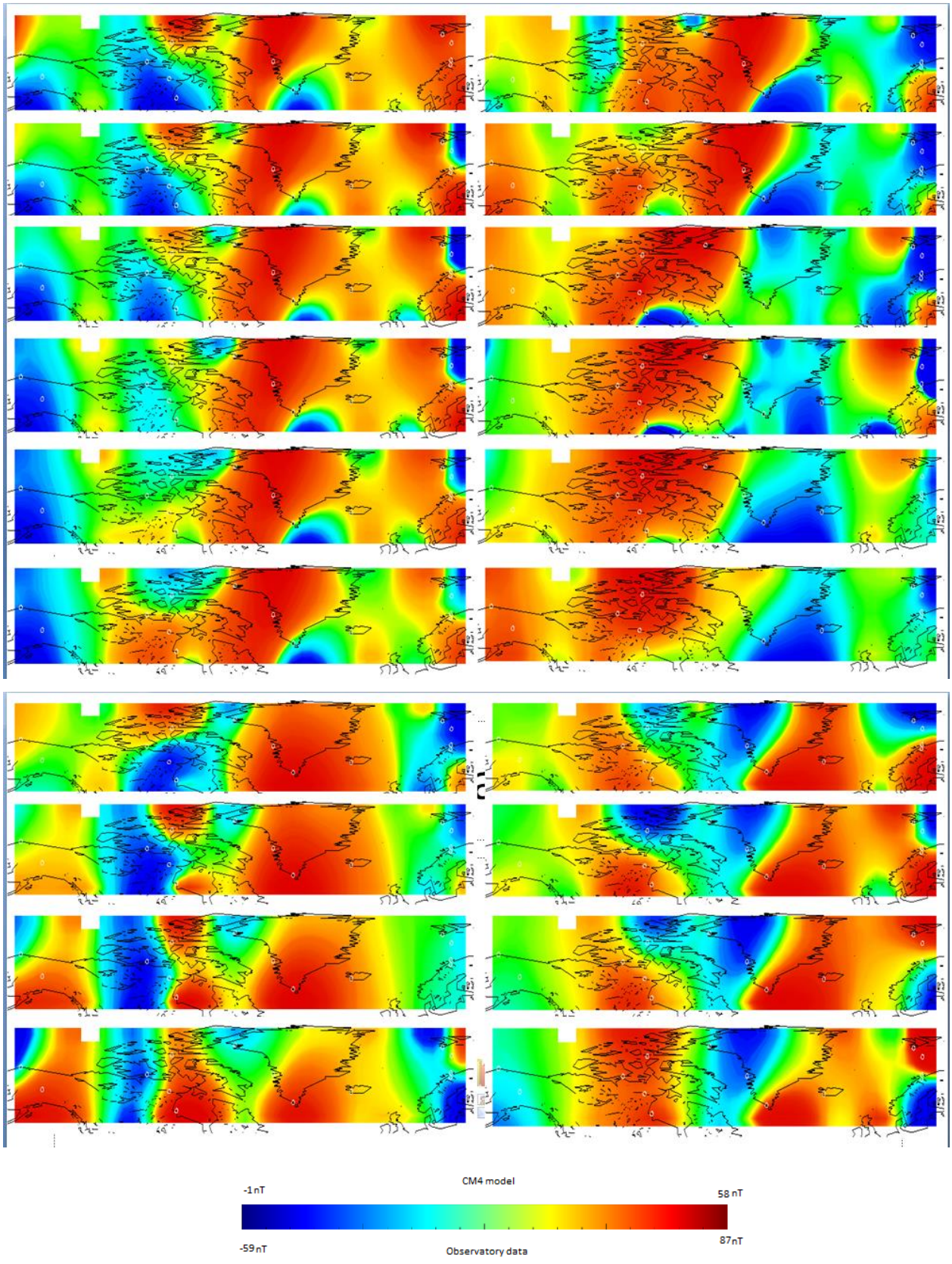

Figure 3.15b Maps showing the CM4 model and observatory data (adjusted) values for each hour time slice, from 07:30 to 22:30. The model data is scaled from 58nT (red) to -1nT (blue). The adjusted data is scaled from 87nT (red) to -59nT (blue)

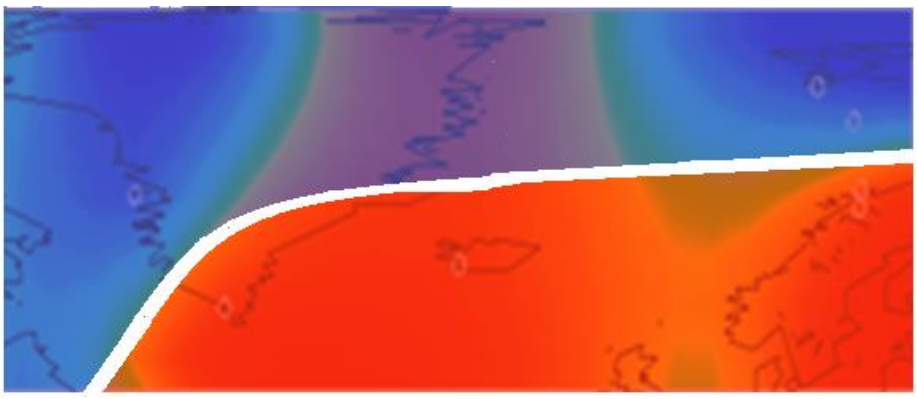

Figure 3.15c The probable approximate location of the split in behaviour across the Atlantic (ignoring gridding effects). Overlay on observatory data from 19:30; the position (and likely the shape) of the dividing line moves through the day.

These results show clear variations in behaviour between latitudes, particularly when comparing the Greenland observatories – when using these stations to correct surveys, there is a definite need to choose the base station location carefully to avoid potential mismatches, and therefore the risk of not correcting data properly, or indeed not being able to correct it at all. This should also remove the possibility of data showing opposite sense peaks (spikes in one station recorded as troughs at another, etc.), as generally stations in the same grouping show the same sense, however if the survey or station are close to a boundary there may be an intermediate stage (as the distance between stations prevents the establishment of exactly how sharp these divisions are) and this could potentially create a situation where something like the overall behaviour of one group is recorded, but with the short period behaviour of the one next to it.

This also translates well to the mismatch of amplitudes generated by CM4, likely due to missing physics in the model– aside from VAL, which may be due to the coast effect, northern stations were consistently noted as having higher amplitudes than the model suggested, while mid-latitude stations were well matched by those in the model data (see chapter 2.1). This also shows that in the high latitude region, CM4 should not be used as a basis for determining these latitude groupings – the model does not see them.

This comparison also shows that while BJN is located on a smaller island than HRN, which is probably showing a true coast effect, this doesn't affect the grouping – BJN still behaves like HRN, but has slightly larger amplitudes and tends to react to disturbed days more than might be expected. Since there is also likely to be some coastal effect at a lot of these high latitude stations, as many are coastal or on islands, it is not easy to pick that specific effect out using this method. It is more noticed in that BJN has a different **model**, rather than the data; this results in CM4 model data separating its behaviour from the other nearby stations (HRN, ABK, TRO) rather than showing the pairs seen in the observatory data. The comparison of increased model components (chapter 2.3)

shows that islands generally have larger variations than inland observatories, and coastal observatories tend to be higher still – but equally, that magnetic latitude (location in the Arctic region) has a similar effect, even for inland stations. If we were to be looking for coast effect in these stations, it would probably be best to compare BJN to ABK, since this would compare an island station with the closest properly inland station; however, this would involve comparing between different latitude sets- thus complicating matters; what is due to which effect?

The maps here are poor methods of comparing the behaviour of the North American stations; while it may be seen which are behaving in a similar manner to the Greenland stations, or if they are all behaving in the same manner, the effects of the gridding cause problems with this type of display. This is probably also confused by the location of the pole within this area – the European observatories are easier to see differences in due to the angle of magnetic latitude in this area, for Canada/N. America, the angle is varying much more substantially, and station coverage would need to be much denser to see variations.

Looking at stations from northern Europe, Greenland and North America, we can see trends in behaviour running both north-south and east-west. It is probable then, that the trends could be traced round into groups on magnetic latitude; it was not possible to test this completely due to unavailability of data from the Russian Arctic regions, and the requirement of denser station coverage to reduce gridding effects.

3.4 Group trends and Short Period Features

Magnetic latitude has a consistent effect on the behaviour of the field, so unless one was attempting to use a base station well outside of the region being surveyed (not a recommended action at the best of times), it is not necessary to correct for it – however, the patterns of behaviour across the region are more important to understand, since locating survey and base station in different regions can have a large impact on the effectiveness of the correction. The correction required therefore is less to remove the effects of high latitude, but to be able to define a method of adjusting data from different regional groups so it can be used in other locations. This involves understanding how the changes between these groups manifest – and also what remains the same. The CM4 model is not so useful for this, since it is only designed to fit well for days of very little disturbance, and while it does seem to perform better than might be expected on days of higher disturbance, the amplitudes it

gives may still be too low (particularly for the Z component) as stations move further north. There is a trend to higher amplitudes and greater response to disturbance in the field as station location moves northwards. There is also a tendency for some features of the variation to act in the opposite sense – e.g. peaks in the data recorded at a more southern station becoming troughs in a northern one (e.g. TRO/BJN, GDH/NAQ, figure 3.16). Some short period features can be used to correlate between stations, as they are recorded at most stations and change orientation between the latitude groups. However, care must be used in this, as some features seem only to be recorded in localised areas.

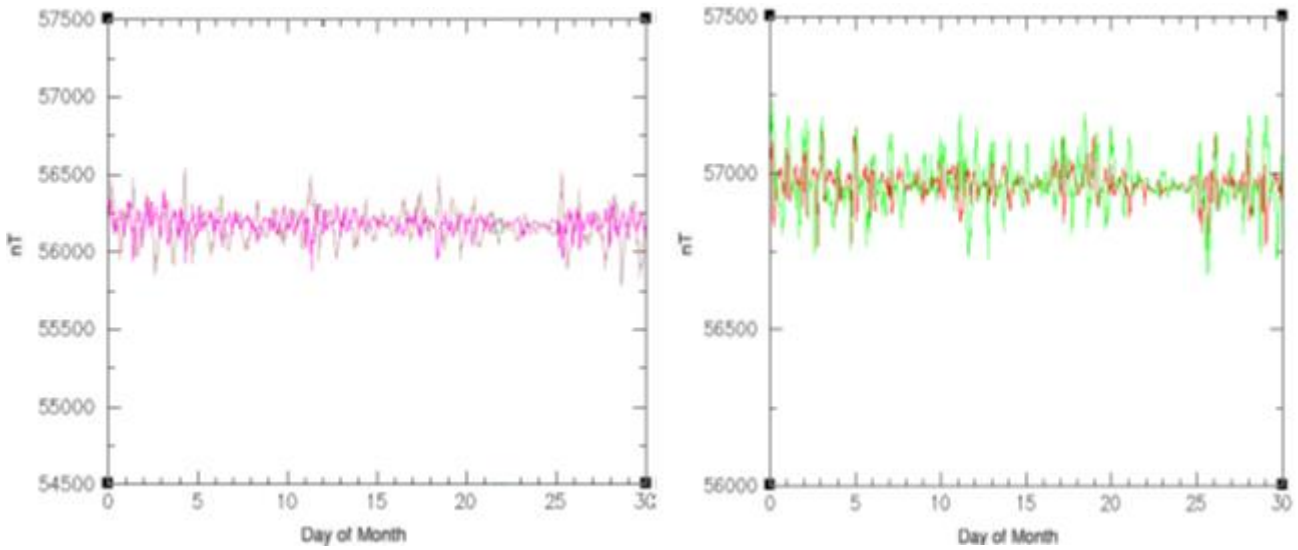

Figure 3.16 F value comparisons at GDH/NAQ (brown/pink) and BJN/TRO (green/red)

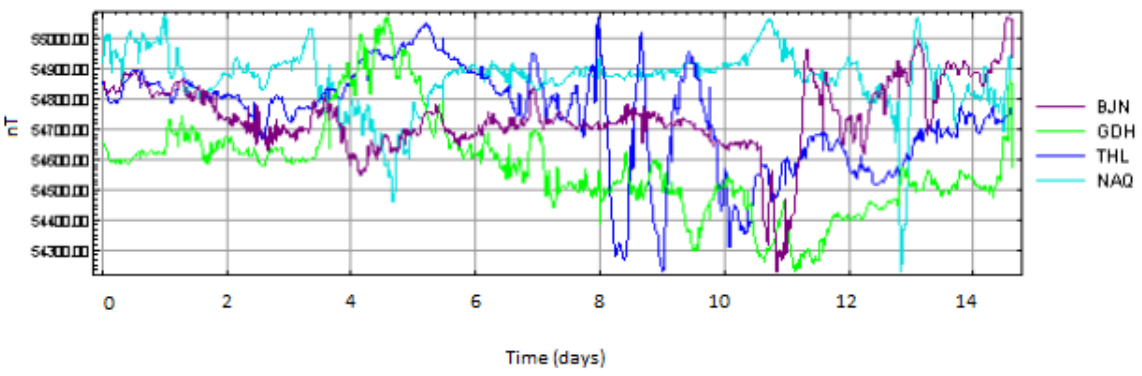

Figure 3.17 Minute F value data from part of July 2006 at BJN, NAQ, GDH and THL, showing short period and longer period features in opposite senses between station groupings. This is particularly noticeable at, for example, GDH and NAQ between days 4-6 showing opposite sense behaviour, and at around 6.8 days, where NAQ does not show the peak seen at the other three stations.

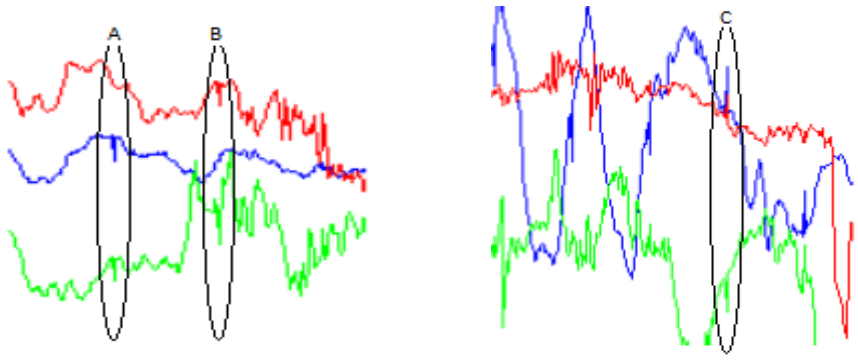

Figure 3.18 BJN (red), GDH (green), and THL (blue) (zooms of above diagram) showing short period features more clearly. Some are not seen at all stations (e.g., a spike seen at GDH and THL but not BJN (A), and one at BJN and GDH but not THL (B)). Some are in opposite senses (C shows a spike seen positive at BJN and THL, but negative at GDH). These features are a few minutes long.

Figures 3.17 and 3.18 show some of the differences between station groupings – as short period features (each around five to ten minutes long) can be seen in data from the Greenland stations and Bear Island, showing features not recorded at all stations, or in opposite sense at some stations. Occasionally these features are not recorded instantaneously by all stations, instead showing lags of up to 10 minutes. Lags in features appear to progress westwards, with delays of up to ten minutes. These only tend to occur with very short duration features, and on the most disturbed days, otherwise lags don't tend to happen- short period features occur simultaneously across a particular area. Sometimes these are 'apparent lags', due to the amplitude of the spike being very different or in the opposite sense at another observatory, rather than a true lag (an apparent lag of ~ten minutes, may actually be that the ten-minute duration event has changed sense, and the next wiggle has been picked as the spike instead).

3.5 Correlating High Latitude Stations

If the difference between stations is due to a non-persistent effect, then it is likely that it will only need to be adjusted for a few hours to a few days, however the changes between groupings are likely to warrant changing all data recorded at the station in order to give a match between the two. It must also be noted that stations with large differences in longitude will need adjusting to use as comparisons, as they will be experiencing different parts of the Sq cycle. If the stations do not have a large longitude split, this will be unnecessary.

Qualitative comparison suggests that the station groupings are quite different from each other, though with some similarities. They tend to record at least some short period features at the same or

similar times, though they may be in opposite senses between groupings. There are also times (especially very quiet days) where station groups seem less distinct, and stations behave more like each other, particularly where these are stations that are closer to each other (e.g. NAQ/GDH, or BJN/TRO). These similarities imply that the stations are all recording some part of their daily variation in the same way, while the groupings show where the recorded field contains effects that vary with latitude. Some results trying to separate/correct for these effects are shown below.

The variation in behaviour between latitude groupings in the Arctic region is most clearly seen in the northward trend of the Scandinavian stations ABK, TRO, BJN and HRN, and can be extended out to other stations in the region. This allows an initial choice in base station to be made more effectively – the station and the survey should fall into the same group in order to show the same variation pattern. It also allows tests to be made to relate stations to each other, in much the same way as with NGK and VAL. In this case, the differences between the stations are not primarily due to the coast effect (many of the Arctic stations are located on the coast, due to the location of settlements/accessibility of terrain) but rather due to the observatories proximity to the geomagnetic pole and the effect of the auroral electrojet. Stations in this region are also much more sensitive to disturbance in the field (see chapter 2), as the polar regions of the geomagnetic field contain areas of increased disturbance, manifesting as polar ionospheric currents and the auroral oval. The geomagnetic field also increases in strength towards the poles, so any externally induced field generated in this region will be proportionally stronger than those at lower latitudes, thus likely to have more of an effect on the data recorded here.

KIR and HRN were chosen for this study, as they are located away from the probable location of the group boundary in this area. The initial RMS misfit between the two observatories is 94.92nT. Looking at DFTs of KIR and HRN (Z component, figure 3.20), it can be seen that there is more power in the 24-hour peak at HRN, so one correction could be to add in a 24-hour cosine wave. However, this is not enough to fit the two stations; even with an additional 24 hour signal they would still be quite different from each other (RMS misfit of 94.55nT with the increase). Looking at the days from the 6th to the 9th of May 2009 (since the disturbance here makes it easier to compare qualitatively), a double peak is seen in one station, but a double trough in the other – the two stations appear to mirror each other (figure 3.19). Flipping the orientation of data from one station (by multiplying the data by -1 and then adjusting the level back up by adding a mean value to all data; in this example, KIR, figure 3.21, is changed) shows that this is indeed the case – the flipped station data matches quite well to the general shape of daily variation at the other (this also reduces

the RMS misfit to 57.16nT – a large drop from the initial misfit). This is not perfect – further correction would be required – but is an interesting first step. It also agrees with previous findings that increasing external field components, particularly the induced elements thereof, results in a mirror of the data pattern. This would fit with the idea that the difference between these stations is due to latitude and to either the auroral electrojets or similar ionospheric currents that are not seen at lower latitudes. This could be due to an ionospheric current passing between the two stations, and the induced magnetic field surrounding it being symmetrical but opposite on either side (using Ampere's right hand grip rule, if the current flows to the west, the magnetic field generated around it will be 'up' to the south and 'down' to the north, but otherwise identical). Short duration spikes seen at both stations match in time, but one set is in opposite sense in the flipped data – peaks in one dataset and troughs in the other. If we want to match all of the signal between these stations then, not all of the signal must be changed in this way. There also appears to be an additional set of these spiky features seen at KIR that is not seen at HRN. HRN and TRO June 1994 shows a similar partial anti-correlation in the Z component. The partial anti-correlation (fitting of flipped data) (figures 3.19 and 3.21, most obviously between the 7th – 9th of the month) again implies that induced fields are part of the difference between these station sets, but also that this is not changing the data entirely – some parts of the signal are still as 'normal' at both sets of stations. Flipping of X at HRN also correlates quite well with Z at TRO. That the X and Z components match is likely at least partially due to a coast effect at HRN, since the coast effect raises the values of the vertical

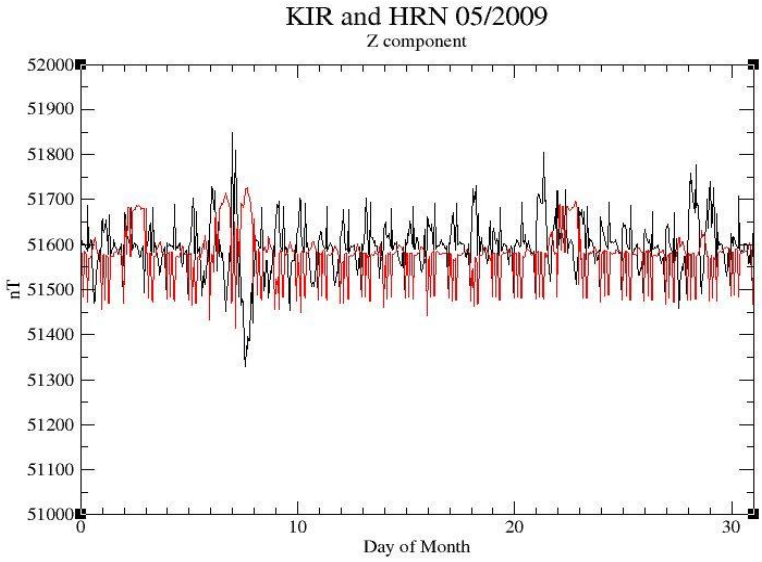

component in proportion to the horizontal component. (Parkinson and Hutton 1989; see chapter 5.3)

Figure 3.19 Comparison of Z component data from HRN (black) and KIR (red)

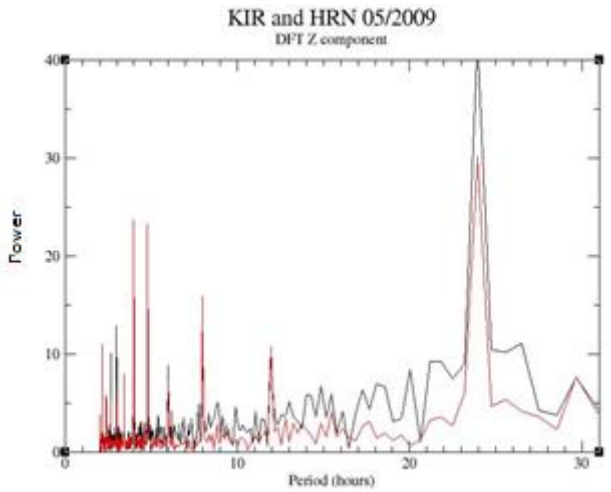

Figure 3.20 Comparison of DFTs of HRN (black) and KIR (red)

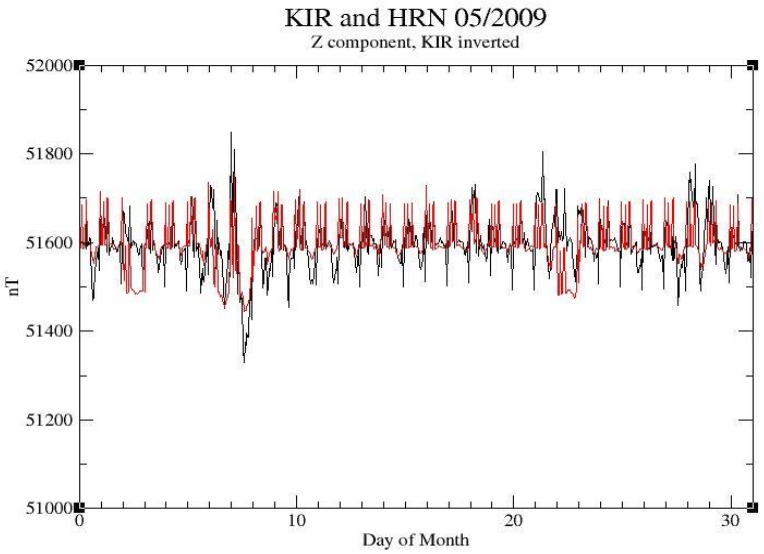

Figure 3.21 Comparison of Z component data from HRN (black) with flipped data from KIR (red).

We also attempt to correlate between NAQ and THL (figure 3.22), using data from June 1994, since these stations are similarly located in different latitude groups (NAQ possibly falling into the same band as KIR in the above example). The initial RMS misfit is 167nT for the X components, and 107.13 for the Z components. Y components at the two stations are very similar, but the match is improved with an 8-hour time shift (THL +8 hours/NAQ -8hours). A similar effect is seen in the X components, but with a 9/10-hour shift (figure 3.23), this shift produces and RMS misfit of 93.04nT. Flipping X component data from THL (figure 3.24) also produces a good match between the stations, and lowers the RMS misfit to 82.79nT. Z components do not seem to have any obvious correlation (or anti-correlation) between the two stations, though flipping Z does produce a better fit between the two stations on the quieter days of the month (e.g. the 23-25th, figure 3.25), with an

RMS of 104.19nT.

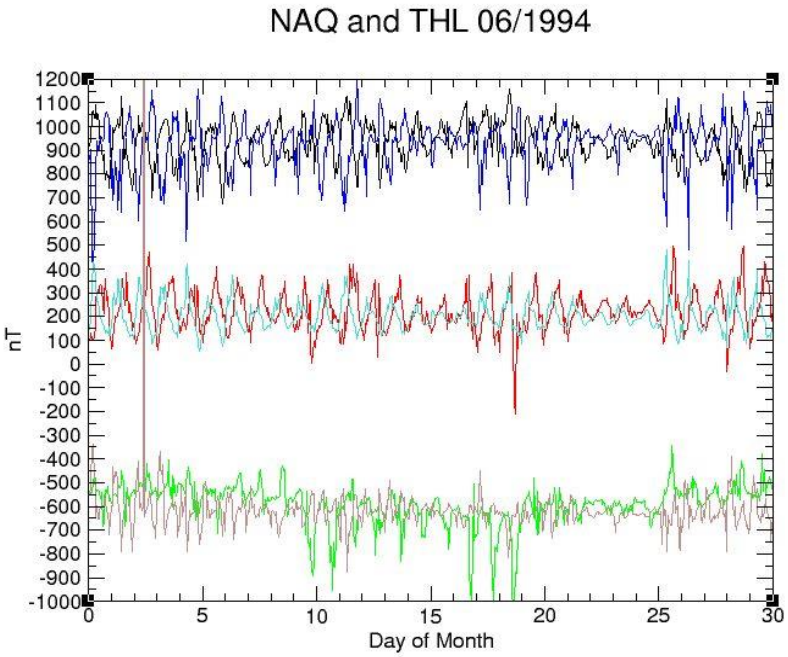

Figure 3.22 Comparison of data from June 1994 for NAQ (X blue, Y turquoise, Z brown) and THL (X black, Y red, Z green)

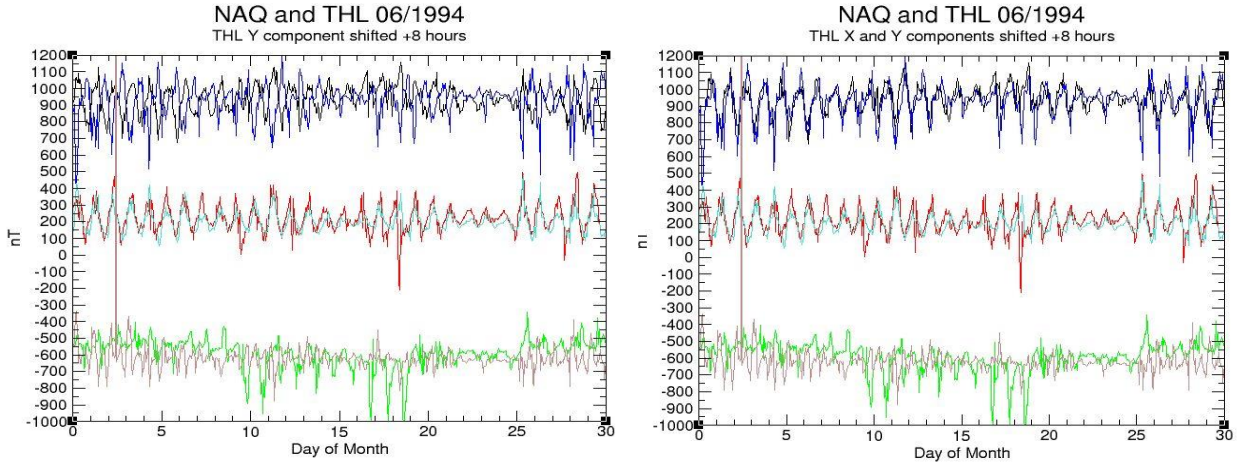

Figure 3.23 Time shifts of THL X and Y components, showing the improved match between the stations

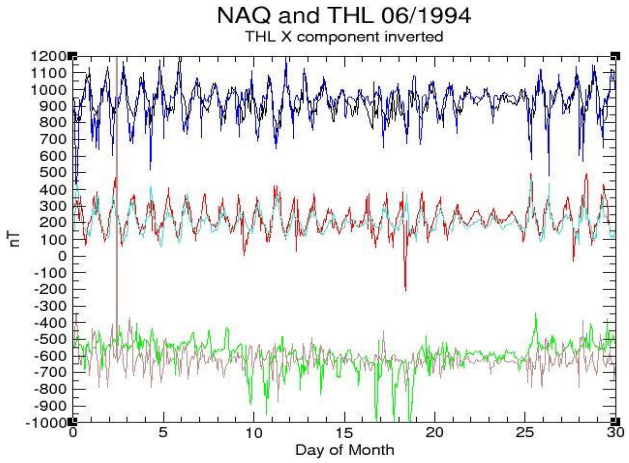

Figure 3.24 Inversion of THL X component, showing improved match between the stations

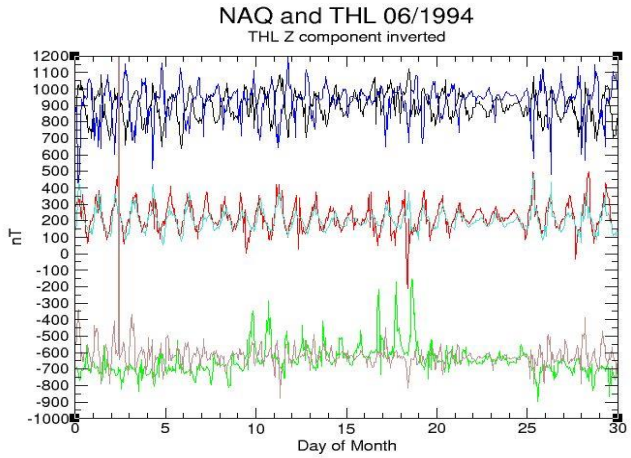

Figure 3.25 Inversion of THL Z component, showing some improvement in correlation, but generally poor match

Since flipping the data from one set of stations produces partial correlations with stations from another set, some of the differences between the high latitude groups are likely due to induced fields, as inversion of the Sq pattern was seen in model data with increasing induced contributions (chapter 2.3). The inducing currents are likely related to the auroral electrojet, and other ionospheric currents in the region. Not all of the fit between the groups is improved by flipping data, showing that some of the data recorded is still primarily due to the main field and not induced fields, so this method does not result in a full ability to correlate data between these observatories, however further work taking into account the induction might be able to define a method of correlation based on this observation.

Results

The previous chapter shows that CM4 cannot model all behaviours in high latitude regions. This section aimed to establish what it can do, and what other observations can be used to aid remote correction in this setting.

The survey considered in section 3.1 showed that, while the base station used could not correct the survey data completely, it was behaving as expected from its CM4 model Surveying other observatories which might have been chosen for the base station showed that while the station used was located at approximately the same geographic latitude as the survey, the offset of the magnetic and geographic poles places it at a different magnetic latitude. A base station located at the same magnetic latitude might have had more success in correcting the survey.

This led to the finding of distinct, latitudinally split, groupings in observatory behaviour in the arctic region. This is seen in both the overall Sq pattern in a month long data series, and in much shorter, minute period variations superimposed on this variation. In particular, some features/observatories seem to display mirror images to data recorded in adjacent groups. Comparison of pairs of observatories in this region was used to try to find any potential method of correlating between these groupings, or correcting for the difference – which would be useful for surveying should the only available base station locations be in a different grouping to the survey location. KIR and HRN show that flipping the data from one station creates a good match to the other; this is also seen at NAQ/THL. Both of these pairs, and HRN/TRO also show partial correlations between X component at one station with Z component of the other. These observations, combined with work on CM4 components in chapter 2 which shows increased induced components can change the phase of the resulting model, suggest that the groupings in this region could be due to the influence of magnetic fields from, or induced by, ionospheric currents. Greater knowledge of these currents and the exact changes seen might result in a better description of the boundaries of the behavioural groupings, and an improved method of correction in the arctic region.

Chapter 4. Disturbed Time and Geomagnetic Storms

Having previously established that CM4 can model for a higher level of disturbance than expected, and that disturbances can be correlated between stations, we now look at the larger disturbance events – geomagnetic storms. Geomagnetic storms often lead to loss of data from magnetic surveys, as information collected is rendered unusable by the storm effects, which are far larger than normal Sq values or any target anomaly. We look for trends in the behaviour of various observatories during geomagnetic storms, and attempt to identify where data may be retrieved from these periods, either through use of models such as CM4, or other methods of correction.

4.1 The Disturbed-time Field

Magnetically disturbed periods are due to higher levels of activity in the Sun, linked in a large part to the 11-year sunspot cycle. Times of high sunspot activity are correlated with higher levels of disturbance in the geomagnetic field (Allen 1944, Papitashvili et al 2000), since their presence increases the likelihood of space weather events, due to increasing the occurrence of solar flares, increasing the overall radiance of the sun, and the decay of sunspots causing greater variation in the solar magnetic field. The field variation is due to the expulsion of toroidal fields which create the sunspot, the flux from which is then mixed by turbulent flow of the solar atmosphere across the area; and also due to the peak in sunspot generation coinciding with reversal of the solar poloidal field. Increased numbers of sunspots therefore make it more likely that patches of south oriented magnetic field can be transferred out to the Earth by the solar wind. Years in which sunspot activity peaks therefore tend to have more geomagnetic storms occur. The solar wind is the stream of charged particles constantly emitted by the Sun, mostly consisting of protons and electrons. The geomagnetic field deflects most of these particles, but some become trapped in the Van Allen belts, and others manage to enter the Earth's field, often deflected towards the auroral zones. The Sun is also constantly emitting electromagnetic radiation on all wavelengths. The radiation is most commonly thought of as visible light, but it also emits high energy ionising radiation (UV, X ray, etc.) and lower frequencies such as infra-red and radio, and various interactions of this radiation with particles creates radiative heat. Gamma ray radiation is generally not emitted beyond the Sun itself (gamma rays are generated by nuclear fusion in the core, but they are mostly absorbed internally) except in the creation of solar flares and coronal mass ejections (which may be thought of as 'super flares', in the sense that they emit far more energy and particles, over larger areas of the solar surface). High energy radiation does not penetrate the Earth's atmosphere, instead being

absorbed at high altitudes, mainly in the thermosphere, except some longer wavelength UV, which is not absorbed, but scattered. The radio waves emitted that reach the Earth with a wavelength of 10.7 centimetres are used to create the F10.7 index, which is used as a proxy for solar activity levels for longer period variations (such as sunspot activity cycles), which is otherwise hard to quantify. Increased solar activity leads to the solar wind becoming denser, faster, or more highly polarised (or any combination of these three). It also increases the potential for solar flares or coronal mass ejections, which gives a specific, strong boost to the solar wind, and causes much more of a response in the geomagnetic field if the Earth is in the path of the flare. Particles leaving the Sun have the magnetic flux of their origin location locked into them as they are emitted; this means the solar wind arriving at Earth may be either north or south polarised, and the dominant polarisation varies in relation to both the rotation of the Sun and the Earth's orbital position. Since the solar magnetic field is much more complicated than that of the Earth, with varying polarities present on its surface and a much faster rotation period, the polarity of solar plasma arriving at Earth varies in polarity over time. If the wind is carrying south polarised charge, it reacts strongly, and more easily, with the polarisation of the geomagnetic field, coupling more easily and creating greater amounts of disturbance. Any of the types of more active solar wind may result in the breaking of magnetic field lines and their later recoupling, allowing solar particles to enter the magnetopause, and also allowing atmospheric particles to be removed and enter the solar wind. This may generate additional currents in the upper atmosphere, or strengthen existing ones. It also changes the composition of the ionosphere, mainly in terms of the amount of charged particles (the solar wind is almost completely made up of charged particles, while regions of the upper atmosphere are incompletely ionised), but also the type of particle, since the plasma making up the solar wind is of a different composition to the atmosphere, which is mostly heavier atomic or molecular gases, unlike the protons and electrons of the solar wind. Influx of charge into the upper atmosphere (and the resulting magnetic reconnection process, where lines of magnetic flux break and rearrange, allowing energy to be released and solar plasma to enter the magnetosphere) is responsible for many of the variations in the behaviour of the geomagnetic field, the largest of which are termed geomagnetic storms and substorms (Campbell 1997, McPherron et al 2013).

The most visual effect of the entry of solar particles into the geomagnetic field is the presence of auroral activity. Aurorae are generally produced within two bands circling the poles, called the auroral ovals. These bands are around 5^{o} wide, located 10-20^{o} from the geomagnetic poles, and centred towards the night side of the planet (Campbell 1997). Aurorae are present at quieter times, as well as times of disturbance, and the normal interaction of the solar wind and magnetosheath can

cause charged particles to be precipitated from the radiation belts in the upper magnetosphere. However, during the squeeze/break/recouple process of field lines forced by higher activity solar activity it is easier for large amounts of plasma to be inserted into the magnetosphere from the solar wind, greatly enhancing the auroral effect. In normal, relatively low-disturbance periods, aurorae are seen within the auroral ovals; however additional disturbance (the presence of additional charged particles) expands the oval. At storm times, this may extend down into mid latitudes, and cause exceptionally bright aurorae to be seen. In either case, the charged particles entering the atmosphere are funnelled towards high magnetic latitudes by the field lines, and when they interact with other particles, and excite them, causing emission of visible light radiation. The colour of light emitted is determined by the type of atoms that are being excited- high altitude atomic oxygen emits red light, at lower altitudes atomic oxygen and nitrogen emit green light, and lower still molecular nitrogen emits blue light. Green is by far the most common of these, since the majority of particles are at this altitude. Most aurorae are therefore green in colour.

Of course, aurorae are only the effect that can be seen visually. The flow of additional plasma also generates and adds to currents flowing in the ionosphere, particularly (in the case of magnetic storms) the ring current (figure 4.1). The increase in the strength of the ring current creates a corresponding low in the horizontal components of the magnetic field; this is the effect measured by the Dst index. The flow of bursts of charged particle into high latitude regions induces magnetic fields which interact with the main field, creating short period disturbance effects in the field. The larger the amount of particles involved, the stronger the effect is, hence why the large solar emission of flares or coronal mass ejections are often associated with geomagnetic storms, as is southward polarisation of the solar wind. The breaking and recoupling of field lines that occurs so much more easily and more often with southward polarisation allows far more particles to enter the magnetopause. These effects are also more likely to extend globally, compared to small injections, which may affect only the polar regions if funnelled there, or have a much subtler effect as they disperse into various current streams. Increased particle density in high latitude regions is also likely to affect the auroral electrojets, since these are also driven by current flow (McPherron 2013, Richmond 2002, Lanza and Meloni 2006).

The auroral electrojets (figure 4.2) are large horizontal currents flowing in the ionosphere in the auroral regions (Campbell 1997). While horizontal currents may flow in the ionosphere at any latitude, the auroral electrojets are particularly strong and persistent currents. This is due to the higher conductivity of the auroral region compared to lower altitudes, since it contains more

charged particles (partly due to particles funnelling along magnetic field lines), and the horizontal electric fields of the ionosphere being stronger in the auroral region. In disturbed times, the electrojets increase in strength, due to the influx of solar charged particles enhancing the conductivity still further, and the electric fields increasing in strength, and the electrojets also expand in extent, both to higher and lower latitudes, as the auroral oval does. Large influxes of solar plasma also inflate the ionosphere, both due to the addition of new particles, and the extra heat generated by emission of radiative energy as particles collide and are ionised or otherwise excited. This expansion of the ionosphere outwards into the magnetosphere allows more particles to be captured by the solar wind, and also adds to the distortion of the magnetic field (Pirjola 1998). The effect of additional solar plasma fades as the energy input is transferred by radiation (or atmospheric particle loss) back out to space or taken up in particle interactions, and 'loose' electrons and protons re-combine in the upper atmosphere. How long this takes is dependent on how much solar plasma is introduced, and for how long, as well as how energetic the particles are (how much energy needs to be lost).

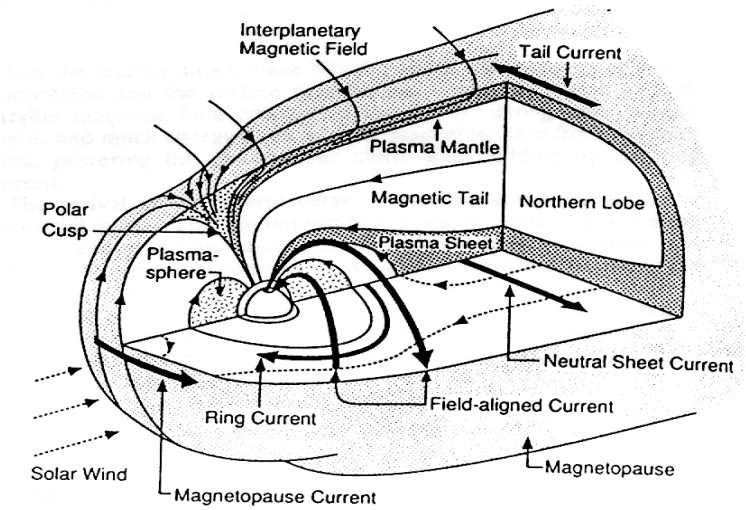

Figure 4.1 Current systems in the magnetosphere (from Russell and Luhmann 1997)

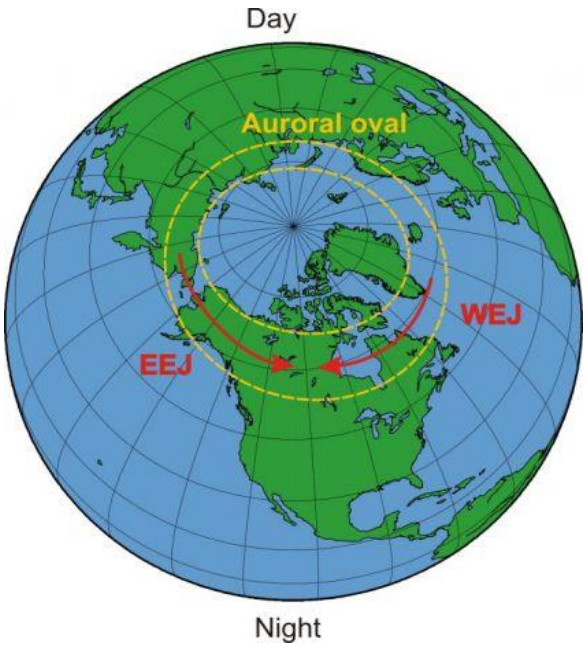

Figure 4.2 Location of the auroral electrojet in the northern hemisphere (INGV)

4.2 Geomagnetic Storms

Particularly large disturbances in the field are termed geomagnetic storms or substorms. Geomagnetic storms are associated with large changes in speed or density of the solar wind, often caused by events such as solar flares. If the solar wind is in the correct orientation, reconnection in the magnetosphere allows large amounts of solar plasma to enter the magnetosphere. This influx of charged particles enhances the ring current, causing a decrease in the strength of the geomagnetic field at the equator. The decrease is mainly in the horizontal components of the field at this point, and is measured by Dst. Storms may be divided into three periods – onset or commencement, the storm itself, and the recovery period following it. Storm commencement is associated with an increase in the X component, although not all storms have commencement periods. The main phase of the storm is a large, rapid, decrease in X (the increase in the strength of the ring current); the main phase lasts for a few hours, and the amount Dst falls to in this period is used to categorise the size of the storm. The recovery period is an initially rapid, then tailing off return to previous values, which may take several days (figure 4.3). Substorms are less well defined, and their relationship with storms is debated (Lakhina et al 2006, Partamies 2013). They are shorter variations in the magnetic field, which occur more frequently than storms, observable primarily in polar regions (or in space). Unlike storms, which are related to large-scale events in solar activity, substorms are a function of the 'normal' solar wind – when southward oriented patches of solar wind reach the

magnetosphere, reconnection allows larger amounts of plasma into the atmosphere; substorms are due to the release of this plasma/related energy from the magnetotail. Substorm events result in widespread auroras, and an intensifying of field aligned currents and the auroral electrojets, which then have an impact on the main field. While storms are primarily characterised by Dst variations, AE is more useful for substorms (Lakhina et al 2006, Liou et al 2013).

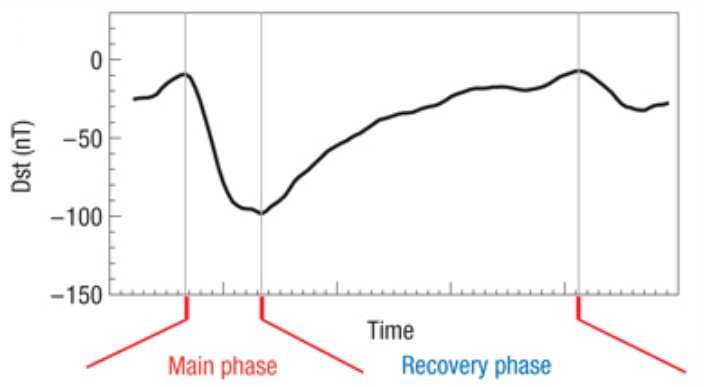

Figure 4.3 Generalised diagram of geomagnetic storm phases (from Chen et al, 2007). The main phase will typically last 2-8 hours, while recovery will be at least the same length, and potentially up to a week.

4.3 Storm Period Data and Models

Disturbed periods of time, where there are higher levels of solar activity, cause short period fluctuations in the magnetic field due to the increasing of ionospheric electric currents. These may build up to longer and higher amplitude periods of differing magnetic field values as the disturbance increases, up to geomagnetic storm level, where the field may be affected for days. Since the effect of short period features, particularly if small amplitude and rare, may be mistaken for geological features, these are important to correct for if at all possible. The more disturbance that can be modelled, the less disturbed times will negatively affect the ability to process survey data. While CM4 is generally expected to only model at low disturbance values, it can be used fairly well at slightly higher values (see chapter 2). The main noticeable feature of this fitting is the ability to fit single days of disturbance better than long periods of disturbance. This is potentially due to the idea that short periods of disturbance only allow a small amount of additional plasma from the solar wind into the magnetosphere, which can affect everything by a small amount for that period of time, before recovering, where long periods of disturbance may not necessarily allow any more plasma to enter, but does allow a cumulative loading effect- in longer time periods, more plasma may enter before the effects of a previous recoupling can 'wear off', giving a greater effect than allowing the disturbance to dissipate quickly.

As has already been noted the CM4 model seems to be able to model disturbances up to around Kp 3 or 4 at quiet stations, and if Dst changes gradually. This is despite only being designed to deal with Kp up to 2. On more disturbed days it is still possible to use data from stations if corrected carefully by local stations. As discussed in chapter 3, this may require careful selection of base stations. If this is done though - can we correct for disturbance effects? Since we understand what is creating the disturbance, is it possible to model disturbed time induced effects, even geomagnetic storms? During storms it is probably not possible to use data, certainly not in the same way as normal, as the storm tends to obscure all other magnetic signals (since it is so much stronger than any other effect).

Much as we previously surveyed months for low activity in order to look at Sq variations, a survey was done here to find months containing geomagnetic storms. In particular, we were looking for months containing a distinct storm (or storms), with relatively undisturbed behaviour for the rest of the month, as this would allow the storm and recovery to be seen more clearly. This would also avoid as far as possible the problem of noise, or overlapping recovery/onset periods in months containing multiple storm or substorm events. Multiple months of data were needed to see if conclusions could be drawn about storms in general, as opposed to one single event. November 2003 (storm on the 20th-21st), August 2005 (storm on the 24th, smaller event on the 31st), August 2011 (storm on the 5th-6th), and October 2011 (storm on the 24th-25th) were chosen as months that might be most useful for this work. As with data in previous chapters, mean values have been removed from the data to aid in their display. Typical storm data can be seen in figure 4.4.

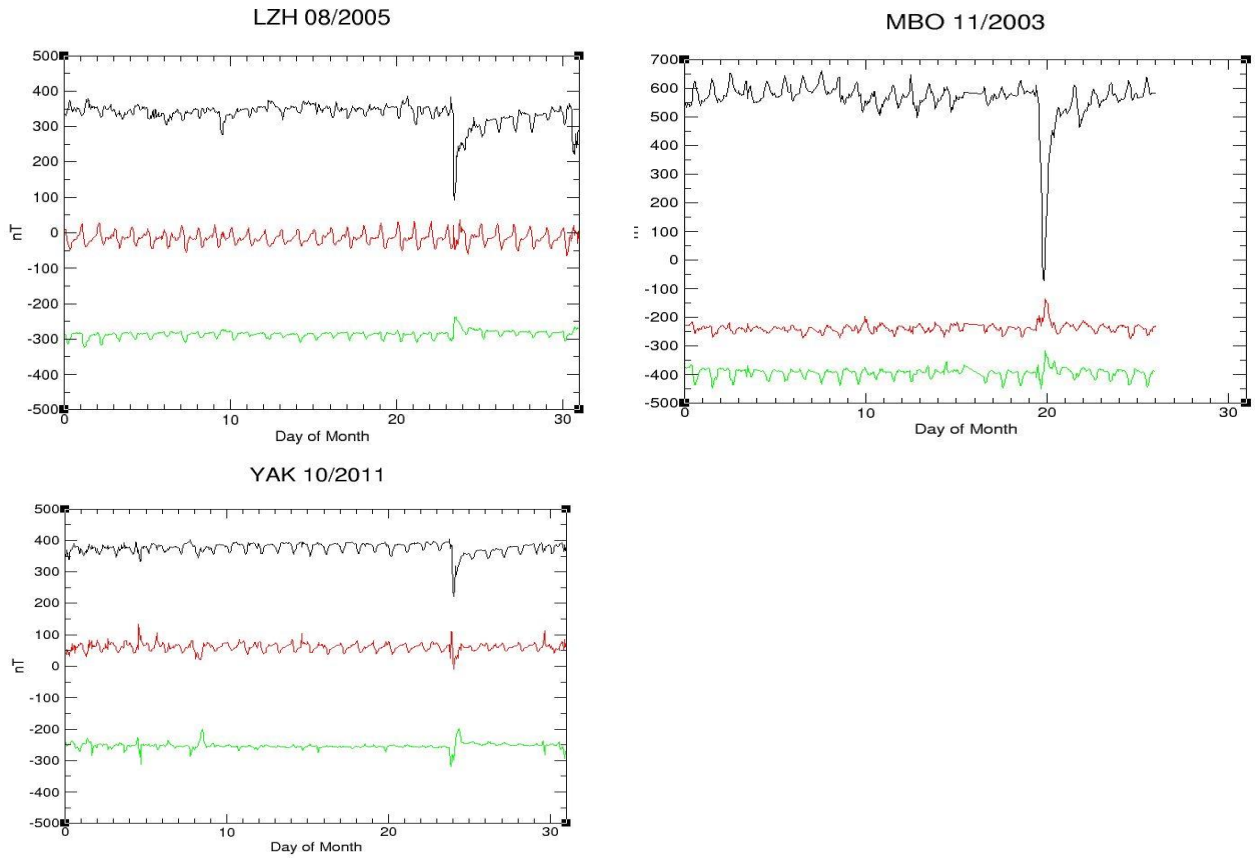

Figure 4.4. Typical data from geomagnetic storms, showing main and recovery phases

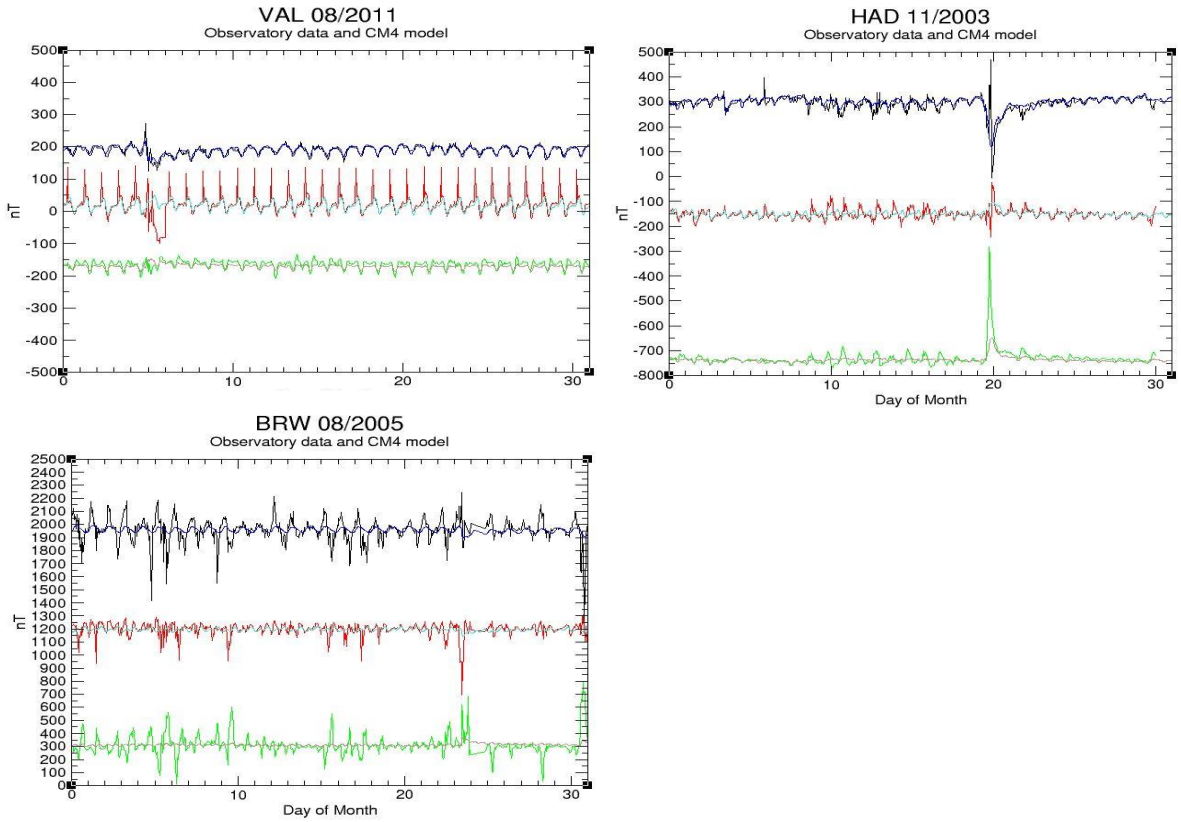

Figure 4.5. CM4 model fit to storm-time data. The fit is generally good, but better for X components. (Observatory XYZ data in black, red, green, CM4 model XYZ in blue, turquoise, brown)

Tests of the CM4 model during storm/substorm periods suggests it is fitting the X component variation well, but is not as successful at fitting the Y and Z components (figure 4.5). The variation in X does seem to contain a larger storm signal at most stations, and X behaves in a much more regular manner than the variation on Z, so this is not unexpected. While the X component data tends to be completely dominated by the storm, Sq variations can often be seen in Y and Z component data (e.g., KOU 10/2011 or KIR 11/2003, figure 4.6).

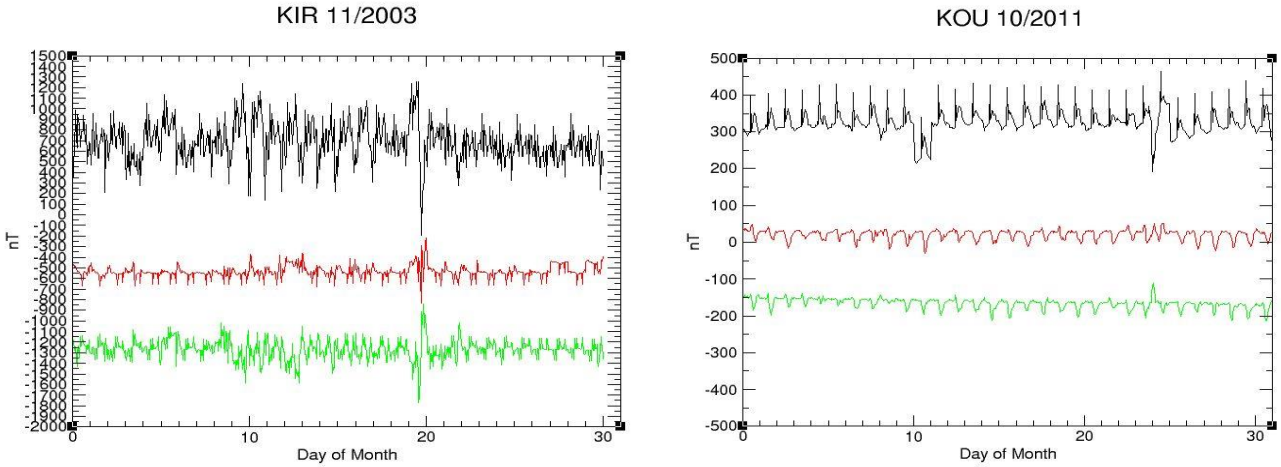

Figure 4.6. Observatory data from KOU and KIR, showing the presence of Sq periods which have not been completely overprinted by the storm in Y and Z components.

This suggests that the storm effect is not so large (at least for certain stations) that it cannot be used – the effect on the data of storms is much smaller than might be expected. Substorm disturbances also make relatively little difference to stations outside of high latitudes, and can in effect be 'ignored' – only the larger storm events are going to be overly noticeable in the data and so need correcting before data can be used. That some storms have less effect than might be expected on the data, and that Sq variations can be seen within storm periods, suggests that with suitable corrections, some data can be used from these periods. This is discussed further in section 4.5.
CM4 is based on quiet-time data, and so is not expected to fit well in high activity periods. However, it does actually model geomagnetic storms quite well, at least at low latitudes (where it generally performs better anyway). For example, for August 2005, there is an RMS misfit of 21.1nT between CM4 and the observatory data at NGK, which is only a little higher than the misfit to a generally more disturbed month such as May 1994; the misfit to the days containing the storm and recovery period (23rd-27th) is 13.53nT, while non-storm days (17th-21st) have a misfit of 6.97nT – the misfit is approximately double for the storm period, and again, similar to the misfit at VAL to more disturbed days (see chapter 2.1).

This suggests that the storm features are not purely due to the ring current. Nearer the equator, the storm disturbance is seen in the X component, and moves to Z as stations become nearer the poles. CM4 does not model this, and will preferentially place the storm signal in the X component. This is also found in tests conducted by Shore 2007. Adjusting the model to use RC as an improvement on Dst might therefore fit more of the disturbed signal, as suggested by Onovughe 2015.

4.4 Discrete Fourier Transforms of Months Containing Geomagnetic Storms

Discrete Fourier transforms are calculated as in chapter 2.4, to show the relative power of different frequencies in the signal recorded at observatories. Power spectra of DFTs from disturbed months (figure 4.7) show relatively more influence from short periods than undisturbed months do (compare to figures 2.12 and 2.13 in chapter 2). However, they are still usually relatively less important than the solar harmonics, showing that even on noisy days the Sq period is controlling most of the variation, but with other periods superimposed due to the disturbance. Some stations show massively increased spike heights at short periods during more disturbed (geomagnetic storm containing) months compared to quiet months. These are not seen in all disturbed months, or at all stations – some (e.g. THL 08/2005) lose the lower period spikes, with most of the power falling into the 24-hour period, and the rest being less coherent. Others show these spikes at stations in several locations, but not others (e.g. NGK and VAL 08/2011). This shows that while the storm may appear to be similar in all locations, the precise effect on the local field behaviour varies with location, and from storm to storm.

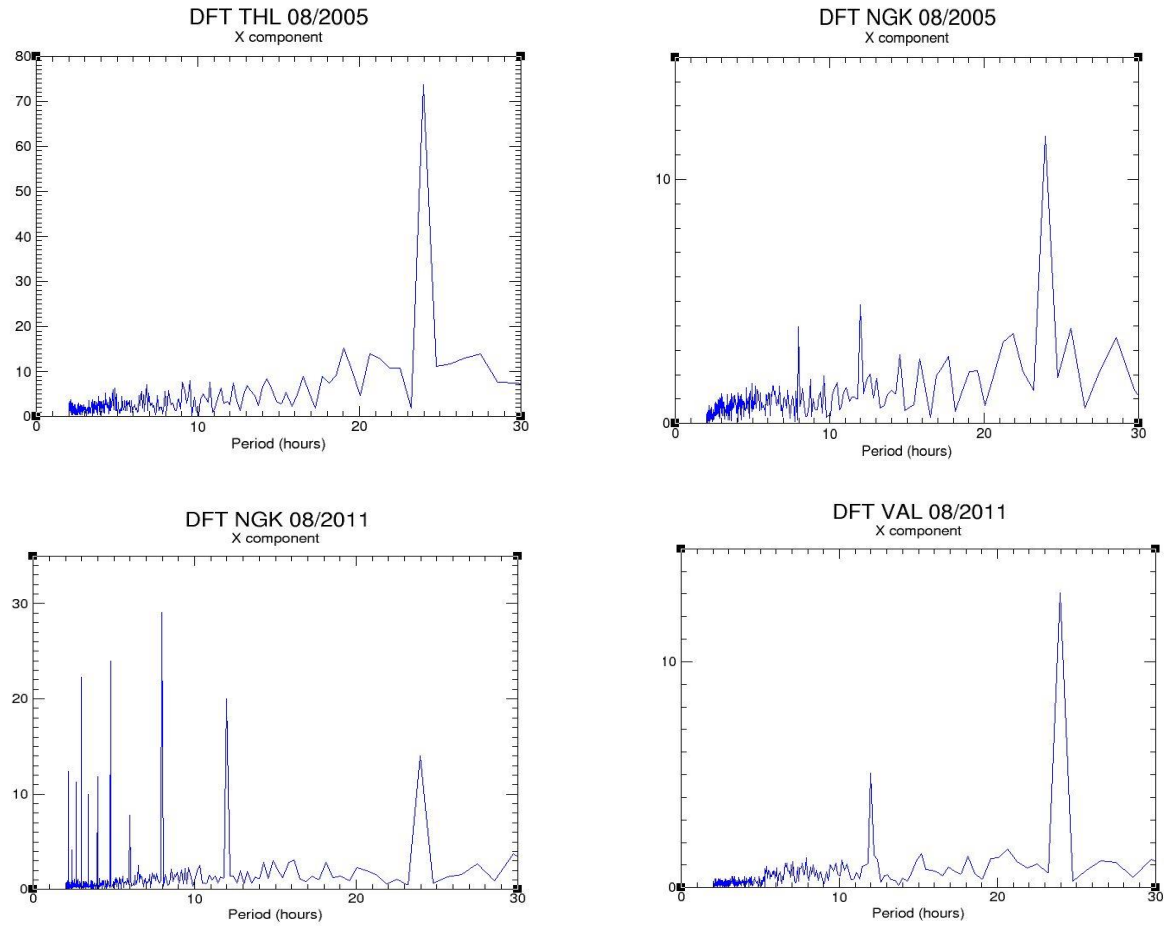

Figure 4.7 DFTs of X component data from various stations in storm containing months. Y axis shows the relative power at each period

4.5 Storm Behaviour Trends

Looking more closely into storm time data then, it can be seen that there are locations/times when this data can be used to a greater extent than might be expected.

Storms may be split into an onset period, the storm period itself, and then the recovery period following the storm. For the purposes of this work, the 'onset' period is either ignored (where it is short, or is a relatively unimportant contributor to the field behaviour), or included as part of the storm period (where larger effects are seen). The storm period is however considered separately from the recovery period. Storm periods therefore last several hours, while the recovery may last several days.

In almost all cases, while the storm period is too complex (varying with location and with different characteristics to each storm) to model simply, and must be discarded for survey purposes, the recovery period contains data which may be treated as normal after a correction is applied for the

recovering field strength. Occasionally, a small amplitude correction might be needed to adjust Sq-type variation on the following day. This would allow recovery period data to be used, even if the survey and base station locations are behaving too differently to be used for a normal remote reference correction.

For most stations, the recovery period follows normal Sq variations, but with a trend up (X) or down (Y, Z) from the storm amplitude. X components tend to show the overall storm feature (as seen in Dst) with an obvious recovery period. Y components are more likely to show a pair or triplet of features that correspond to the storm, and are often modifications of the underlying Sq pattern. Z components behave in a much less consistent way, which may be due to varying induced effects at each location. Generally, the effect on Z is smaller than that seen in X, however it may be expressed in various different ways, and Sq variation can often be seen in the disturbed period. The recovery period is most commonly a raised overall value returning to normal, but the following days may show increased or decreased amplitude variation compared to Sq days surrounding it, or indeed very little recovery time may be needed, with the data showing a near immediate return to standard Sq values. Where the effect of the storm is smaller (closer to normal Sq variation values), the recovery period is shorter than for larger events, and for Y and Z may be less than a day long (HON 08/2005, LZH 08/2005, or ASP 11/2003, figure 4.8).

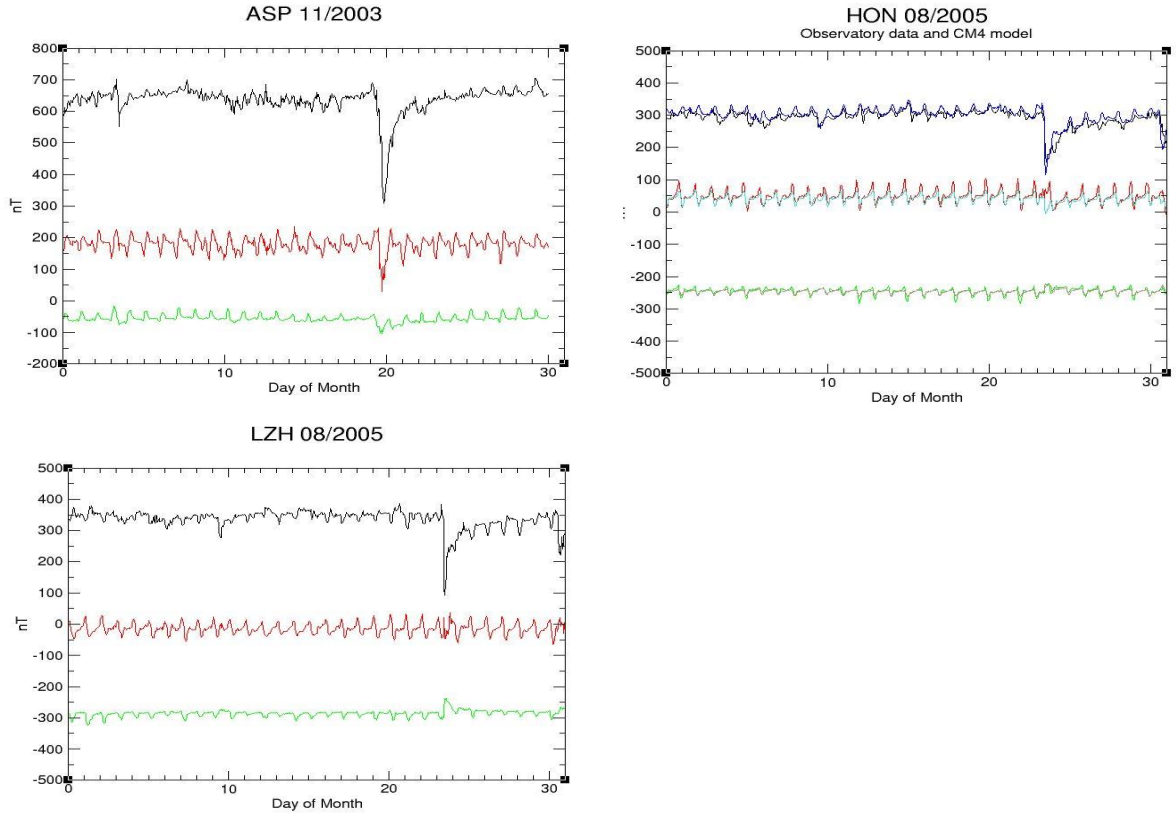

Figure 4.8. Short recovery periods seen for Y and Z components at several observatories, with much longer recovery periods in X

While there are variations between stations in how storms affect the recorded data, each station tends to behave consistently within itself, and regarding those observatories nearby (in same setting bracket). During some storms, features of the Sq field can be seen underneath the storm signal on the Y and Z components, particularly in stations where the storm is of relatively lower amplitude compared to the Sq (e.g., figure 4.6). Since Sq features can still be seen, and given that storms have consistent effects at each station, this suggests that storm signals could be removed from Y and Z components in some cases. X components generally do not have the underlying Sq pattern, and so it is less likely that storm signals could be removed from X component data. It is possible that for stations where this Sq pattern can be seen and/or smaller storms, some data could be extracted from the storm period. This might be useful in some situations, but is likely to be constrained to very specific locations and conditions.

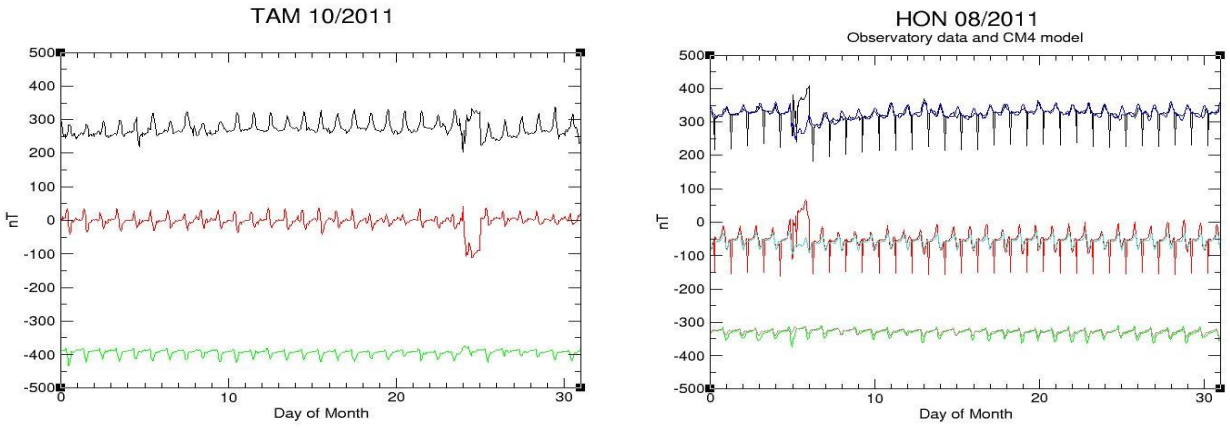

Figure 4.9. Smaller response to storms seen in equatorial observatories, particularly for Z components

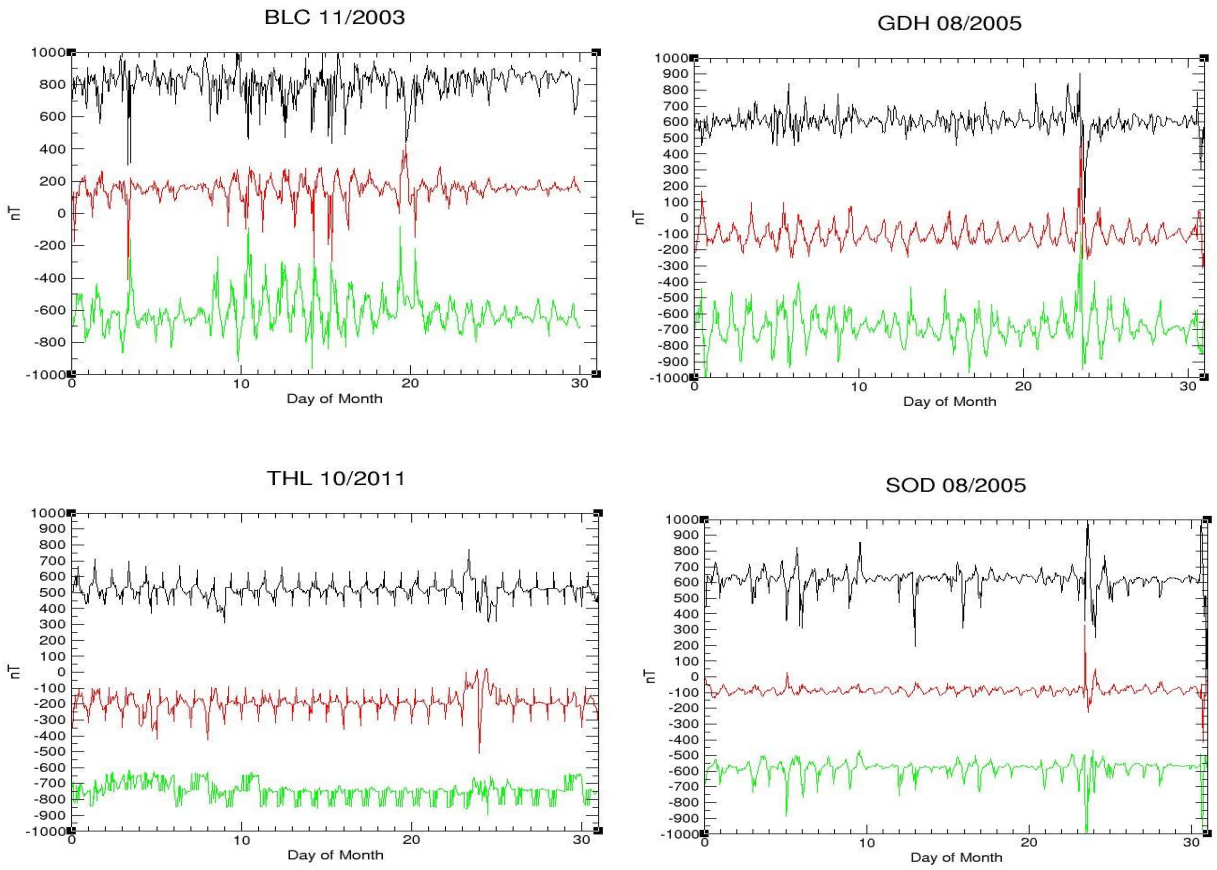

Figure 4.10. Storms recorded at Arctic observatories, showing common onset spikes in X components, and larger response to disturbed periods of any sort

Stations nearer the equator tend to have less response on the Z axis, and particularly for island stations overall less of a response to the storm (in amplitude terms and relative to the size of normal Sq variations – ref. GUI, HON, TAM, figure 4.9). Stations in the Arctic region (figure 4.10) tend to show a spike on the X axis before the expected trough, and have a proportionally much larger response overall (both to geomagnetic storms, and to smaller disturbance events), as do coastal stations compared to inland stations at the same latitude. The Arctic stations often have more power at higher frequencies compared to lower latitudes, which also suggests that they are affected much more by short period fluctuations (both those peculiar to the region, and those related to Dst wobbles). DFTs of disturbed months show that short period variations of the field may become significantly more important to the behaviour of the whole field. The effect is not consistent to all disturbed times however, and may be related to the level of disturbance (see chapter 2.2).

4.6 Restoring the Recovery Period

The recovery period is the period of several hours to several days following a geomagnetic storm, where the field strength is returning to normal values. For most storms surveyed in this study, the recovery period appears to show Sq variations, within a trend to normal from the storm value. CM4 also models the recovery period well, even at high latitudes, which agrees with the idea that the recovery period is mostly composed of normal Sq type variation, superimposed on a curved increase or decrease in overall intensity. This suggests that a method to restore the data could be found, potentially by using regressions. Tests of several types of regression were run on the recovery period of several stations, after cropping the data to remove the storm itself, to see which best removed the recovery trend (figures 4.12, 4.13, and 4.14, for the X, Y and Z component respectively at GUI; figure 4.15 for CLF). A quadratic regression seems to restore the recovery period back to where it would be without the disturbance. Cubic regression is also a potentially good option. Linear, exponential or logarithmic regressions tend to over correct the middle part of the recovery, but would also at least partially restore the data. This is most obvious, and also most useful for the X component, which tends to have a longer recovery period, and also a larger difference from normal values. The shorter the recovery period (as in Z, GUI 08/11) the less difference a regression makes, though this is mainly because there is less need for correction here.

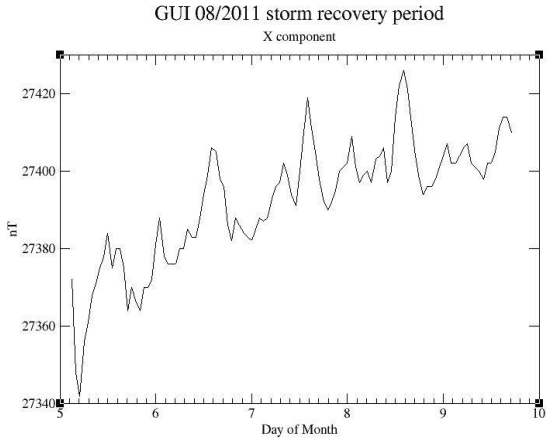

Figure 4.11 Storm recovery period at GUI (for geomagnetic storm on the 5th August 2011) X component

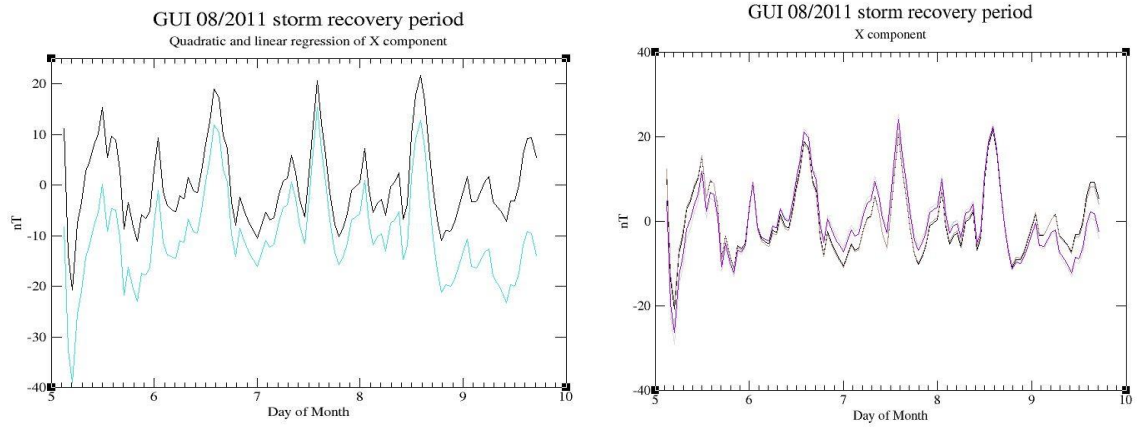

Figure 4.12 Regressions of the GUI recovery period (X component). Linear regression (turquoise), quadratic regression (black), cubic regression (brown), exponential regression (grey), logarithmic regression (purple). Quadratic regression provides the best restoration of the data. Cubic is similar to quadratic, others are similar to linear

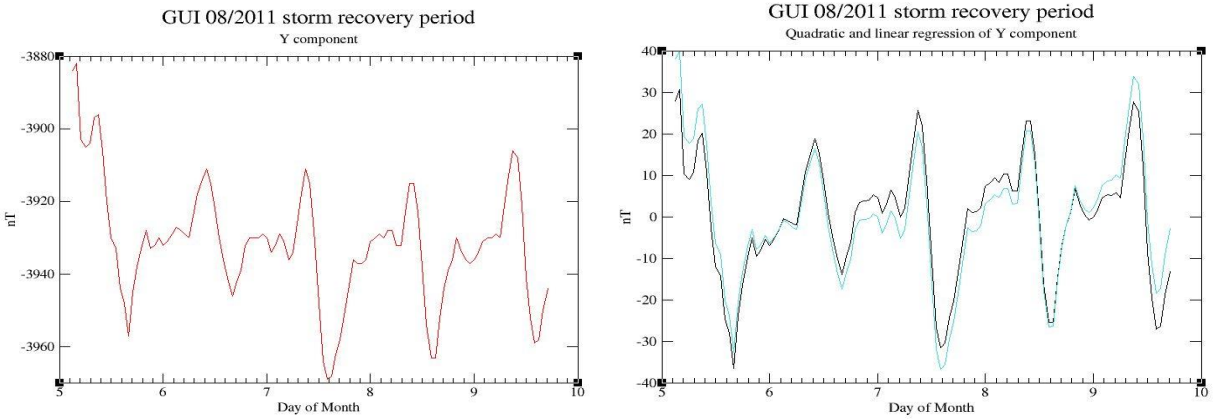

Figure 4.13 Storm recovery period at GUI (for geomagnetic storm on the 5th August 2011) Y component (red). Quadratic (black) and linear (turquoise) regressions

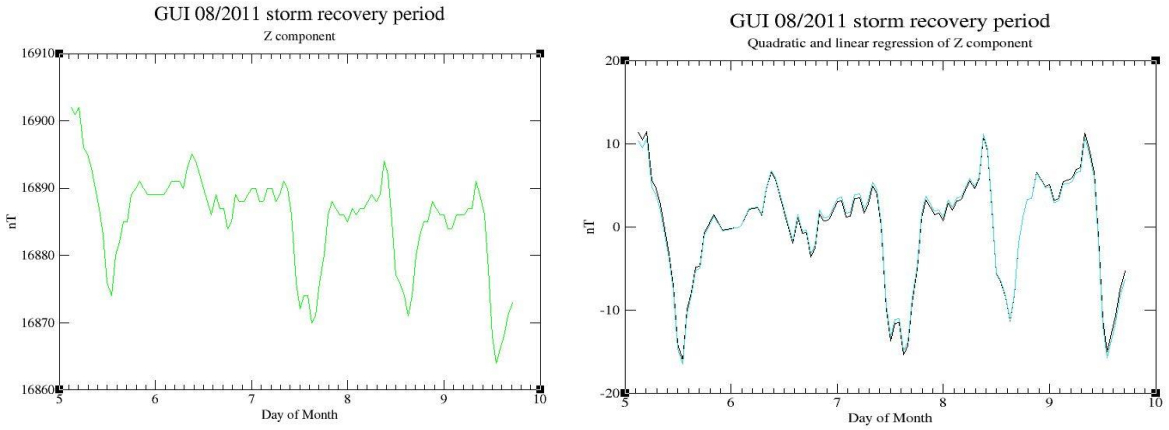

Figure 4.14 Storm recovery period at GUI (for geomagnetic storm on the 5th August 2011) Z component (green). Quadratic (black) and linear (turquoise) regressions. There is less difference in the regressions for the Z component, as less overall correction is required than for X

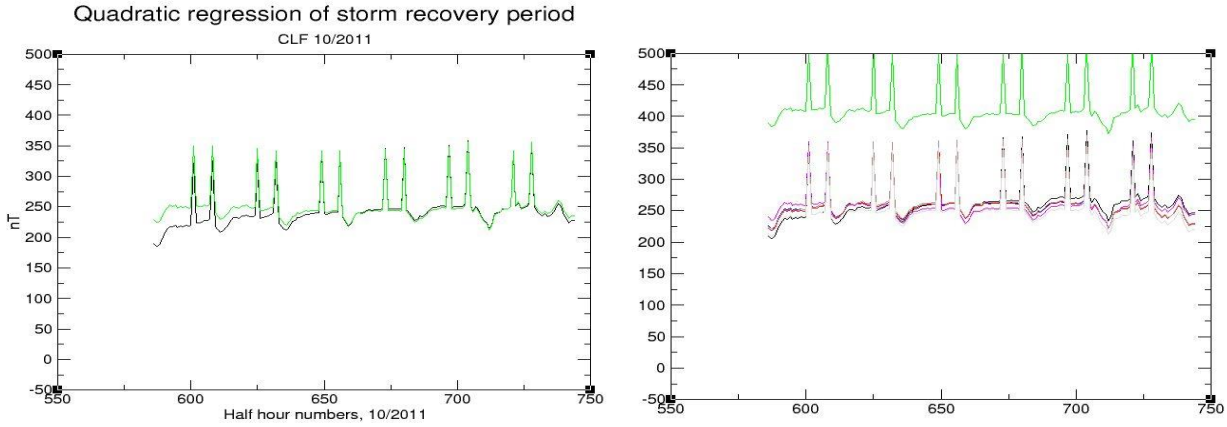

Figure 4.15 Regressions of the recovery period at CLF (for geomagnetic storm on the 24th/25th October 2011). Recovery period data (black). Quadratic regression (green), linear regression (red), cubic regression (pink), logarithmic regression (grey), exponential regression (brown), power regression (blue). Quadratic and cubic regressions are near identical (the quadratic has been shifted up by 200nT to aid viewing)

While several types of regression appear to be successful at restoring this data, the simplest one that works is to be preferred. In this case, that appears to be quadratic regression, as there is not a significant difference between it and a cubic regression in these tests (this is not to say that a cubic regression would be unacceptable, more that the additional complexity doesn't seem to be required). The linear, log and exponential regressions in this case appear to under correct the beginning and end of any series, so are not as successful at removing the recovery effect. Restoring the data in this manner would remove any additional complication from differing recovery experiences between survey and base locations, and allow the period after the storm to be used as normal. This greatly reduces the amount of time considered to be affected by the storm, and so the amount of data 'lost' due to storm effects. The recovery period is usually of significantly longer duration than the storm itself, and may extend for several days, so the ability to use as much of this data as possible reduces the disruption caused by the storm. This is particularly important for surveyors, as surveys often have very tight time constraints, and any delay can greatly impact the size or quality of the survey. For the storms seen in these examples, the main phase lasts around 6-10 hours, while the recovery phases are 4 to 6 days. Being conservative to allow for onset periods and later storm effects, only 12-16 hours of data at most is actually overprinted by the storm. Even for events with a shorter recover period (such as 10/2011, which seems to be around four days in this data), this could still rescue 80% of storm time data that might otherwise be discarded.

Results

Disturbance in the geomagnetic field is related to solar activity. The largest events are geomagnetic storms and substorms – periods of large, rapid variation in the field related to the influx of solar plasma, and the resulting changes and recovery this causes.

Geomagnetic storms may be split into three periods – onset, main phase, and recovery. These phases may last hours (onset/main phase) or days (recovery). CM4 makes a reasonable attempt to model the effect of storms, but is not enough to completely fit the effects caused.

CM4 is better at modelling the changes on the X component, however X component data is generally completely overprinted by the storm, and thus unsuitable for use in magnetic surveys. Y and Z components may show some evidence of Sq signal within storm times, and with further work it might be possible to remove the effect of the storm and use some of this data. Since storms are at least partially modelled by CM4, this suggests that the ring current is not the only component of storm variation.

DFTs show that while Sq periods still tend to be visible in periods containing storms, the field contains other effects – short period features may become much more important to the overall variation (especially in high latitude areas), or the field may become more incoherent, with only the 24-hour period being successfully resolved. This suggests that while storms may appear similar at first glance, the effects on a given location may be quite different to any other, and there are many layers of complexity involved.

While, as noted above, storms appear to be very complex, and the main period renders data collected during the storm unsuitable for surveys, the longer recovery period after the main phase seems much more promising for retaining usable data. Indeed, for many locations, the recovery period appears to contain mainly Sq variations, with a trend from storm values to normal over days, with the amount of change and the time taken depending on the size of the storm. Tests of simple regressions show that quadratic or higher (e.g., cubic) regressions restore the recovery period data to normal looking Sq variation. This could then be used as normal for remote reference corrections – and indeed, if the recovery period is similar between locations, this suggest that no additional correction would be needed to use the majority of the recovery period data.

Chapter 5. Induction effects

5.1 Induction

Induction is a feature of the relationship between electric currents and magnetic fields (electromagnetism). When a conductor is moved within a magnetic field, a current is generated within that conductor. Equally, when current flows within a conductor, it generates a magnetic field around it.
These relationships are defined by Maxwell's equations:

$$\nabla \cdot \mathbf{D} = \rho$$
$$\nabla \cdot \mathbf{B} = 0$$
$$\nabla \times \mathbf{E} = -\frac{\partial \mathbf{B}}{\partial t}$$
$$\nabla \times \mathbf{H} = \mathbf{J} + \frac{\partial \mathbf{D}}{\partial t}$$

These are Gauss's law, Gauss's law for magnetism, the Maxwell-Faraday equation, and Ampère's law (with Maxwell addition), respectively; the electric field strength is denoted by **E**, the magnetic induction field/flux density **B**, the magnetic field intensity **H**, the electric displacement **D**, ρ is the electric charge density, and **J** is the electric current density (Griffiths 1999).
Gauss's laws describe how electric and magnetic fields behave in a given space, while Faraday and Ampère's laws describe how the magnetic and electric fields may induce each other. (Maxwell-Faraday covers electric currents and fields induced around time-changing magnetic fields, while Ampère-Maxwell is magnetic fields around time-changing electric currents and fields).

EM relationships, as defined in these equations, allow induced magnetic fields and electrical currents to form at a variety of scales around the Earth, since there are several sources of flowing currents whose strength and position varies with time (giving rise to magnetic fields as shown by Ampère's law), large changes in conductivity across the surface, and the geomagnetic field also varies in strength with time (giving additional magnetic fields from induced electrical currents – a compounding of both Ampère's law and the Maxwell-Faraday equation).
Another type of induced effect of importance to magnetic surveys is the effect of geomagnetic storms, driven by the ring current and solar interactions. However, the most important persistent effect (the one that may be seen at all times and in all field conditions) is the coast effect, which is

important mainly due to the location of both survey areas and many observatories. Induction effects are also generated by other things, mainly due to differences in electrical conductivity; the tides can have a relatively large effect, as can changes in rock type, or man-made features, such as telephone cables. This means that large metal objects, such as telephone cables, or electricity grids, are vulnerable to damage by geomagnetic storm-induced currents. In surveys, induction features become problematic if they are generated at one part of the survey but not another, for example if the survey area crosses from land to ocean, if the base station is much further inland or nearer the coast compared to the survey, or if there is a large conductivity contrast between the two areas, for example due to them being in very different geological settings (Parkinson and Hutton 1989).
If magnetic surveys could be conducted on a fine enough scale, the induced effect of conductive ore bodies could be used to pinpoint extraction locations. Indeed, this is effectively what is measured in surveys using other geophysical methods, such as Self Potential or Induced Polarisation (SP and IP) surveys (albeit by means of voltages generated), magnetotellurics, and EM coil methods of surveying (Milsom 2003). Due to the fact that the induced fields are much weaker compared to the overall geomagnetic field, they are often a modification of the overall field, making it relatively stronger or weaker than the background level without their influence. The induced effects important to surveys are mostly seen in the Z axis, though they also affect the horizontal components of the field. The most obvious induced effects in survey data are the time varying ones, such as the effect generated by the tide, which may be seen in the time series data (Maus and Kuvshinov 2004). Time invariant effects, like the coast effect, are more easily seen when comparing data series, by presence or absence in one location (Kuvshinov et al 2007). Sq also causes an induced effect (Maus and Lühr 2005), however this effect is unlikely to be distinguishable from the Sq variation in the data used in this work.

The following chapter is split into three sections – first (section 5.2) those dealing with the fields induced by the motion of electrically conductive material within the geomagnetic field, here exemplified by the tidal effect; and second (section 5.3), those generated by the varying of the magnetic field with time over regions of large conductivity contrasts (the coast effect). In both of these sections, the aim was to investigate if these effects could be seen in observatory data, how large an effect they might have, and if they could be corrected for in some way.
The final section (5.4) contains work on induction effects that are geographically contained – observations of effects seen only in stations at the equator or in the arctic regions.

5.2 Tidal effects

The tidal effect is due to the motion of conductive material within the geomagnetic field, due to the gravitational pull of the moon and sun. The motion is primarily taken up by sea water, but the effect is strong enough to also move solids, such as lithospheric rock, and liquid phases of the core. This generates a current, and so an induced magnetic field, as shown by Ampère's Law. The dominant period is 12.4 hours, half a lunar orbit, otherwise known as the M_2 tidal constituent. This is different enough from the solar period to modulate its effect, although there is also a modulating solar influence here - the Sun generates an additional gravitational effect, seen in spring and neap tides. Tidal effects are strongest in areas on the coast, and more so in areas with high tidal ranges, as this generates the greatest flow of current. It is primarily seen in the Z component, as the tidal rise is the major part of the motion, but is also present in the X and Y components, since there is a horizontal component to the motion as water moves around the Earth. Higher harmonics of M_2 may also be seen in areas of shallow water.

In order to look at 'normal' behaviour of the magnetic field, and pick out any motional induction effect present without unnecessary additional complications, an undisturbed month was chosen for these tests. Surveying Kp values over several years suggested that 2009 as a whole was very magnetically quiet, and May of 2009 in particular would be appropriate, since most days are very quiet (Kp of 0 or 1) and the most disturbed days have Kp values of 2 (with one or two exceptions).

Using discrete Fourier transforms, different periods can be picked out within the three component station data (figure 5.1). The daily 24hr solar period is in almost every case the dominant one, followed by twelve, eight and six hours, each becoming less significant. In some cases, another signal can be seen, at around 12.4 hours (12 hours 25 minutes). This is mainly seen in the Z axis. In the case of Valentia and other coastal stations, it is a discrete peak next to the 12hr in the Fourier transforms, while in others, such as Niemegk, it is a slight widening or distortion of the 12hr spike. In some stations (e.g. VAL) it can also be seen in the X axis data, though not nearly as strongly. Much smaller peaks exist at shorter time periods, however given the observatory data used is in half hourly means, and month long time series, short features are not likely to be well resolved. Given the relative heights of the short period peaks, they also make up a significantly lower portion of the signal all together, and so are less important to account for in this instance.

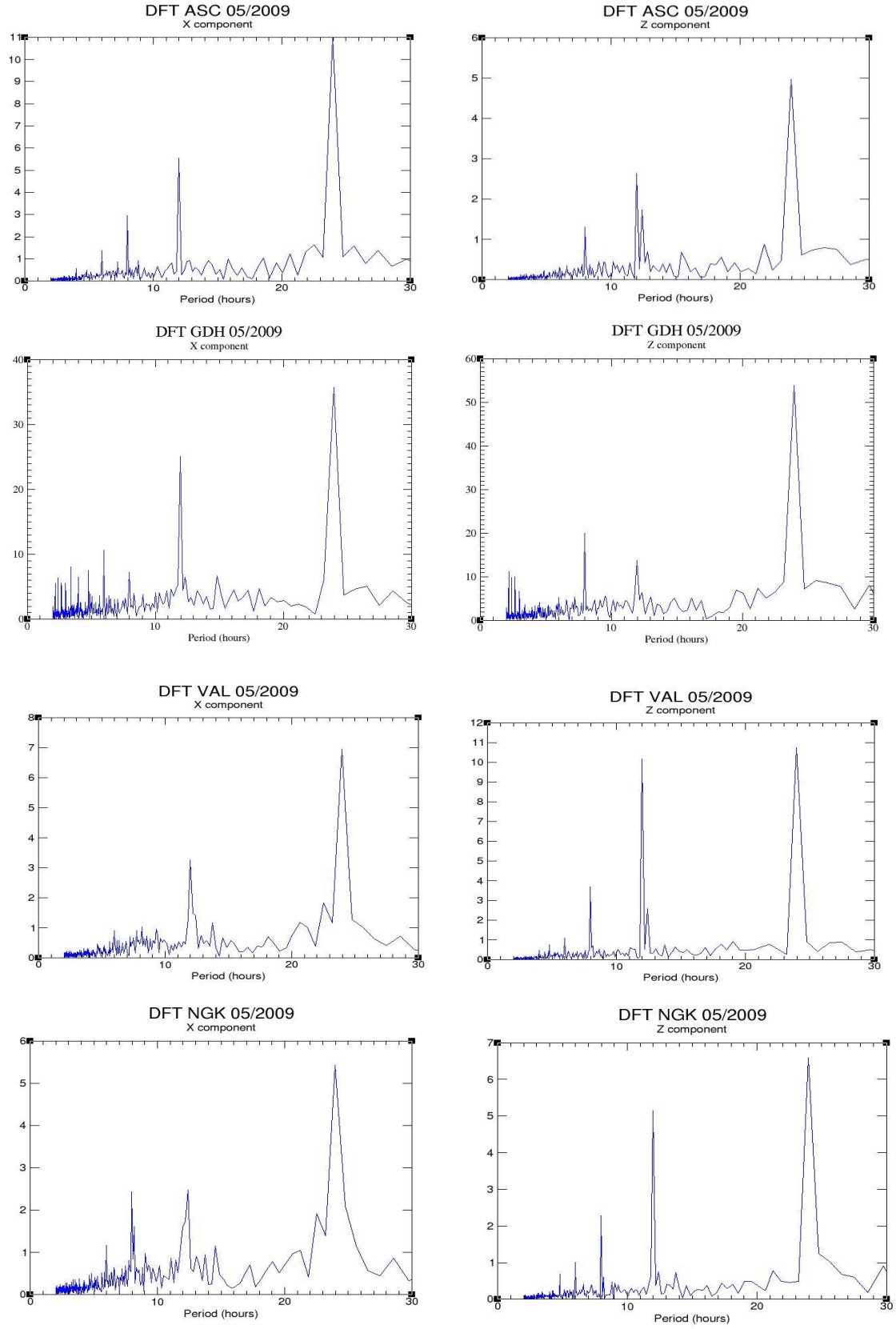

Figure 5.1 DFTs of quiet months at ASC, GDH, NGK and VAL. 12.4 hour (M_2 tidal peak) can be seen on Z, and for VAL and GDH, X component. Y axis shows the relative power at each period

The 12.4 hour, or 12 hour 25 minute signal is almost certainly due to tidal effects. This signal corresponds almost exactly (within 5 minutes either way at most stations used in this study – at some stations it appears to be peaking at 12.3 rather than 12.4, though this may be due to using hourly-mean data, and not resolving to enough detail) to the M_2 tidal constituent. M_2 is the principal lunar semi-diurnal, the dominant tidal period in most places. It is exactly half a lunar day, 12 hours 25.2 minutes. This is the component most people think of as a 'tide' as seen at the coast. Since the high (and low) points of the tide rotate with the orbit of the moon, the bathymetry of the ocean and the shape of continents affect the range of the tide in each location. The Atlantic coast of Europe has a particularly high M_2 tidal range, while others, such as the Caribbean, have very low ranges, since they are close to amphidromic points, where lines of constant tidal amplitude meet, generating no motion at all (Maus and Kuvshinov 2004). This is seen in the magnetic data, as a smaller tidal related effect is observed in data from observatories in areas of lower tidal ranges (GNA, KOU), and a much larger and stronger signal at VAL (Irish Atlantic coast). There is possibly also a ~6.2-hour signal in areas of shallower water, which is M_4, a higher harmonic of M_2 – though to properly distinguish this from the Sq harmonic at 6 hours would require very quiet, minute data over a longer time span (Schnepf 2014). Since surveys do not generally run to the length of time needed to resolve such data, only months at a time have been looked at to establish the lunar diurnal signal. Though higher harmonics may well be recorded at some locations, it is unlikely they will make up a large portion of any signal and will not be present everywhere; as a certain depth of water and strength of M_2 is required for them to be generated consistently, it is not vital that higher harmonics are corrected for. Should they become important for a given survey, this could be accomplished in much the same way as for the M_2 tide. As a rule of thumb, we can resolve to half wavelength –we will only see signals in 15min breaks with half hourly data, though this will improve with longer time periods of repeating signals – which are effectively stacking (Kuvshinov 2008).

The tide is not only present in the ocean, for the gravitational effect of the moon also affects the fluids within the Earth, and the solid Earth itself; tides within the solid Earth are of much lower amplitudes than the oceans, since water may flow significantly more easily than rock. The effect of tidal motion of the oceans can be seen inland, although at a reduced amplitude compared to areas nearer the coast. This is seen in the presence of a smaller, or less easily separated, M_2 tidal signal in data from inland stations such as Niemegk. The position of the Sun also influences the tides, though it's effect is only strong enough to be noticed at spring and neap tides, where the solar and lunar gravitational forces are directly in alignment and either cancelling out or reinforcing each other. The gravitational effect of the sun is not likely to be picked out of magnetic data, since it will correspond well to Sq, which is due to solar radiation, and so has the same period and alignment.

Since a large portion of the signal within the monthly data appears to be made up of a few dominant components of different periods, sine and cosine wave fitting was considered as a method of modelling. By fitting single frequency sine or cosine curves to the data the effect of the tidal signal can be better seen. First, the times which are misfit by a given wave were calculated (figure 5.3). These fall at 24 hours (the largest peak) and 12 hours for all stations, some then showing smaller 8, 6, and 4 hours, and some showing a second peak at 12.4. Some of the stations also have lobes around the 24-hour signal, which may also be a modulation related to the tidal components. The largest misfits are covered by the 24 and 12 hour periods, so cosine waves of these periods, at an appropriate amplitude for each station, were generated, and compared to the data. Using a combination of a 24hour period wave and a twelve-hour period, much of the pattern and amplitude of the data recorded at each station can be replicated (figure 5.2). This is a simple method of representing the variation due to the dominant signal frequencies; it is useful as it is quick and easy, and while it does not cover as much variation as using a full model, it is much less computationally intensive, and can be easily adjusted for any location, using any selection of periods one chooses.

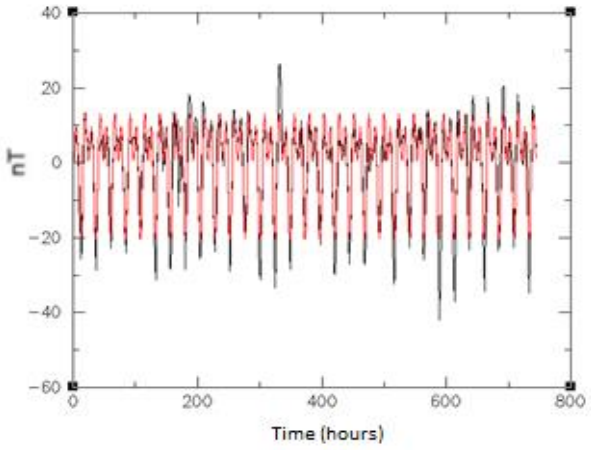

Figure 5.2 VAL observatory data (black) compared to 24+12-hour curve (red)

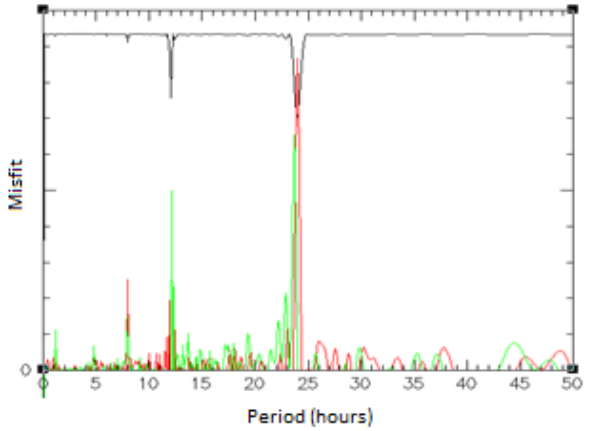

Figure 5.3 Misfit curve, black line shows the size of the misfit between observatory data and a cosine curve (period in hours)

While the amplitudes are not always perfect, the difference in inland stations appears to be mostly due to Dst effects in the data, which are not of a consistent period, and so not modelled. Small differences are also due to signals with much smaller or larger periods, which while having much less of a contribution to the overall signal, are still important. Stations at the coast, such as Valentia have an additional misfit, seen in the data as a variation in the relative heights of the 24 and 12 signal. This produces a 'double peak' in the daily variation for the station, with a larger 12+24-hour peak followed by a smaller 12+12-hour one, preceding the trough at local midnight (figure 5.4).

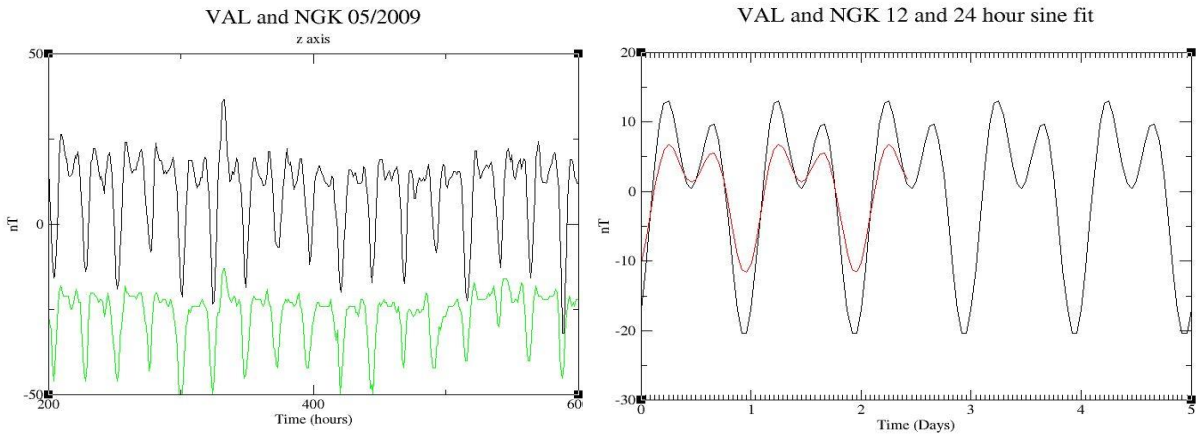

Figure 5.4. Comparisons of z axis data (left), and 12+24 hour curves (right) for VAL (black/black) and NGK (green/red), showing the differences in the double daily peak at each observatory.

While for stations such as Niemegk the heights are quite consistent, in VAL there is a distinct asymmetry in the double peak effect, and the relative heights of the two peaks changes over the course of the month, which is not modelled by using only 24 and 12 hour waves. This shape is also not modelled by CM4- CM4 tends to give flat-topped peaks in the daily variations in Z for VAL, which fit the overall shape, but not the amplitude, which is both generally larger, and varying through the month. The pattern in real data does not show flat topped peaks, but sharper points; the double peak shows the presence of higher harmonics. Adding in a wave with a 12.4-hour period produces a much better fit to the Z axis data at VAL, and to a lesser extent, NGK. This also applies to other coastal stations (figures 5.5 and 5.6). Using both 12 and 12.4 hour waves, the varying relative height of the double-peaked effect of the VAL Z axis data can be replicated. It also replicates the longer period amplitude changes in the data (variations over the course of the whole month as opposed to single days) due to their interference. The overall daily amplitude variation given by this method is lower than that recorded in the observatory data, although the difference between the two is not consistent – some days show less difference than others, so this may be due to Dst variations – adding in Dst or RC values might improve this further.

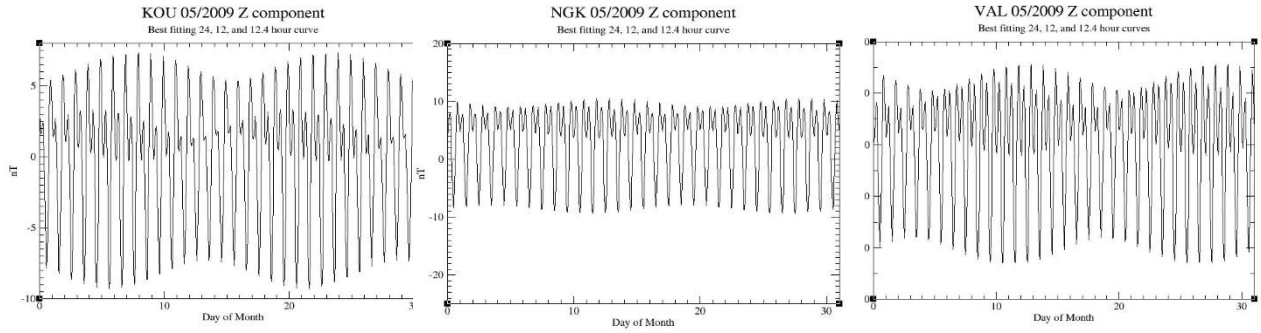

Figure 5.5 Best fitting curves for KOU, NGK and VAL, combining 12, 12.4 and 24 hour curves

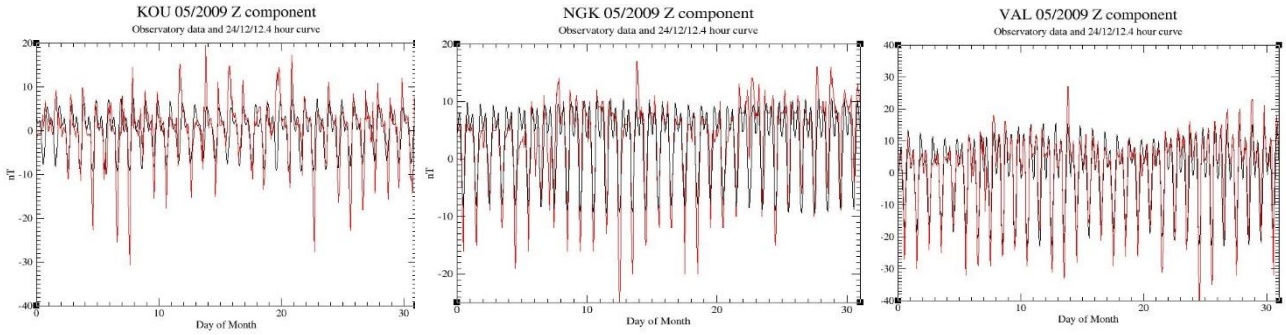

Figure 5.6 Observatory data (red) compared to the best fit curves (black) for KOU, NGK and VAL, Z components

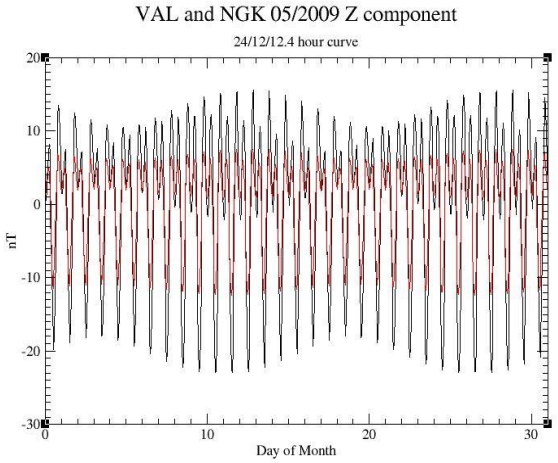

Figure 5.7 Comparison of the best fit curves for NGK (red) and VAL (black), showing the much larger effect of the tidal period at VAL

	RMS misfit to 12+24-hour curve (nT)	RMS misfit to 12+12.4+24-hour curve (nT)
NGK	4.31	4.28
VAL	5.33	5.01
KOU	5.11	5.06

Table 5 RMS misfits for sine wave curves with and without the tidal period

The 12.4 wave in the Z axis data has an amplitude range of around 4.5nT at VAL, while the 12hour is around 18nT and 24hr around 22nT. While the effect at VAL is probably particularly large, due to the very large tidal range in the area, that the effect can also be seen (to however much of a lesser extent) at NGK shows this is therefore a significant effect, and correctly taking it into account is important to understanding the data (figure 5.7 and table 5). Since the tidal period is very consistent, it could easily be corrected for in survey data by the addition or removal of a sine wave with a period of 12.4 hours and an amplitude appropriate for the location, with the phase based on local tide tables. In areas of more complicated tidal patterns, such as high latitudes or enclosed systems, multiple tides may be recorded in a day, or varying numbers of tides per day through the month; this may be trickier to correct, but still possible. The period of the signal would have to be adjusted for the local tidal frequency in this case. If there is a consistent separation of tides, the correction would simply have to be changed from 12.4 hours to the appropriate local frequency. If the separation is not consistent, it may be possible to instead model this as two or more superimposed sine waves, or using different corrections for different days. For stations near to the coast, in a location with a large tidal range, this signal is up to +/- 5nT, while for other stations it would be much lower, acting more as an additional complication/source of noise, rather than really benefiting from a fine-tuned correction.

5.3 The Coast Effect

5.3.1 The Coast Effect

The coast effect is an unusually large increase in the vertical component of the geomagnetic field, which correlates positively with the inland horizontal field. It is created due to the differing conductivities of land and sea, with the Sq change of the magnetic field during the day providing the motion to generate the current. The size of the effect is proportional to both the strength of the existing field and the contrast in conductivity. Treating the salt water/land boundary as a uniform half space, (e.g. Dosso and Meng 1992; Kellett et al 1991, Parkinson and Hutton in Jacobs 1989), the relative conductivity difference generates an increase in the Z component of the field relative to the distance from the coastline, with the largest difference seen nearest to the coast (figure 5.8).

Since the coastal effect is a steady feature at the coast in many areas, any survey conducted over or near this area, or using a base station located near the coast, is likely to be affected by it. This is therefore an important additional correction for improving remote referencing.

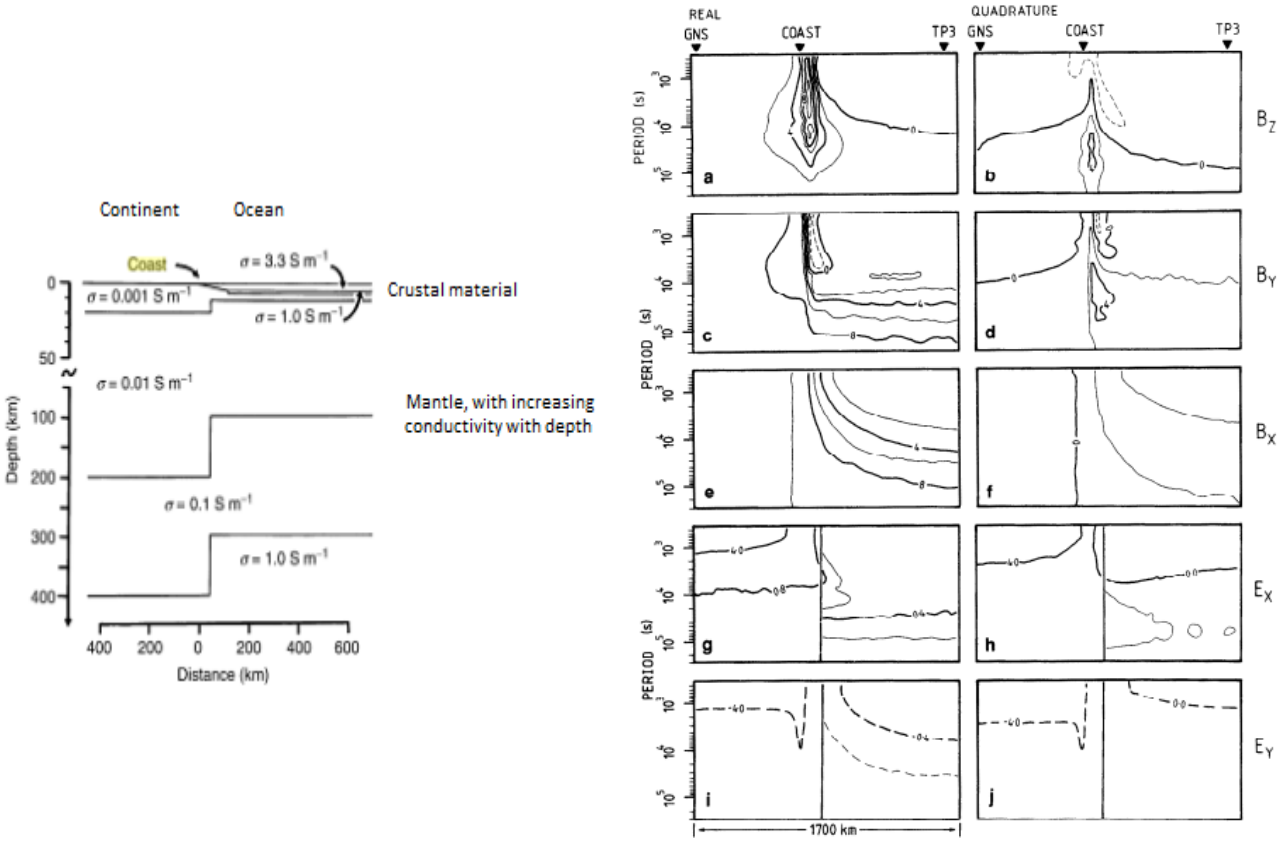

Figure 5.8 2D coastal conductivity model, and the resulting magnetic and electrical fields generated (Kellett et al 1991)

5.3.2 Numerical Conductivity Modelling

Assuming a time-varying source of EM fields can be converted into the frequency domain by Fourier transformation, the electric and magnetic fields, **E** and **H**, obey Maxwell's equations

$$\nabla \times \mathbf{H} = \sigma\mathbf{E} + \mathbf{j}^{ext}; \nabla \times \mathbf{E} = i\omega\mu_o\mathbf{H}$$

where $\mathbf{j}^{ext}$ is the impressed (extraneous) current (given source), $i = \sqrt{-1}$, σ is the conductivity distribution, and the time factor is $e^{-i\omega t}$. The magnetic permeability is μ_o. Above the conducting Earth (r > a, a = 6371.2 km is the mean Earth's radius) and beneath the external (magnetospheric and ionospheric) sources, the Fourier component of the magnetic field, $\mathbf{B}(\omega) = \mu_o\mathbf{H} = -\text{grad } V(\omega)$, can be derived from a scalar magnetic potential, V, which is represented by a spherical harmonic expansion

$$V(r,\vartheta,\varphi,\omega) = a\sum_{n=1}^{\infty}\sum_{m=-n}^{m}\left[\varepsilon_n^m(\omega)\left(\frac{r}{a}\right)^n + \iota_n^m(\omega)\left(\frac{a}{r}\right)^{n+1}\right]P_n^m(\cos\vartheta)\,e^{im\varphi}$$

where r, υ and φ are the distance from the Earth's centre, co-latitude and longitude respectively, ε^m_n and ι^m_n are the complex expansion coefficients of the external (inducing) and internal (induced) parts of the potential, and $P^m_n(\cos\upsilon)$ are associated Legendre polynomials. Components of the magnetic field follow from this potential expansion as

$$B_r(r,\vartheta,\varphi,\omega) = -\sum_{n=1}^{\infty}\sum_{m=-n}^{m}\left[n\varepsilon_n^m(\omega)\left(\frac{r}{a}\right)^{n-1} - (n+1)\iota_n^m(\omega)\left(\frac{a}{r}\right)^{n+2}\right]P_n^m(\cos\vartheta)\,e^{im\varphi},$$

$$B_\vartheta(r,\vartheta,\varphi,\omega) = -\sum_{n=1}^{\infty}\sum_{m=-n}^{m}\left[\varepsilon_n^m(\omega)\left(\frac{r}{a}\right)^{n-1} + \iota_n^m(\omega)\left(\frac{a}{r}\right)^{n+2}\right]\frac{dP_n^m(\cos\vartheta)}{d\vartheta}e^{im\varphi},$$

$$B_\varphi(r,\vartheta,\varphi,\omega) = -\sum_{n=1}^{\infty}\sum_{m=-n}^{m}\left[\varepsilon_n^m(\omega)\left(\frac{r}{a}\right)^{n-1} + \iota_n^m(\omega)\left(\frac{a}{r}\right)^{n+2}\right]\frac{im}{\sin\vartheta}P_n^m(\cos\vartheta)\,e^{im\varphi}$$

From these equations it is seen, in particular, that the radial component is influenced by induction to a greater extent than the horizontal component. For the horizontal components the degree of this influence is governed by the (complex) Q-response, which is the ratio of the internal to external coefficients for a specific degree, order and frequency. In the case of a 1-D conductivity distribution ($\sigma \equiv \sigma(r)$), each external coefficient induces only one internal coefficient (of the same degree n and order m); their ratio Q is independent of m

$$Q_n(\omega) = \iota^m_n(\omega) / \varepsilon^m_n(\omega)$$

and can be calculated using appropriate recurrence formulas. For the radial component, the degree of the influence is governed by the quantity

$$Q^{(r)}_n \equiv \frac{n+1}{n} Q_n(\omega)$$

This means that the relative amount of induction (compared with the external part) in the radial component is $\frac{n+1}{n}$ times larger for individual terms than for the horizontal components. In addition, due to subtraction in the radial component, the ratio of induced signal to total (external + induced) signal is much bigger (Kuvshinov 2008).

The Q function is a ratio of the induced and external coefficients of the field, in real and imaginary parts. For a perfect conductor, there is no penetration, making the radial field zero. Using Olsen 1998, and Olsen 1999, the induced component in this case is therefore half the external, giving a Q of 0.5 for a perfect conductor. This separates into real and imaginary parts (for perfect conductor, as with the external and induced components, real = 0.5, imaginary = 0). The amplitude and phase of the data can therefore be calculated, and this could be used to establish the external and induced fields and currents generated around a particular conductor.

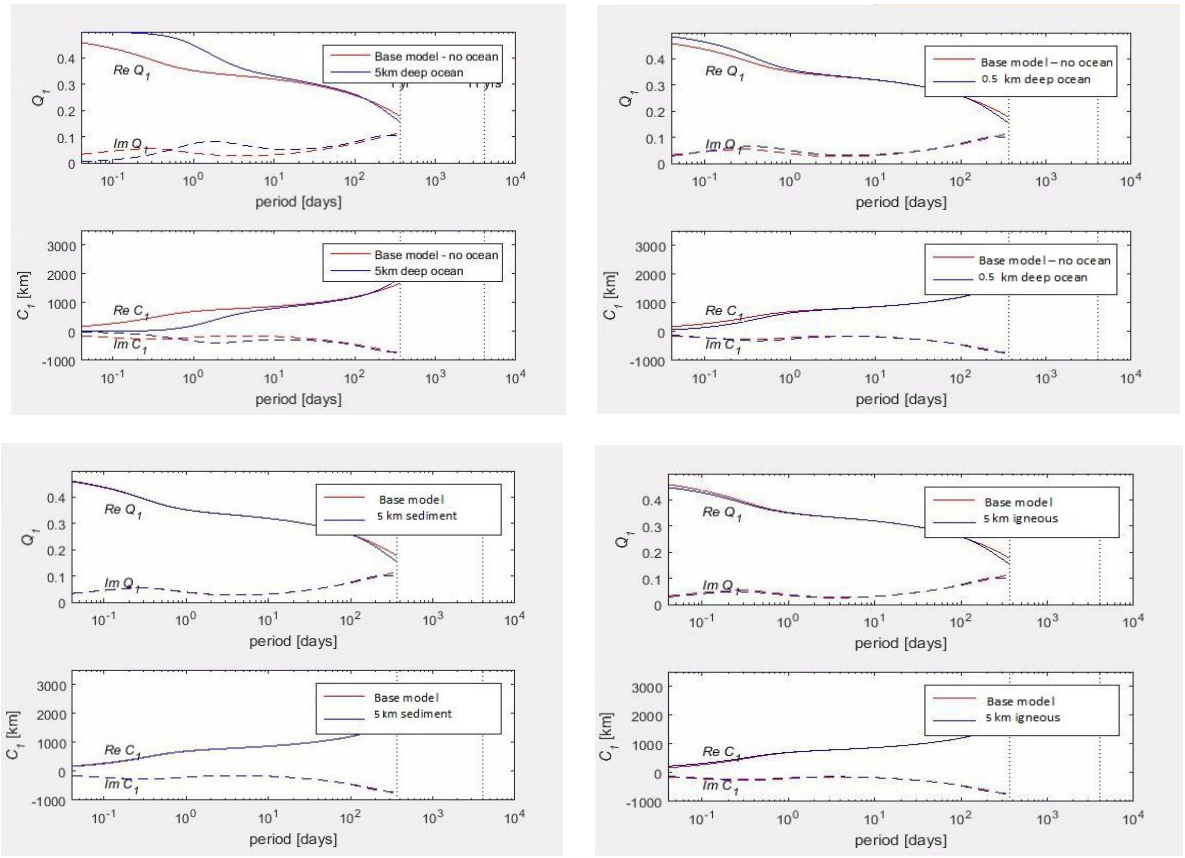

Figure 5.9 Q and C functions for a selection of conductivity models. In all cases, the base model has no conductivity contrasts, and a conductivity of 0.4 S/m. The ocean conductivity is set as 400 S/m. Igneous and sedimentary values are set at 0.001 S/m and 0.1 S/m respectively; values from McNeill 1980.

Looking at various model sections (figure 5.9), the effect of a deep ocean can be seen up to periods of 100 days, although the major differences are up to 1 day, with most of the remaining difference up to 10 days. Beyond 100 days, the difference between the presence/absence of ocean appears to increase again, but since this is beyond the scope of most surveys, it is unlikely to be able to be picked up in the length of this type of series of data, so it may not be necessary to model it in this

context. The deeper the water, the longer the effects can be seen for, and the larger the effect. These models contain average conductivities for a selection of rock types and average sea water. The largest change observed is between deep ocean and poorly conductive rock, but differences can be seen even in small conductivity contrasts, such as between different average rock types. This means that while a coast effect is the most obvious expression of induced fields, a change in rock type can also generate a similar effect. This could be taken into account if there is a known (or suspected) change in rock, e.g. along the boundary of a deep sedimentary basin, or where large plutons meet basement rock. Of course, the conductivity difference in rock types is relatively small (igneous rocks have resistivities in the range of $10^2 – 10^7$, while sediments may range from 1 to 10^8, McNeill 1980) so whether these changes are large enough to be observed in magnetic data is another matter. This is likely to only be seen for very large features; the effect of such a change in rock type is considered in d'Erceville and Kunetz 1962, which studies the effect of a fault on electromagnetic fields.

If induction effects due to conductivity contrasts can be successfully identified and corrected for, particularly if this could be done on a finer scale than simply showing the ocean/land boundary, it may be possible to take the induction feature and invert it to give the conductivity. This would allow the conductivity structure of the subsurface to be imaged, and so giving an additional observable to be added to the survey dataset, for no extra effort or equipment in surveying. At the finest detail, this would give results comparable to a local ground based potential or EM survey, without having to actually complete a survey of this type. While this is not the primary goal of this work, and indeed unlikely to be a method that can be reliably used with current data collection methods, it does present an interesting prospect for future, improved surveys.

An attempt was made to mathematically define external and induced values at 24-hour harmonic time periods at several stations; the best fit sine and cosine waves of these periods could then be used to generate phase and amplitude, and thus Q functions for these time periods. This work was unsuccessful, as working with the equations (as above, from Kuvshinov 2008, Olsen 1998) gave nonsensical values. Previous induction work at other periods, and the maths which this method was based on, assumes a uniform inducing effect - Sq has a much more complicated structure than this assumption allows for. If we were interested in induction we would avoid such periods, however we are interested in explaining the data, so these are important signals. This was not therefore continued with.

5.3.3 The Coast Effect in Observatory Data

A coast effect has been noted at many sites in previous work (Southern Australia, California, Western Canada, Nova Scotia/Newfoundland, Chile, western Ireland, Japan) and is also occasionally conspicuously absent for example Sable Island, Southern Peru, most of the British Isles - except western Ireland, some parts of the Mediterranean coast, Genoa, large parts of northern Europe (Parkinson 1962, Parkinson and Jones 1979, White and Polatajko 1977, Srivastava et al 2001, Neumann and Hermance 1985, Schmucker 1973, Rikitake 1965, and many others). Most of these absences are attributed to unusually conductive underlying geology (either at or near to the areas where measurements were taken from), or particularly shallow water, which does not provide enough contrast in conductivity to generate a strong magnetic effect. Some similar effects/modification of the coast effect have also been noted, mainly attributed to highly conductive underlying geology (e.g., San Joaquin valley California, Alert Canada, Brittany), or channelling of seawater currents (e.g. (possibly) Straits of Gibraltar, Cabot Strait). Similar effects could be seen away from the coast if current flow and rock/rock contrasts are strong enough. Most of the coast effect variation is seen in the Z component, though coastal stations may also show differences in X and Y components compared to their inland counterparts. The amount of change seen in X or Y might be related to direction of field/current flow at the location. One characteristic of the coast effect is that Z components will show strong correlation with H components, e.g. figure 5.10, White and Polatajko 1978. The effect may be defined as the ratio of horizontal to vertical components, transfer functions, or by induction vectors, particularly when considering magnetotellurics (Worzewski et al 2012, Key and Constable 2011).

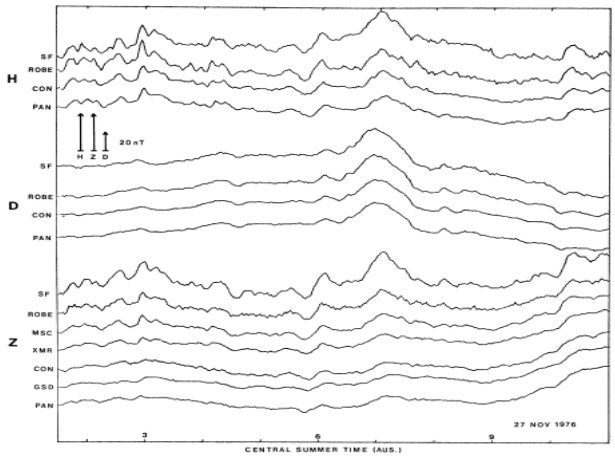

Figure 5.10 The coast effect: correlation of Z and H components from magnetometers in South Australia (from White and Polatajko 1978)

Previous work has found a normal coast effect at VAL (Parkinson 1962). This is seen in the observatory data used here primarily as a much larger amplitude variation in the Z component of Sq, as well as differences in response to larger disturbances such as geomagnetic storms (see chapter 4). The initial empirical suggestion of this effect is in the comparison of VAL to an inland station, such as NGK. Both have nearly identical CM4 models, but while the observatory data is similar, the differences are noticeable by eye, without any further statistical analysis. Looking at discrete Fourier transforms of the data, the main differences between the two stations are the lack of a prominent 8-hour X component spike at VAL, and the much higher 12-hour spike relative to the 24-hour spike on the Z component at VAL (see chapter 2, figure 5.18 below). VAL also shows a relatively larger 12.4-hour spike, which is related to the position on the coast, but not specifically the coast effect (rather being due to the greater effect of tidal variation since the station is closer to the sea). Since conductivity analysis suggests that the major differences caused by conductivity contrasts would be seen over short periods of time (see above) it is probable that the coast effect will be seen in the datasets used in this work, mainly as an amplification of Sq, though it is also likely the coast effect will make VAL more sensitive to Dst variations than inland stations (Kuvshinov 2008).

We look at observatory data to see if we can identify locations which show the features expected from the presence of a coastal effect. For several stations located at the coast, increased amplitude and variability is consistently present. When looking at increasing parts of CM4 to more successfully fit to station data (see chapter 2.3), the coastal stations all required a higher level of correction than the inland stations, particularly in the Z component. This is consistent with both the behaviour of the coast effect, and the limitations of CM4. In the cases of the high latitude stations, a similar sized correction is required to make the model fit the latitude related variation that is also seen, so it is less certain how much of the difference here is due to the coast effect. In the chain of stations running north in Scandinavia to Svalbard, the latitude change appears to be more important, though since the CM4 models do not take account of the coast effect or the effect of the auroral region, and generally are not well fit to high latitudes, it is possible that the effects are related, or indeed one and the same, since many high latitude stations are also coastal, due to access in the region/location of settlements. NAQ does however show the coast effect characteristic of correlated X and Z components (figure 5.12). When increasing the ion_pri values of CM4 to improve the fit to data (chapter 2.3), coastal stations tended to have higher values than inland stations. The exception to this (in the small sampled dataset) is HLP, which while located near the coast, doesn't require as big an increase in the model to fit observatory data (figure 5.11). This would agree with findings

from previous studies (Untiedt 1970) that there is little coast effect generated by the Baltic – possibly due to the water being too shallow to generate a significant conductive effect, or the underlying tectonics.

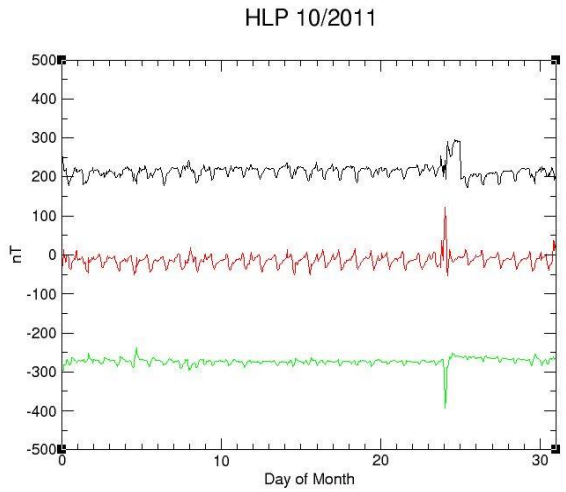

Figure 5.11 Data from HLP, October 2011, showing relatively little response to the geomagnetic storm, and generally small variations in the Z component, agreeing with previous findings that there is not a significant coast effect here

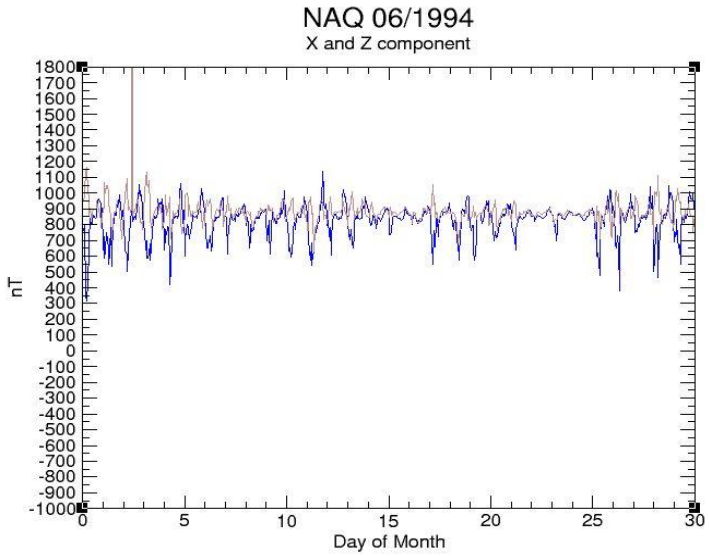

Figure 5.12 Correlation (and anti-correlation) between X (blue) and Z (brown) components at NAQ

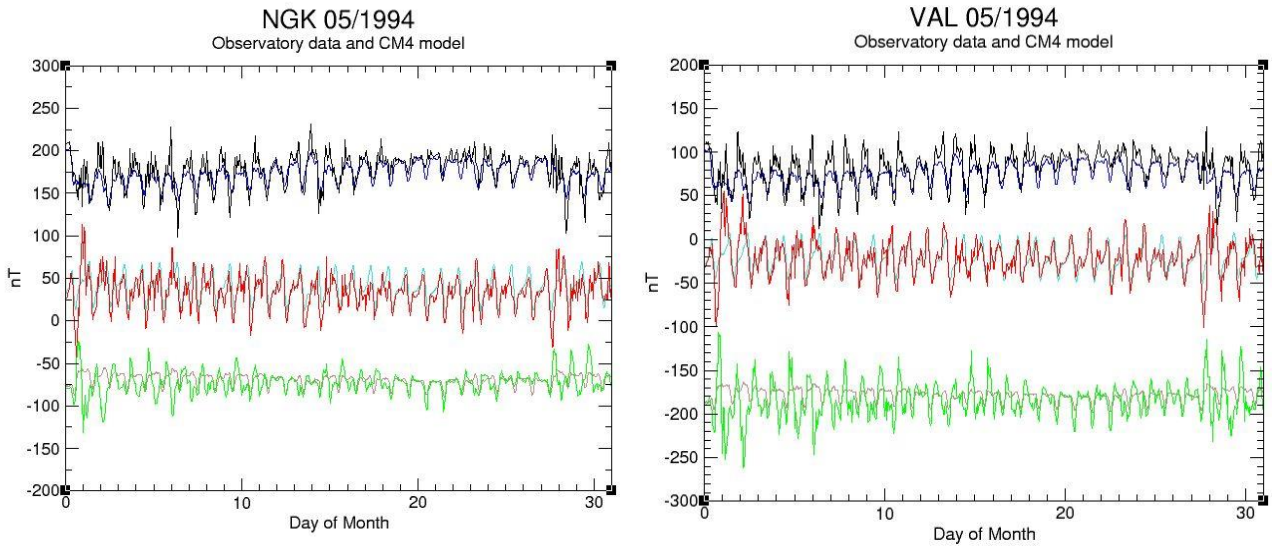

Figure 5.13 Increased response to disturbed days at VAL compared to NGK

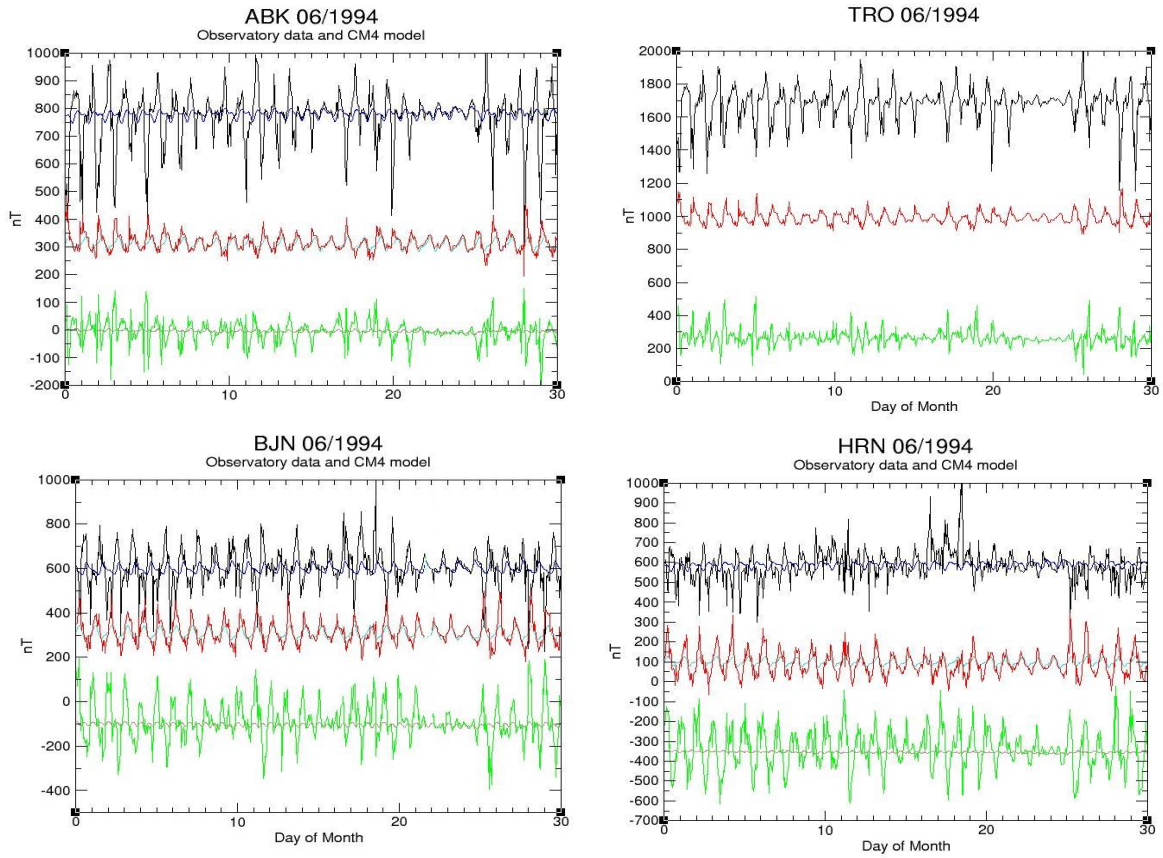

Figure 5.14 Diagrams showing the increase in amplitude of (particularly) the Z component moving from inland (ABK) to coastal/islands (BJN and HRN)

Increases in Dst or Kp tend to be more obvious in coastal stations (figures 5.13 and 5.14), showing that as well as producing an amplification of Sq values, disturbances in the main field are amplified. Geomagnetic storms appear to have a stronger effect on coastal locations (figure 5.15; Olsen and

Kuvshinov 2004), and months with higher disturbance levels affect coastal locations more than those inland. Since the coast effect is generated in part by the variation with time of the magnetic field, this is to be expected. This is potentially due to the coastal stations behaving as if they were oceanic – with the higher conductivity levels underlying them effectively amplifying any changes in the geomagnetic field.

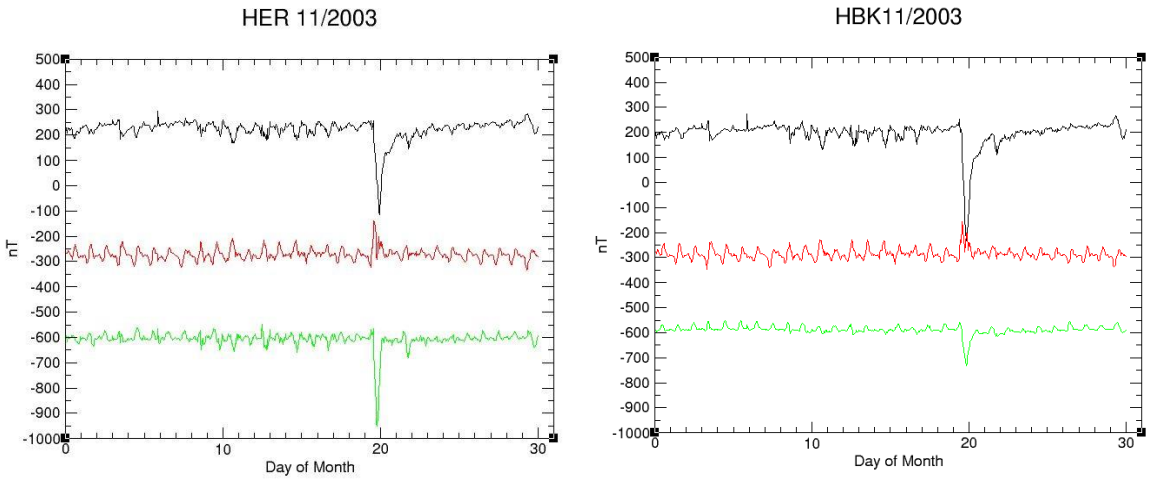

Figure 5.15 The difference in the effect of a geomagnetic storm between HER (coastal), which shows more effect in the Z component, and HBK (inland), showing the larger response in the X component

Correcting for the coast then, could be achieved by taking the data, and reducing (or amplifying) by the relative strength of the effect at each location. This would require knowing the amount of difference the effect is making on a station dataset, so a nearby inland station to compare to would be needed. A possible rough method of adjusting data for this effect is shown below, using increased 12 and 24-hour period signals to raise an inland station to the values seen at the coast.

5.3.4 Correcting For The Coast Effect

VAL and NGK

Looking at DFTs (chapters 2.4 and 5.2) and the difference in the best fit period curves used to model the tidal effect (figure 5.16), it can be seen that there are several differences between NGK and VAL, despite the fact they are quite close together, and the CM4 model for each is almost identical. That CM4 doesn't change between the two is unsurprising, as it doesn't contain lateral variations, but the amount of difference seen between the stations is significant. This sort of

difference in station behaviour is important to be able to correct for if one wishes to use one (or both) as a base station for a survey.

DFTs (figure 5.18) suggest that the major difference between these two stations is in the 8-hour period, and the 12/12.4 hour signals, as well as in overall amplitude. DFTs of VAL show much less power in the 8-hour period compared to NGK, but more is present in the 12 and 12.4 hour periods. This is confirmed by the best fitting sine curves at these periods – the curves for VAL are larger than NGK, and the 12-hour curve is of similar amplitude to the 24 hour one.

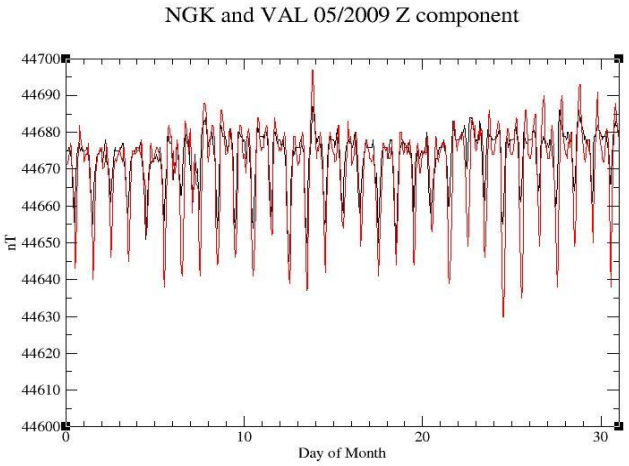

Figure 5.16 Comparison of VAL (red) and NGK (black) Z component data for 05/2009

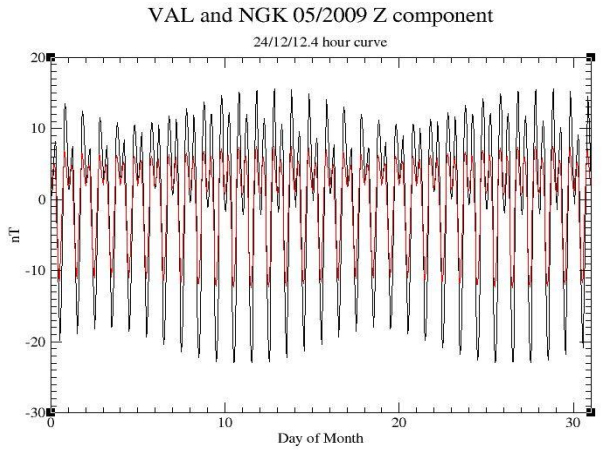

Figure 5.17 The best fit 12/12.4/24 hour periods curve for VAL (black) and NGK (red)

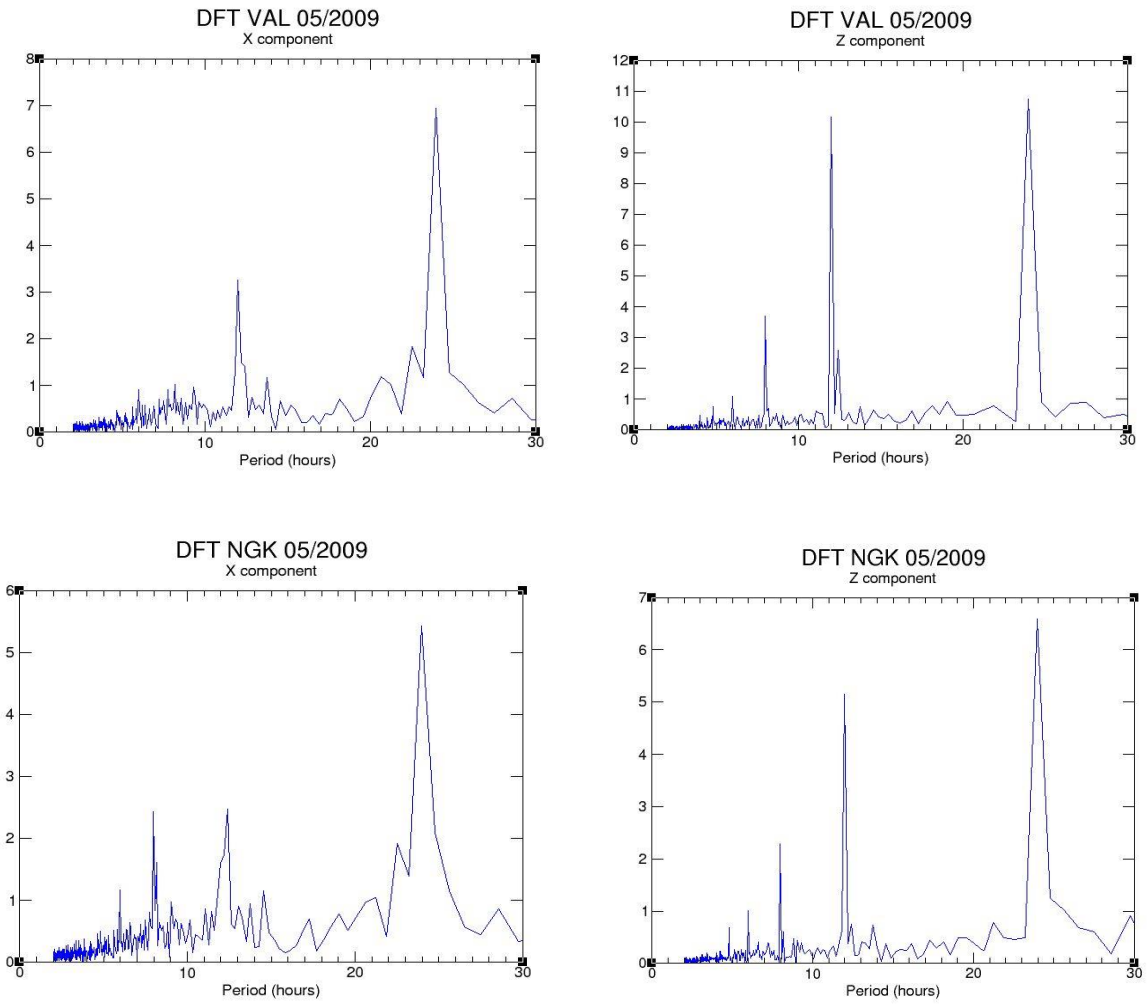

Figure 5.18 DFTs of VAL and NGK X and Z components, showing the difference in power of Sq periods at each station. Y axis shows the relative power at each period

Increasing the 12-hour signal at NGK would appear to fix much of the misfit (see figures 5.19 and 5.21, and table 6) between the two stations – it starts to raise the amplitudes to a similar level, and also emphasises the double peaked shape of days towards that of VAL. Based on a visual comparison of the shape, 1.5 times the 12-hour signal is doing a good job of transforming the NGK data to match VAL (figure 5.19). Looking at the DFT, figure 5.20, however, shows that there is too much power in the 12-hour period from this (unlike VAL, which has a 12-hour peak almost as high as the 24 hour one, this increase at NGK gives a higher 12-hour peak). Lowering the amount the 12-hour signal is increased by (figure 5.22) doesn't help the fit however, as it doesn't produce enough of a change in the double peak shape, and also doesn't increase the overall amplitudes enough (see

table 6 for RMS misfits). Increasing much further starts to over-exaggerate the double peak, especially on the quieter days. The ideal for adjusting NGK towards VAL therefore, is probably somewhere between 1.5 and 1.75 (figure 5.21) times the best fit cosine wave (RMS misfits of 6.51nT and 6.43nT respectively). Of course, some of this signal is also overlapping the 24-hour variation, which must also be increased to fit the overall amplitudes at VAL.

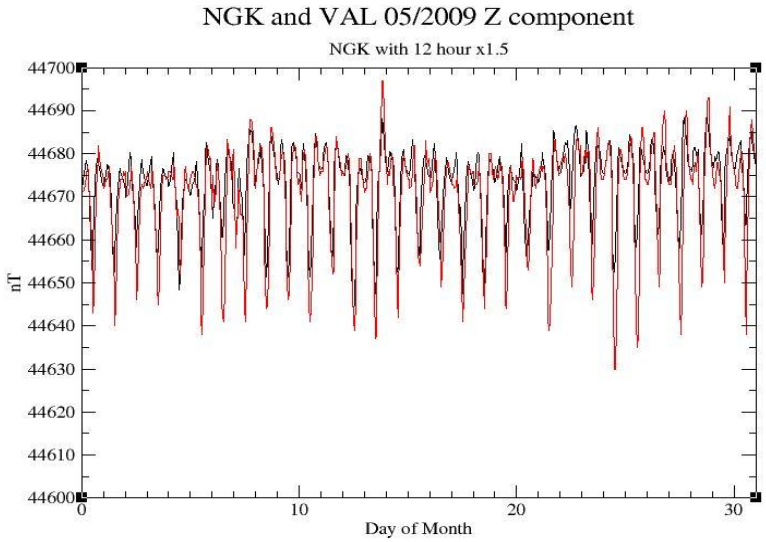

Figure 5.19 Comparison of VAL (red), and NGK (black) with 1.5x increased 12-hour period signal

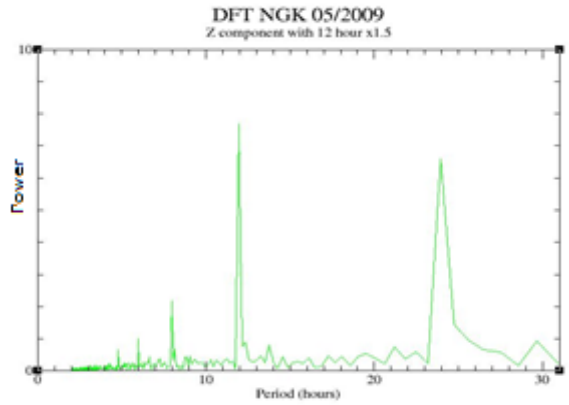

Figure 5.20 DFT of the increased NGK data

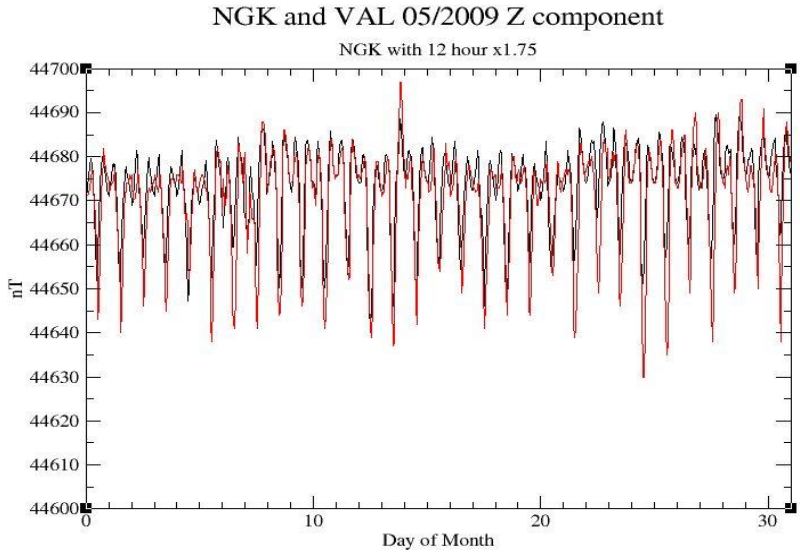

Figure 5.21 Comparison of VAL (red), and NGK (black) with 1.75x increased 12-hour period signal

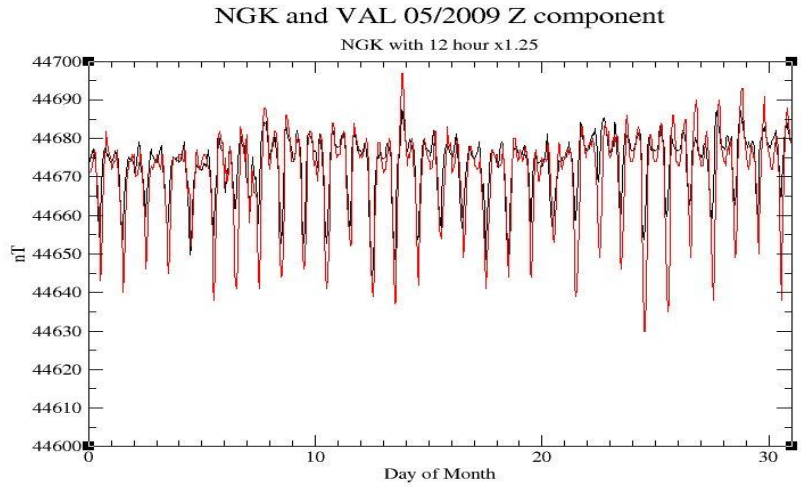

Figure 5.22 Comparison of VAL (red), and NGK (black) with 1.25x increased 12-hour period signal

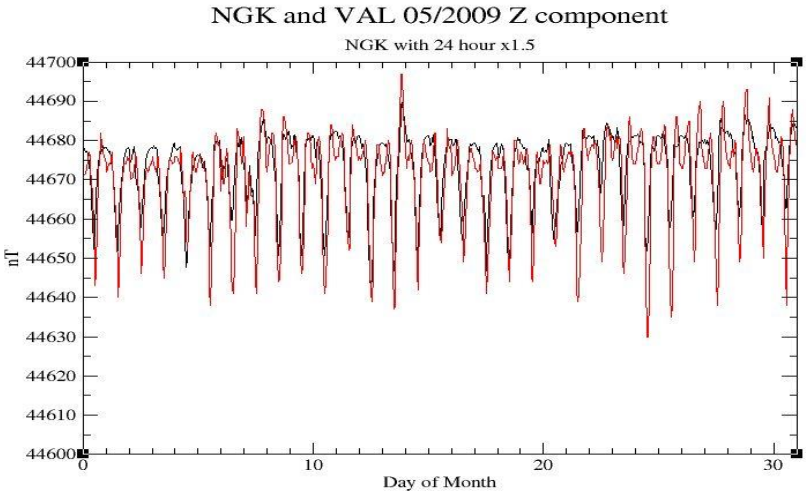

Figure 5.23 Comparison of VAL (red), and NGK (black) with 1.5x increased 24-hour period signal

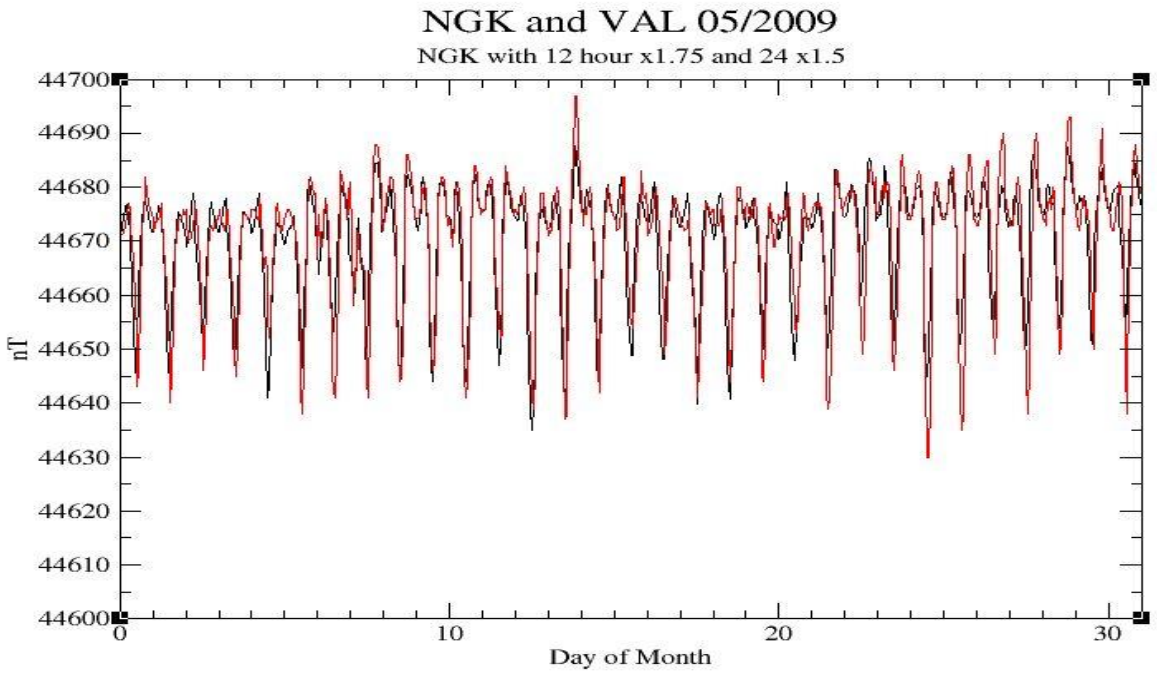

Figure 5.24 Comparison of VAL (red), and NGK (black) with 1.75x increased 12-hour and 1.5x increased 24-hour period signal

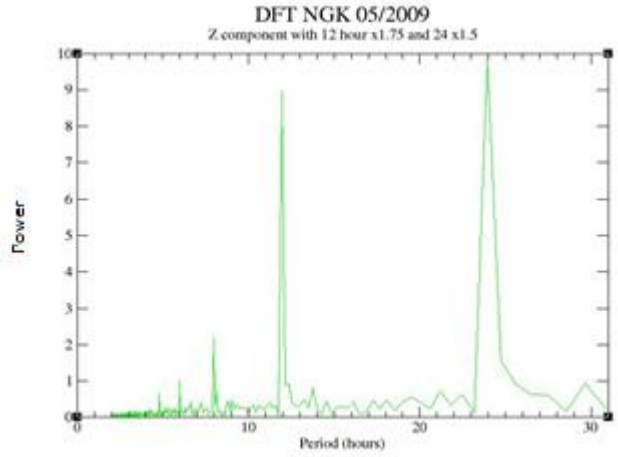

Figure 5.25 DFT of NGK with increased 12 and 24 hour

Increasing NGK signals	RMS misfit (nT)
No increases	7.03
1.25*12 hour	6.72
1.5*12 hour	6.51
1.75*12 hour	6.43
1.5*24 hour	6.45
1.75*12 and 1.5*24 hour	5.79

Table 6 RMS misfits to various increases in the amplitude of the 12 and 24-hour period signals at NGK

Increasing the 24-hour signal (figure 5.23) does increase the amplitude fit, but does nothing to match the double peak shape of the variation (as expected). However, increasing both the 24 hour and the 12-hour period results in a much better fit to VAL (figure 5.24, table 6; this gives an RMS misfit of 5.79nT). The DFT of this also shows that the proportion (and to an extent the absolute heights of the peaks) are much more similar to VAL, with the exception of the 12.4-hour tidal signal, which has not been increased here (figure 5.25). Increasing this as well would likely create the slight changes in the relative heights of the double peaks, and the trough depth variation through the month, which is not currently seen in the NGK data as it has a lower amount of tidal influence. This shows that the data from NGK could be transformed to match that of VAL by using sine/cosine waves of 24 and 12 hour periods, to make up the difference in the two sites. This could also be used in reverse to match data from VAL to NGK. In essence, this is correcting for the coast effect, removing a 24/12-hour period signal which is seen at the coast but not inland. This method could be used at other stations, requiring only a pair (or set) of stations that should otherwise be expected to be similar, and DFTs to show the relative differences in signal power of each period at those stations. This can then be used to determine the value of the sine or cosine wave to be added/subtracted from the station data to match the stations. The precise values would need fine tuning depending on the way in which the stations differ from each other, and the relative dominance of each period in the signal. Adding the increased tidal signal (12.4-hour curve) seen at VAL would also improve the correction, as shown in section 5.2. Shorter periods may have to be taken into account if the data is from a more disturbed time, or short features are relatively more important at a given observatory. Features at one station which are not required to match could be ignored, edited out, or corrected for in another way depending on their source, frequency characteristics as needed. Should a feature be identified which is not desired to be matched, but cannot be removed or otherwise accounted for, this method would not be appropriate.

Other Stations

Similar adjustments also seem to improve the match of stations in other locations, such as TAM/MBO, and ASP/GNA.

Compared to MBO, TAM has more power in periods below 6 hours, which we have not attempted to match here, but also relatively less power in the 24-hour period (figure 5.27). Adding in an extra 24-hour period signal to the data from TAM increases the fit to MBO (figure 5.28 and 5.29). The RMS misfits for this are 29.95nT for 1.5*the 24-hour signal, and 28.97nT for the 1.75*24-hour. The step like drop in overall strength (edited out of the diagrams for clarity) and large daily peaks

present at TAM, make this month difficult to compare easily using RMS, though it is seen by a visual comparison.

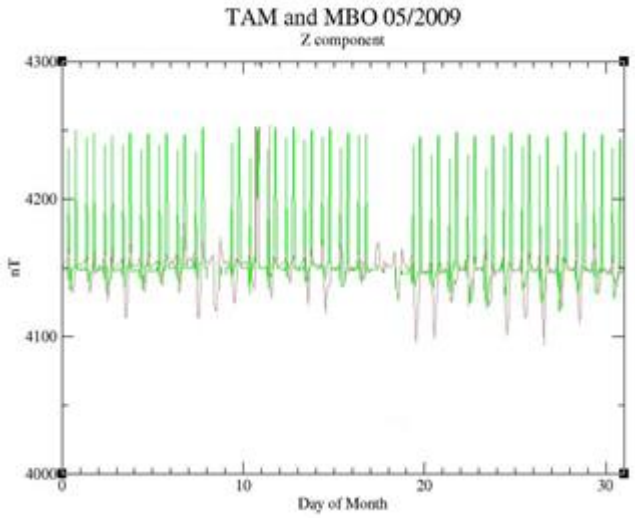

Figure 5.26 Comparison of Z components at Tam (green) and MBO (brown). Anomalous data has been removed from TAM on the 9th – 10th and 18th – 20th for clarity of viewing.

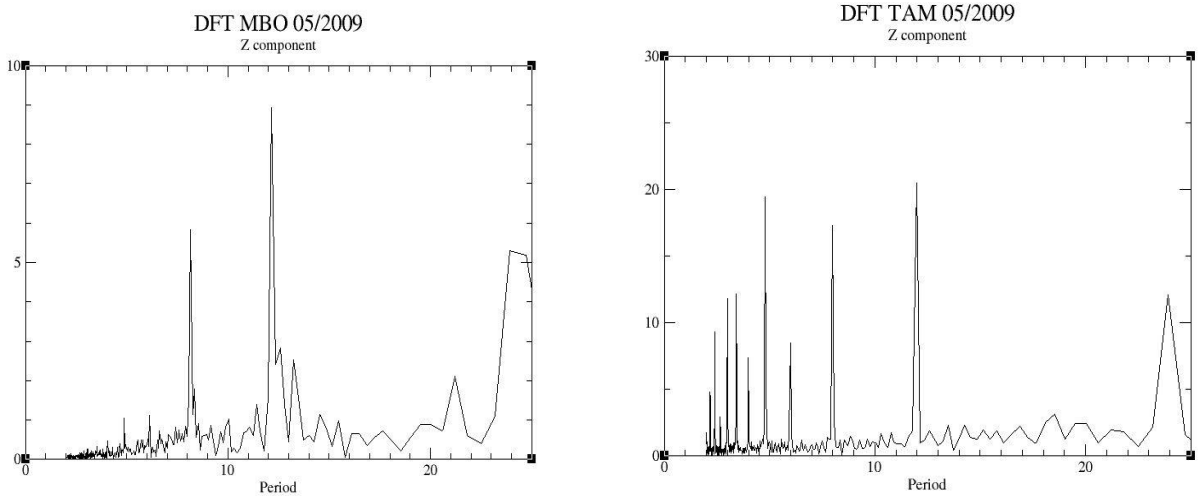

Figure 5.27 DFTs of MBO and TAM Z components. TAM shows much more power in shorter periods, while MBO has a relatively larger 24-hour peak. Y axis shows the relative power at each period

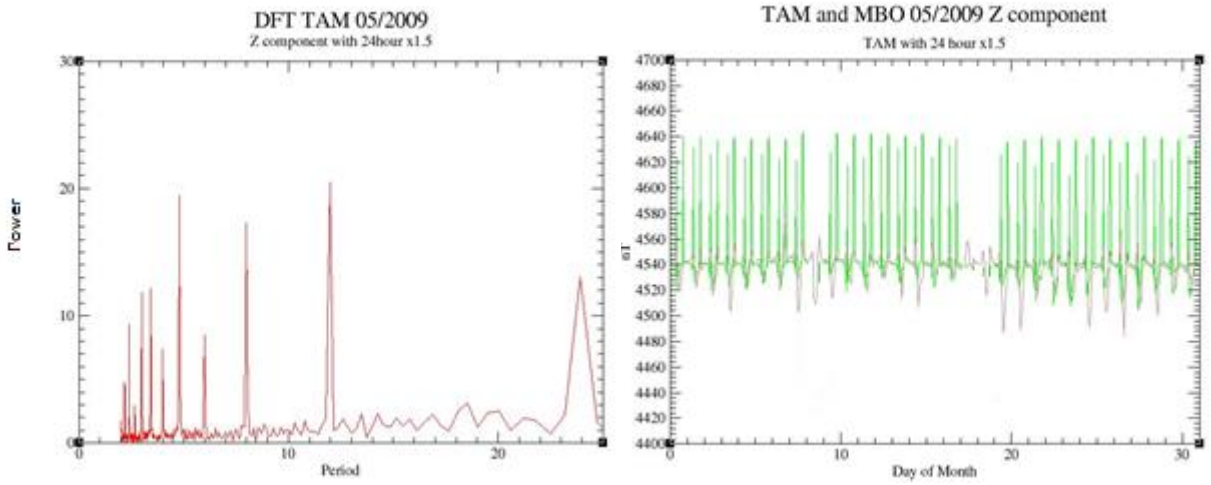

Figure 5.28 DFT of TAM with an increased 24-hour period signal, and comparison of the increased TAM (green) with MBO (brown)

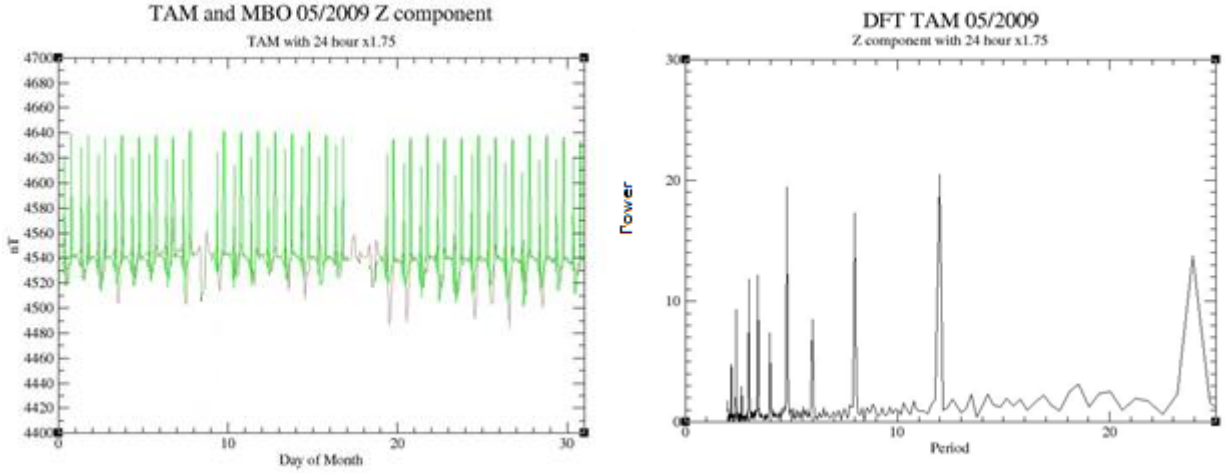

Figure 5.29 DFT of TAM with further increased 24-hour period signal, and comparison of the increased TAM (green) with MBO (brown)

For ASP/GNA, it can be seen that much like VAL/NGK, the coastal station GNA has relatively higher power in the 12-hour period, the peak in the DFT being almost as high as the peak for 24 hours (figure 5.30). Adding extra 12-hour signal to ASP improves the match, but doesn't correct this difference completely (figure 5.31). This can be improved by also adding an extra 24-hour period signal. The fit between the two stations is improved in some places, but not in others – it is probably that this misfit is due to the timing of the 12-hour period signal, as the increase in ASP is not in quite the right place (the additional 12 hour signal we have added to the data is in phase with the 24-hour signal, but it comparing to GNA suggests that it should be offset by a few hours, figure 5.32). This is also shown by the RMS misfit, which is 14.11nT for the 1.5*12-hour increase, and 14.26nT for the increase in both 12 and 24-hour periods, showing that this method is not correcting the overall fit for the month, but may be fitting parts of it.

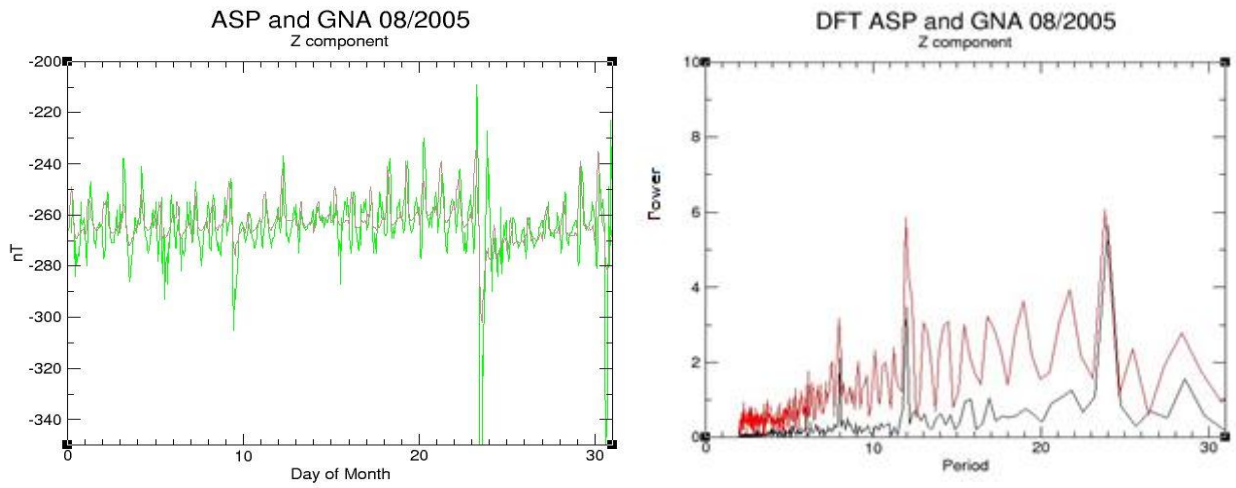

Figure 5.30 Comparison of ASP (brown) and GNA (green) Z components, and the DFT for each (ASP black, GNA red)

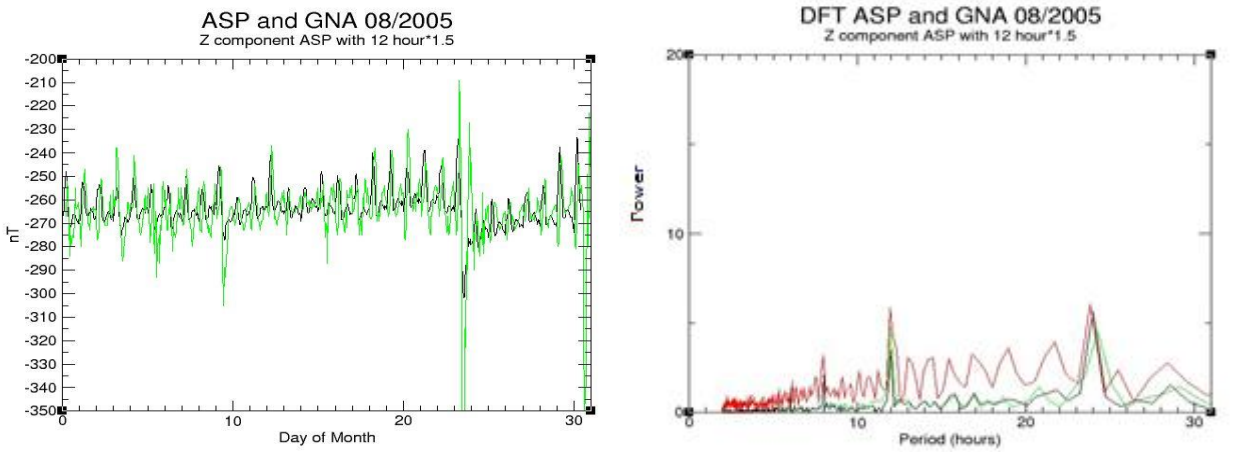

Figure 5.31 Comparison of ASP with an increased 12-hour signal (black) with GNA (green). DFT of the data from GNA (red), ASP (black) and ASP with increased 12 hour (green)

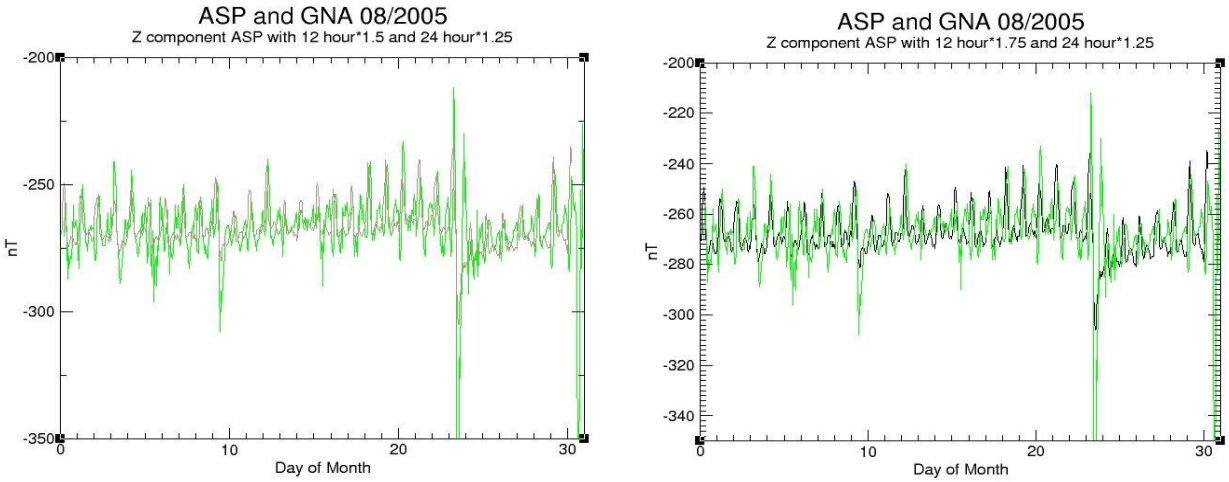

Figure 5.32 Comparison of ASP with an increased 12 and 24-hour signal (brown) and GNA (green), and comparison of a further increased ASP (black) with GNA (green)

This is a relatively crude correction, and further work would be required to refine it, but it does seem that increasing Sq periods can provide an approximation to the coast effect.
This (if improved) could be used to adjust a survey (or base station) to account for a coast effect in one area. This could also be used to adjust CM4 model outputs to account for the coast effect which it does not currently do, without adding extra parameters or complex conductivity models.

5.4 Geographically Localised Induction Effects

The following section details induction-related effects seen in the equatorial and arctic regions. These are different to those seen due to tidal and coast effects, as they seem likely to be related to the positions of ionospheric currents and the electrojets, rather than the underlying conductive medium.

5.4.1 Equatorial Induction Effects: GUI and TAM

At some stations (e.g. GUI) the effects of geomagnetic storms are smaller than might be expected. Compared to its normal Sq variation, the storm of 17th March 2015 only produces a signal of three times the amplitude of Sq at GUI. Dst (provisional) falls to -223 nT at the peak of the storm. GUI only falls to around -170nT, while TAM, situated inland but on approximately the same latitude shows a much larger variation, falls to -240nT (figure 5.33). The days preceding this storm show larger amplitudes at TAM, and other months show similar values at both stations. While TAM does tend to have larger values, the amount of difference is perhaps surprising. This suggests that there is some kind of dampening effect occurring at GUI, possibly related to it being a few degrees further north, and thus avoiding more of the influence of the equatorial electrojet, or possibly due to the relative orientation of the electrojet here meaning it doesn't contribute as strong an influence. The difference in behaviour here would not seem to be (purely) an island effect, since for HON, which is at a similar latitude, variation in X and Y seems to be similar to (or higher than) TAM. HON however does have a relatively reduced amount of variation in the Z component, which again suggests that induced fields are having less of an effect here (Denardini et al 2013, Rastogi 2004).

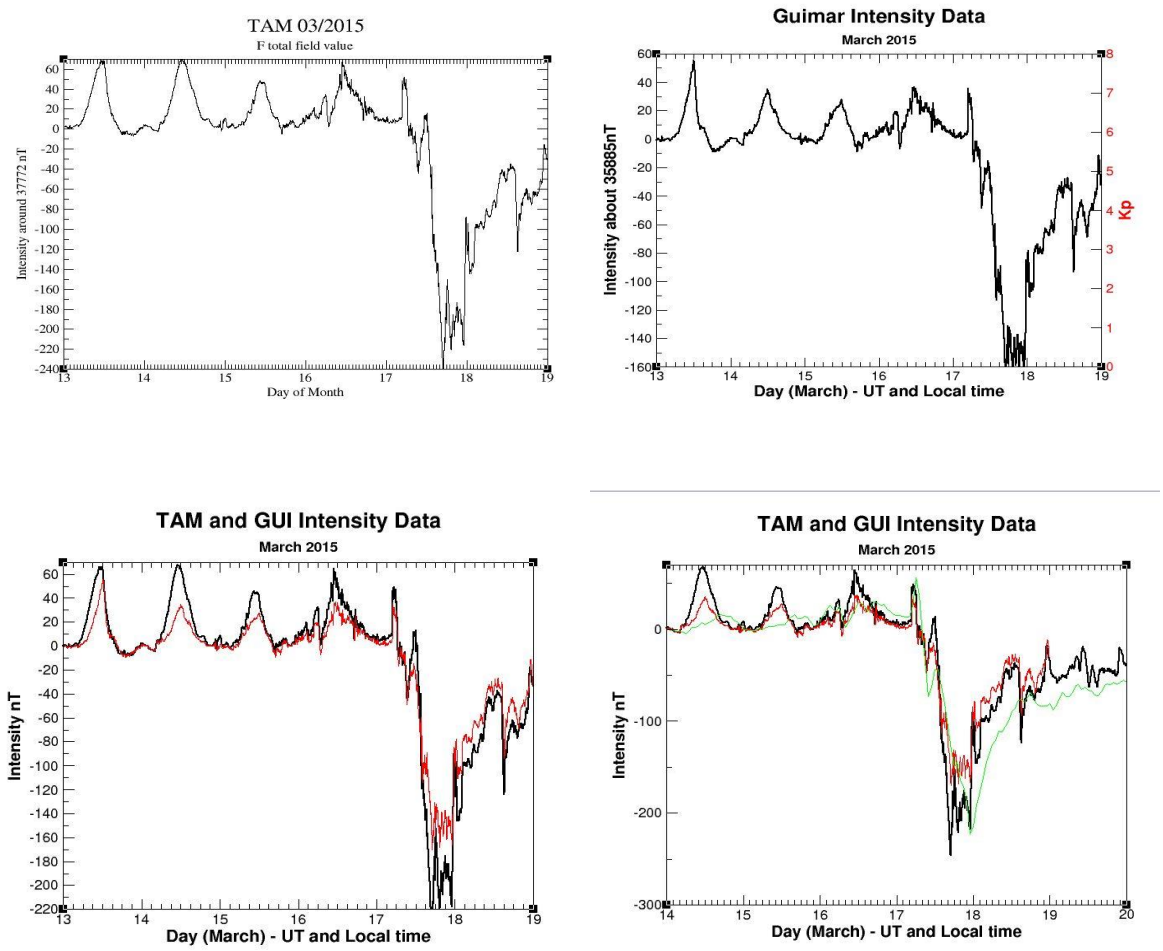

Figure 5.33 Comparisons of F values for storm period at TAM and GUI. TAM in black, GUI red, Dst (provisional) green

5.4.2 High Latitude Induction Effects

The 'opposite' effects seen at some high latitude stations are likely due to the increase of induced parts of the ionospheric or magnetospheric field in the auroral region, hence why they tend manifest in differences between north and south groups, as well as not appearing in the CM4 models. This was seen as an effect of increasing the induced components of the CM4 model (see chapter 2.3), while not increasing the primary field. Since short period features showing this trend tend to be occurring more often in disturbed periods (and seem confined to the auroral region, having not been seen at other, lower latitude, stations), they are likely related to the induced magnetic fields created by increased current flows in the ionosphere. This would also explain why they are non-persistent features – the effect will only be seen on days with the appropriate ionospheric conditions, where one station or group of stations is experiencing an unusual induced effect. Their larger cousin

however is the persistent differences in station groups, probably due to ionospheric currents, and features such as the auroral electrojet and related Hall currents; the effect of these features is related to the distance from the geomagnetic pole. These locations may adjust with the activity levels of the field, but will tend to affect limited localities, and crucially, flow latitudinally. Large parts of the difference between high latitude station groups is therefore likely to be due to induced fields (Ritter et al 2004).
Based on grip rule, it is possible that some of the differences between stations in the arctic region - particularly where they show the same feature in opposite phases - is due to large currents flowing east-west between them. This would generate a circular magnetic field around the current flow, which while much weaker than the geomagnetic field, has the appropriate geometry to produce the observed differences - with one side flowing ‘up’ to give a positive anomaly, and the other ‘down’ to give a negative anomaly, which are in other respects the same size and shape.

It might be possible to model the latitude variations seen in the Arctic region by using the SECS method. This method uses spherical elementary currents placed in the ionosphere to upward continue the magnetic field measured at the ground. This can be used to show the effect ionospheric currents have on the disturbance measured on the ground. This method is suitable for analysing small areas which might be difficult with spherical harmonic analysis methods, and is also usable without the need for regular gridding of ground-based measurements. Use of SECS could show if ionospheric currents are indeed the cause of the field variation between stations in this location, as is suspected. The precise location of the differences could then be pinned down (geographically and/or temporally). Additionally, this might allow a correction for drifting short-period features, which are also possibly related to ionospheric currents, as well as add an additional constraint on the location of features such as the auroral oval. SECS would be especially useful as a method of analysing and correcting disturbed periods, since such disturbance is due to ionospheric or magnetospheric current changes (Amm and Viljanen 1999, Juusola et al 2006).

Results

Induced magnetic fields can make a large difference to the behaviour of the overall field measured in a given area, and they occur on a variety of different scales.

Tidal generated fields can be seen in work undertaken here on relatively short periods of magnetic data, especially where the tidal range is high, such as VAL. These are seen as a 12.4-hour period spike in DFTs, and the increased fit to data of model sine waves when the tidal period is included. The additional effect of the tide can generate a signal of up to ~5nT amplitude. The appropriate value for a given location can be easily added/subtracted using a sine wave of the local tidal period.

The coast effect is another induction effect of importance to surveyors. Mathematical conductivity models show that the largest effect is due to a land/deep water boundary, but smaller effects may also be generated by shallower water, or contrasts in rock type. The effect is noted in many locations (though is also absent in areas of conductive underlying geology, strong electrical currents, or particularly shallow seas). The coast effect tends to amplify Z axis features (seen notably at VAL, compared to inland stations such as NGK). Disturbance is also seen more prominently at coastal stations. Comparing pairs of inland/coast observatories, it can be seen that subtracting or adding Sq period signal from the Z axis data can approximately correct for the coast effect. This is a relatively crude transformation, but with fine tuning it could be used (for example) to remove a coastal effect from one part of a survey (or adjust model outputs which do not take the coast effect into account).

The equatorial stations TAM and GUI show an induction effect related to the position of the equatorial electrojet. Unlike the tidal and coast effects, here there seems to be a damping of disturbance features, which may be related to the relative orientation of the field around the electrojet at GUI, though further investigation is needed here.

High latitude stations tend to show opposite sense features between latitudinal groups (peaks at one observatory seen as troughs at another). A likely explanation for this is the effect of the induced fields created by ionospheric currents. Further work using the SECS method could provide greater detail of the position and strength of these currents (as well as confirming if they are indeed the cause). This would allow the separation of high latitude groups to be defined more accurately, and possibly also provide a method of correcting drifting disturbance features.

Chapter 6. Conclusions and Future Work

6.1 Aims and Results

The aim of this project was to attempt to improve the remote referencing of aeromagnetic surveys. Surveys are referenced to a base station to remove time-varying effects from the data collected; this assumes that these effects occur simultaneously at both the survey location and the base station, and that the base station and survey area are recording similar variations in the external magnetic fields. There are many reasons why this assumption might not be the case, particularly when the base station is far from the survey area. To improve the correction in these situations, we first established, using CM4 models and observatory data, where observatories that are close together are not behaving in the same way – in which case these observatories would be difficult to use as base stations for each other, thinking in terms of survey correction.

Use of the CM4 model and comparison of observatory data has led to a classification of differences based on the activity level of the geomagnetic field, the latitude of the observatory, and the distance of the observatory from the coast.

6.2 Latitude

The latitude of the observatory becomes important when it is located near the auroral (or equatorial) electrojets. This is particularly important for high latitudes, as the polar magnetic field is both more complicated, and more likely to show disturbance that is not seen elsewhere, as charged particles are often funnelled to the polar regions, and sub-storms show their greatest effect here. The location of the auroral electrojet (and other latitudinally flowing currents, such as the DP2 Hall current system) has a strong influence on the behaviour of high-latitude stations, causing them to correlate poorly with each other. This is a problem when attempting to remote reference surveys, as was seen with the survey considered in chapter 3.1. However, a simple method of avoiding this issue would be to choose as a base station an observatory which falls into the group around same geomagnetic latitude as the survey area. The use of two observatories, instead of only one, would also allow for the removal of short period features seen in the region more easily, since features in this region seem to have a geographic limit to their extent, and may be seen at one observatory but not a more distant one. This would also allow a check on whether a given observatory will work successfully as a base station – if the short period features are in phase in both the observatory and the survey

data, they are more likely to be compatible. Comparisons of observatory data shows that stations in different groupings may show anti-correlated features. Work with models (chapter 2.3) suggests that this effect is due to the presence of a large induced field component; this would imply that the use of a method of modelling that incorporates inducing ionospheric currents, for example spherical elementary current systems (e.g. Amm and Viljanen 1999), would provide a better method of converting between these station groupings. Use of satellite data or ionospheric electrical studies to locate more precisely the boundaries between the latitude groupings would also allow more confidence in using remote referencing in this region.

Around the EEJ, a similar effect can be seen (possibly also related to the direction of the EEJ as well as its position) – the effects of geomagnetic storms are noticeable lower than might be expected at GUI, which lies just off the path of the EEJ. This shows that when carrying out surveys in this area, again, remote base stations must be located carefully in relation to the survey area – preferably so that both see similar influences from the EEJ and ring current. The effect of the electrojet in this region does not seem to be of as great a significance to surveys as the auroral electrojet is in its region.

6.3 Induction

Other induction effects are found, notably the coast effect, which has been seen in many locations (see chapter 5 for references). The conductivity contrast of the ocean and land creates anomalously large vertical components in data recorded in this area, as well as amplifying any activity in the main field (as described by Kuvshinov 2008, and seen in section 5.3, as the greater variation with Dst noted at coastal stations and the reduced effect of geomagnetic storms at observatories without a coast effect, such as HLP). This effect is important to note when carrying out surveys over the coast, or when either the survey or base station are located near to it. A simple approximation of the coast effect can be seen in chapter 5.4, showing that adding/removing Sq period cosine waves to the data results in a correction for the coast effect seen at one location. This work could be further refined, to make a better approximation. Work from magnetotellurics has also encountered the coast effect (e.g. Key and Constable 2011, Worzewski et al 2012) and it is likely to be of great use in making a better correction. Conductivity modelling and electrical work has also resulted in some methods of correcting for the coast. While these are unlikely to be directly relevant to remote referencing, or the type of data collected in aeromagnetic surveys, they may in the future result in an appropriate correction method.

The tides also have a smaller, but not insignificant effect on magnetic data. Tides may also be

approximated by a cosine wave with a period of 12.4 hours (for the M_2 tidal constituent), which would allow removal or addition of the tidal effect as necessary at a base station. The amplitude of the wave required can be determined using the power ratio of the 12.4-hour peak in discrete Fourier transforms of the observatory data, or by finding the best fit curve by matching sine/cosine waves, as presented in chapter 5.2.

6.4 Disturbance Levels

The overall disturbance level of the geomagnetic field presents issues to surveying work, particularly when in conjunction with an induction effect, as discussed above. Times containing geomagnetic storms are often seen as unusable for surveying purposes. Comparison of the effect of storms at various locations in this work has shown that the recovery period after a storm can be corrected for by simple fits to the recovery phase, thus allowing this data to be used as normal, and potentially recovering 80-90% of data that might otherwise be discarded (chapter 4.6). We have also seen that Sq period data can be seen under storm signals in some Y and Z component data, implying that stations showing this would still be appropriate to use with some care. The lower than expected effect of the geomagnetic storm at GUI in March 2015 also implies that there are locations where the effect of a geomagnetic storm is not as strong, and more data could be retrieved. This would bear further investigation. Comparison of the GUI data to the RC index at this point may shed further light, as it has been noted that the RC index is a better proxy for disturbance than Dst in some cases.

6.5 Global Field Models

Finally, this work has focused on the use of CM4, finding that it a good model for the areas it is designed to fit, and reasonable for many it is not, e.g. times of higher disturbance ($2< Kp <4$). Further insights could be gained by comparing data with other models, to investigate if the findings from other models agree with those we have seen using CM4, or if other effects can be separated and corrected for. This would be particularly interesting if data was compared to a model designed to fit where CM4 does not, such as a high latitude model.
Since this work was completed, a new comprehensive model, CM5, has been developed (Sabaka et al 2015). CM5 is derived from SAC-C, Ørsted, CHAMP and observatory data covering the period from August 2000 to January 2013. It builds further on previous CM versions, by including a 3-D conductivity model (allowing for coastal features to be modelled) and the ability to model M_2 tidal

constituents, as well as including more polar and high disturbance data in the parametrisation. CM5 therefore, seems to account for most of the major noted exceptions found during this work, and is likely to produce an improved model of geomagnetic field behaviour compared to CM4. It would be interesting
to compare the results from this work to results using CM5, to determine how much improvement has been made in areas which were problematic using the older model.

6.6 Recommendations for remote referencing of geomagnetic surveys

The findings of this work (along with previous understandings) lead us to make the following recommendations for those wishing to improve remote correction of geomagnetic surveys:

- Locate remote base stations as close to the survey location as possible.
- Re-occupy base stations if they are located within or close to the survey.
- Try to avoid locations containing effects which are not found in the survey region (such as coast effects, electrojets, dramatically different geomagnetic/conductive properties).
- Times containing geomagnetic storms are unlikely to be usable for survey purposes, although some locations may still contain usable data. Recovery periods after the storm, however, should be usable as normal, or with small corrections made.
- Base stations should be located at the same magnetic latitude as the survey – for high latitudes, this is particularly important, so the base and survey fall into the same behavioural group. If it is possible, two base stations, one north and one south of the survey region can be used (at least for a short period) to establish if there are strong latitude-related effects which will hinder the use of a particular base location. Different base locations may be used for different parts of the survey region if it covers a wider area.
- If either the base station or survey are located near the coast, consider adding/removing Sq period data to correct for any coast effect. Curves of the local tidal period can be used to correct for tidal effects. The tidal range in the region will determine the size of the correction needed – this is more important in areas with a high tidal range.
- CM4 (or CM5, if this is indeed an improvement on CM4) can be used as a check for unusual measurements, and possibly as a base station, if used for inland, low-mid latitude regions. It is not suitable for higher latitudes, or coastal regions, without some sort of correction.

Appendix 1: Observatory Locations

Station Code	Name	Latitude	Longitude	Altitude	Location (operating country)
AAE	Addis Ababa	9.035°N	38.77°E	2441.0m	Ethiopia
ABK	Abisko	68.358°N	18.823°E	380.0m	Sweden
AIA	Faraday Islands	-65.245°N	295.742°E	10.0m	Antarctica (Ukraine)
AMS	Martin de Vivies	-37.8°N	77.57°E	50.0m	Ile Amsterdam (France)
ARS	Arti	56.433°N	58.567°E	290.0m	Russia
ASC	Ascension Island	-7.949°N	345.624°E	177.0m	(United Kingdom)
ASP	Alice Springs	-23.762°N	133.883°E	557.0m	Australia
BLC	Baker Lake	64.318°N	263.988°E	30.0m	Canada
BEL	Belsk	51.837°N	20.792°E	180.0m	Poland
BJN	Bear Island	74.5°N	19.2°E	80.0m	Norway
BRW	Barrow	71.3°N	203.38°E	12.0m	USA
CBB	Cambridge Bay	69.123°N	254.969°E	20.0m	Canada
CBI	Chichijima	27.096°N	142.185°E	155.0m	Japan
CLF	Chambon-la-Foret	48.025°N	2.26°E	145.0m	France
CMO	College	64.87°N	212.14°E	197.0m	USA
CWE	Cape Wellen	66.163°N	190.165°E	10.0m	Russia
CZT	Port Alfred	-46.431°N	51.867°E	155.0m	Archipel Crozet (France)
DED	Deadhorse	70.36°N	211.207°E	10.0m	USA
DMC	Dome Concordia	-75.25°N	124.167°E	3250.0m	Antarctica (France/Italy)
ESK	Eskdalemuir	55.314°N	356.794°E	245.0m	United Kingdom
FCC	Fort Churchill	58.759°N	265.912°E	15.0m	Canada
FUQ	Fuquene	5.47°N	286.263°E	2543.0m	Colombia
FUR	Furstenfeldbruck	48.17°N	11.28°E	572.0m	Germany
GDH	Qeqertarsuaq	69.252°N	306.467°E		Greenland
GNA	Gnangara	-31.78°N	115.947°E	60.0m	Australia
GUI	Guimar	28.321°N	343.559°E	868.2m	Tenerife (Spain)
HAD	Hartland	50.995°N	355.516°E	95.0m	United Kingdom
HBK	Hartebeesthoek	-25.882°N	27.707°E	1555.0m	South Africa
HER	Hermanus	-34.425°N	19.225°E	26.0m	South Africa
HLP	Hel	54.608°N	18.816°E	1.0m	Poland
HON	Honolulu	21.32°N	202.0°E	4.0m	USA
HRN	Hornsund	77.0°N	15.55°E	15.0m	Svalbard (Poland)
KIR	Kiruna	67.8428°N	20.4201°E	395.0m	Sweden
KOU	Kourou	5.21°N	307.269°E	10.0m	French Guiana
LER	Lerwick	60.138°N	358.817°E	85.0m	United Kingdom
LRV	Leirvogur	64.183°N	338.3°E	5.0m	Iceland
LZH	Lanzhou	36.087°N	103.845°E	1560.0m	China
MBO	Mbour	14.38°N	343.03°E	7.0m	Senegal
MEA	Meanook	54.616°N	246.653°E	700.0m	Canada
MMB	Memambetsu	43.91°N	144.189°E	42.0m	Japan
NAQ	Narsarsuaq	61.167°N	314.567°E	4.0m	Greenland
NEW	Newport	48.267°N	242.883°E	770.0m	USA
NGK	Niemegk	52.072°N	12.675°E	78.0m	Germany
NGP	Nagpur	21.1°N	79.0°E		India
OTT	Ottawa	45.403°N	284.448°E	75.0m	Canada
PBQ	Poste-de-la-Baleine	55.277°N	282.255°E	40.0m	Canada
PPT	Pamatai	-17.567°N	210.426°E	357.0m	French Polynesia
PST	Port Stanley	-51.704°N	302.107°E	135.0m	Falkland Islands (United Kingdom)
RES	Resolute Bay	74.69°N	265.105°E	30.0m	Canada
SCO	Scoresby Sund 2	70.483°N	338.033°E		Greenland
SOD	Sodankyla	67.367°N	26.633°E	178.0m	Finland
TAM	Tamanrasset	22.7925°N	5.532°E	1373.0m	Algeria
THJ	Tonghai	24.0°N	102.7°E	1820.0m	China
THL	Qaanaaq	77.483°N	290.833°E	57.0m	Greenland
TRO	Tromso	69.663°N	18.948°E	105.0m	Norway
TSU	Tsumeb	-19.202°N	17.584°E	1273.0m	Namibia
VAL	Valentia	51.933°N	349.75°E	14.0m	Ireland
YAK	Yakutsk	61.96°N	129.66°E	100.0m	Russia

Appendix 2 – Observatory Location Maps

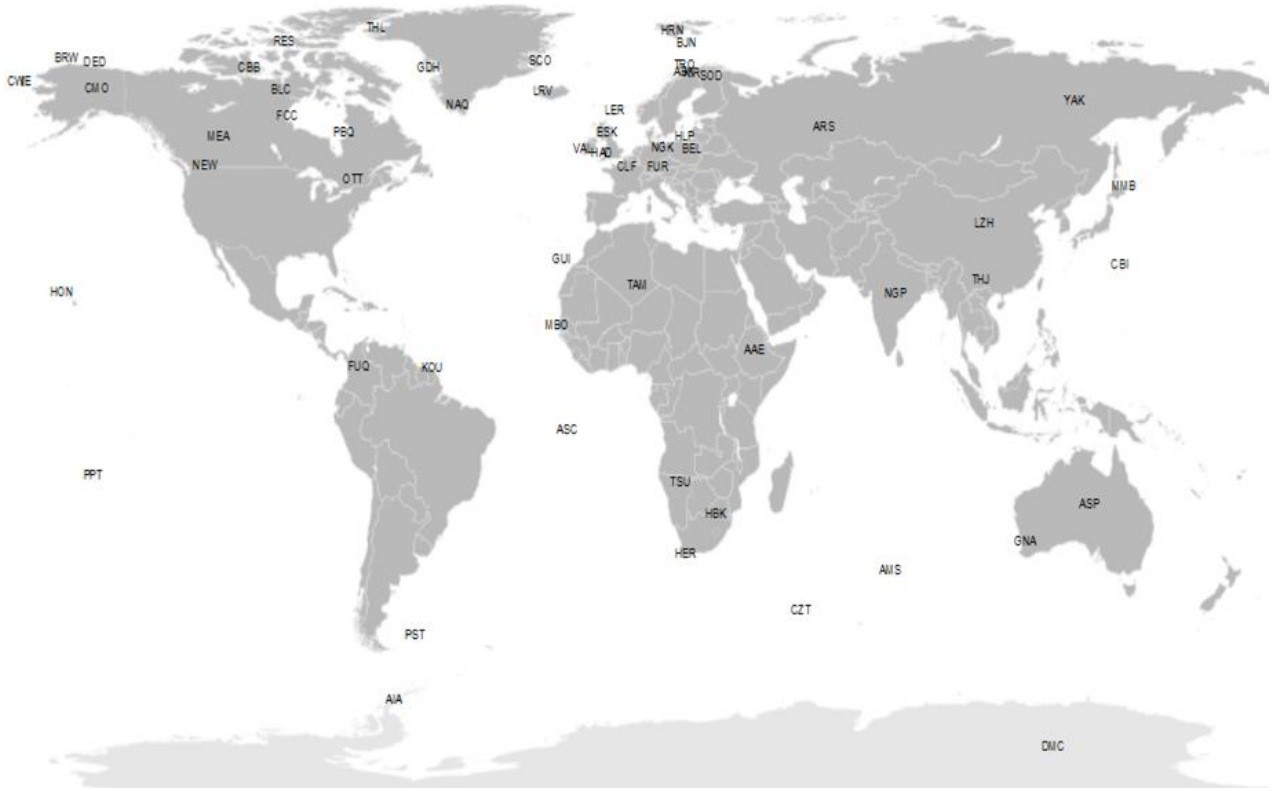

References

Allen, C.W. 1944. Relation Between Magnetic Storms and Solar Activity. Monthly Notices of the Royal Astronomical Society. 104, 1, 13-21.

Amm, O., and Viljanen, A. 1999. Ionospheric disturbance magnetic field continuation from the ground to the ionosphere using spherical elementary current systems. Earth Planets Space, 51, 431–440.

Blakely, R.J. 1996. Potential Field Theory in gravity and Magnetic Applications. Cambridge University Press.

Campbell, W.H. 1997. Introduction to Geomagnetic Fields. Cambridge University Press.

Chen, Y., Reeves, G. D., and Friedel, R.H.W. 2007. The energization of relativistic electrons in the outer Van Allen radiation belt. Nature Physics 3, 614 – 617.

d'Erceville, I., and Kunetz, G. 1962. The Effect of a Fault on the Earth's Natural Electromagnetic Field. Geophysics. 27, 5, 651-665.

Denardini, C.M., Aveiro, H.C., Sobral, J.H.A., Bageston, J.V., Guizelli, L.M., Resende, L.C.A., and Moro, J. 2013. E region electric fields at the dip equator and anomalous conductivity effects. Advances in Space Research. 51, 10, 1857-1869.

Dosso, H.W., and Meng, Z.W. 1992. The coast effect response in geomagnetic field measurements. Physics of the Earth and Planetary Interiors, 70 39—56.

Gambetta, M., Armadillo, E., Carmisciano, C., Caratori Tontini, F., and Bozzo, E. 2007. Magnetic Base Station Deceptions, a magnetovariational analysis along the Ligurian Sea coast, Italy. Annals of Geophysics. 50, 3.

Griffiths, D. 1999. Introduction to electrodynamics 3rd edition. Prentice Hall.

Haymes, R.C. 1971. Introduction to Space Science. John Wiley & Sons.

Hinze, W.J., von Frese, R., and Saad, A. 2013. Gravity and Magnetic Exploration: Principles, Practices, and Applications. Cambridge University Press.

Hitchman, A., Lilley, F., and Campbell, W. 1998. The quiet daily variation in the total magnetic field: global curves. Geophysical Research Letters, 25, 11, 2007-2010.

Juusola, L., Amm, O., and Viljanen, A. 2006. One-dimensional spherical elementary current systems and their use for determining ionospheric currents from satellite measurements. Earth Planets Space, 58 (No. 5), 667-678.

Kellett, R.L., Lilley, F.E.M., and White, A. 1991. A two-dimensional interpretation of the geomagnetic coast effect of southeast Australia, observed on land and seafloor. Tectonophysics. 192, 3-4, 367-382.

Kelley, M.C., 2009. The Earth's Ionosphere: Plasma Physics & Electrodynamics. Academic Press (Elsevier).

Key, K., and Constable, S. 2011. Coast effect distortion of marine magnetotelluric data: insights from a pilot study offshore northeaster Japan. Physics of the Earth and Planetary Interiors. 184, 3-4, 194-207.

Knecht, D. J., and Shuman, B.M. (1985), The geomagnetic field. In Jursa, AS. Handbook of geophysics and the space environment, fourth ed., Chapter 4, 1–37, Air Force Geophysics Lab, Hanscom AFB, MA.

Kuvshinov, A.V. 2008. 3-D Global Induction in the Oceans and Solid Earth: Recent Progress in Modeling Magnetic and Electric Fields from Sources of Magnetospheric, Ionospheric and Oceanic Origin. Survey in Geophysics. 29, 139–186.

Kuvshinov, A., Manoj, C., Olsen, N., and Sabaka, T. 2007. On induction effects of geomagnetic daily variations from equatorial electrojet and solar quiet sources at low and middle latitudes. Journal of Geophysical Research. 112. B10102.

Lanza, R. and Meloni, A. 2006. The Earth’s Magnetism, An Introduction for Geologists. Springer.

Lakhina, G.S., Alex, S., Mukherjee, S., and Vichare, G. 2006 On magnetic storms and substorms. ILWS Workshop Goa, February, 19-24.

Liou, K., Takahashi, K., Anderson, B.J., Nose, M., and Iyemori, T. 2013. Assessment of the auroral electrojet index performance under various geomagnetic conditions. Journal of Atmospheric and Solar-Terrestrial Physics. 92, 31–36.

Lowrie, W. 2007. Fundamentals of Geophysics. 2nd Edition. Cambridge University Press.

Maus, S., and Kuvshinov, A. 2004. Ocean tidal signals in observatory and satellite magnetic measurements. Geophysical Research Letters. 31, 15.

Maus, S. and Lühr, H. 2005. Signature of the quiet-time magnetospheric magnetic field and its electromagnetic induction in the rotating Earth. Geophysical Journal International, 162, 755–763.

Mayaud, P.N. 1980. Derivation, Meaning, and Use of Geomagnetic Indices. Geophysical Monograph Series, vol. 22, AGU, Washington, D. C.

McNeill, J.D. 1980. Electrical Conductivity of Soils and Rocks. Geonics Limited. Report No.: TN-5

McPherron, R.L., Baker, D.N., Pulkkinen, T.I., Hsu, T.-S., Kissinger, J., and Chu, X. 2013. Changes in solar wind–magnetosphere coupling with solar cycle, season, and time relative to stream interfaces. Journal of Atmospheric and Solar-Terrestrial Physics. 99, 1-13.

Milsom, J. 2003. Field geophysics. Third edition. John Wiley and Sons.

Neumann, G., and Hermance, J. 1985. The geomagnetic coast effect I the Pacific Northwest of America. Geophysical Research Letters. 12, 8, 502-505.

Olsen, N. 1998. The electrical conductivity of the mantle beneath Europe derived from C-responses from 3 to 720 hr. Geophysical Journal International. 133, 298–308.

Olsen, N. 1999. Induction studies with satellite data. Surveys in Geophysics. 20, 3, 309-340.

Olsen, N. and Kotsiaros, S. 2011. Magnetic Satellite Missions and Data. In Mandea, M. and Korte, M. Geomagnetic Observations and Models IAGA Special Sopron Book Series Volume 5.

Olsen, N., and Kuvshinov, A. 2004. Modeling the ocean effect of geomagnetic storms. Earth Planets Space. 56, 525-530.

Olsen, N., Lühr, H., Finlay, C. C., and Tøffner-Clausen, L. 2014. The CHAOS-4 Geomagnetic Field Model. Geophysical Journal International. 1997, 815–827

Onovughe, E. 2015. Geomagnetic Diurnal Variation Studies Using Global Models & Observatory Data at Quiet & Moderately Disturbed Times, PhD thesis, University of Liverpool

Parkinson, W.D. 1962. The influence of continents and oceans on geomagnetic variations, Geophysical Journal of the Royal Astronomical Society. 6, 441-449.

Parkinson, W.D., and Hutton, V.R.S. 1989. The electrical conductivity of the Earth. In Jacobs, JA, Geomagnetism Volume 3. Academic, London, 261-321.

Parkinson, W.D., and Jones, F.W. 1979. The Geomagnetic Coast Effect. Reviews of Geophysics and Space Physics. 17, 8, 1999-2015.

Papitashvili, V. O., Papitashvili, N. E. and King, J. H. 2000. Solar cycle effects in planetary geomagnetic activity: Analysis of 36-year long OMNI dataset. Geophysical Research Letters. 27, 17, 2797 – 2800

Partamies, N., Juusola, L., Tanskanen, E., and Kauristie, K. 2013 Statistical properties of substorms during different storm and solar cycle phases. Annales Geophysicae. 31, 349-358.

Pirjola, R.J. 1998. Modelling the electric and magnetic fields at the Earth's surface due to an auroral electrojet. Journal of Atmospheric and Solar-Terrestrial Physics. 60, 11, 1139-1148.

Rajaram, M. 1993. MAGSAT's contribution to geophysical surveys. Advances in Space Research. 13, 33-42.

Rastogi, R.G. 2004. Electromagnetic induction by the equatorial electrojet. Geophysical Journal International. 158, 16-31.

Reeves, C. 2005. Aeromagnetic Surveys: Principles, Practice and Interpretation. Geosoft.

Richmond, A.D. 2002. Modeling the geomagnetic perturbations produced by ionospheric currents, above and below the ionosphere. Journal of Geodynamics. 33, 143-156.

Rikitake, T., 1965. Some characteristics of geomagnetic variation anomaly in Japan, Journal of Geomagnetism and Geoelectricity. 17, 95-97.

Ritter, P., Lühr, H., Viljanen, A., Amm, O., Pulkkinen, A., and Sillanpää, I. 2004. Ionospheric currents estimated simultaneously from CHAMP satellite and IMAGE ground-based magnetic field measurements: a statistical study at auroral latitudes. Annales Geophysicae. 22, 417-430.

Russell, C.T., and Luhmann, J.G. 1997. Earth: Magnetic Field and Magnetosphere. In Shirley, J.H., and Fainbridge, R.W. Encyclopedia of Planetary Sciences, 208-211, Chapman and Hall, New York.

Sabaka, T., Olsen, N., and Langel, R. 2002. A comprehensive model of the quiet-time, near-Earth magnetic field: phase 3. Geophysical Journal International. 151, 32–68.

Sabaka, T., Olsen, N., and Purucker, M. 2004. Extending comprehensive models of the Earth's magnetic field with Ørsted and CHAMP data. Geophysical Journal International. 159, 521-547.

Sabaka, T., Olsen, N., Tyler, R., and Kuvshinov, A. 2015. CM5, a pre-Swarm comprehensive geomagnetic field model derived from over 12 yr of CHAMP, Ørsted, SAC-C and observatory data. Geophysical Journal International. 200, 1596-1626.

Schmucker, U., 1973. Regional induction studies. Physics of the Earth and Planetary Interiors. 7, 365-378.

Schnepf, N.R., Manoj, C., Kuvshinov, A., Toh, H., and Maus, S. 2014. Tidal signals in ocean bottom magnetic measurements of the Northwestern Pacific: Observation versus prediction. Geophysical Journal International. 198, 1096-1110.

Shore, R. 2007. Geomagnetic Storms and Magnetic Models of the Earth, Undergraduate dissertation, University of Liverpool.

Srivastava, B., Abbas, H., RamaGopal, T., Rao, D.R.K., and Pathan, B.M. 2001. Geomagnetic coast and other effects deduced from the new observatory at Visakhapatnam, India. Geophysical Journal International. 146, 3, 827-832.

Torta, J.M., Curto, J.J., and Bencze, P. 1997. Behaviour of the quiet day ionospheric current system in the European region. Journal of Geophysical Research. 102, A2, 2483-2494.

Untiedt, J., 1970. Conductivity anomalies in central and southern Europe, Journal of Geomagnetism and Geoelectricity. 22, 131-149.

White, A., and Polatajko, O.W. 1977. The coast effect in geomagnetic variations in South Australia, Journal of Geomagnetism and Geoelectricity. 30, 109-12.

Worzewski, T., Jegen, M., and Swidinsky, A. 2012. Approximations for the 2-D coast effect on marine magnetotelluric data. Geophysical Journal International. 189, 357-368.

Websites

CM4 code:

http://core2.gsfc.nasa.gov/CM/

Geomagnetic data and services:

www.intermagnet.org
www.wdc.bgs.ac.uk/catalog/master.html
wdc.kugi.kyoto-u.ac.jp/kp/index.html
www.gfz-potsdam.de/en/section/earths-magnetic-field/services/kp-index/
www.geomag.bgs.ac.uk/research/modelling/IGRF.html

Geomagnetic satellite missions:

www.esa.int/
www.nasa.gov/missions
op.gfz-potsdam.de/champ/
www.space.dtu.dk/english/Research/Projects/Oersted

Other information/diagrams:

ftp.ngdc.noaa.gov/STP/space-weather/solar-data/solar-features/solar-radio/noontime-flux/penticton/documentation/miscellaneous/penticton.txt
www.geomag.bgs.ac.uk/education/earthmag.html
roma2.rm.ingv.it/en/themes/23/geomagnetic_indices/26/auroral_electroject_indices